Cape Peninsula University of Technology

Biofouling Mitigation of Polyamide Reverse Osmosis Membranes using Polymer Grafting and Nanoparticle Coating in the Treatment of Municipal Secondary Effluent.

by

GODWILL KASONGO WA KASONGO

Thesis submitted in fulfilment of the requirements for the degree

DOCTOR of ENGINEERING: CHEMICAL

in the

FACULTY OF ENGINEERING AND THE BUILT ENVIRONMENT

at the

CAPE PENINSULA UNIVERSITY OF TECHNOLOGY

Supervisor: Prof Mujahid Aziz

December 2025

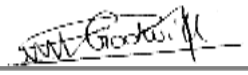
CPUT copyright information

The dissertation/thesis may not be published either in part (in scholarly, scientific or technical journals) or as a whole (as a monograph) unless permission has been obtained from the University.

Cape Peninsula University of Technology

DECLARATION

I, **GODWILL KASONGO,** declare that the contents of this dissertation/thesis represent my own unaided work and that the dissertation/thesis has not previously been submitted for academic examination towards any qualification. Furthermore, it represents my own opinions and not necessarily those of the Cape Peninsula University of Technology.



19 December 2025

Signed **Date**

ABSTRACT

Reverse osmosis (RO) is suitable for treating municipal secondary effluent to produce high-quality water for reuse applications. However, polyamide (PA) RO membrane fouling remains the key challenge as it causes RO membrane degradation and poor performance, resulting in a significant economic impact on the overall RO process. Microbial fouling (biofouling) particularly accounts for 45% of membrane fouling. Fouling mitigation techniques, such as membrane active-layer modification, provide a viable route to tailoring membrane surface physico-chemical properties. In this research project, a novel membrane surface modification approach is initiated to mitigate biofouling of PA RO membranes. The membrane was chemically grafted with 3-Allyl-5,5-dimethylhydantoin (ADMH), a titanium dioxide (TiO_2)-silver (Ag) nanocomposite, and a combined ADMH-TiO_2-Ag nanocomposite layer. Modified membrane structures were characterised using SEM-EDX, ATR-FTIR, NMR, TEM, TGA, contact angle and zeta potential. Membrane performance was evaluated for water permeability, salt rejection, flux decline, and bacterial adhesion using *Escherichia coli* and *Staphylococcus aureus*, as well as real municipal secondary effluent.

Initially, the graft polymerisation of N,N′-dimethylaminoethyl methacrylate (DMAEMA) was investigated to enhance fouling resistance against secondary effluent constituentsSubsequently, 3-allyl-5,5-dimethylhydantoin (ADMH) was grafted at varying concentrations to enhance antimicrobial activity against both Gram-negative (Escherichia coli) and Gram-positive (Staphylococcus aureus) bacteria. Finally, a hybrid modification combining ADMH with titanium dioxide–silver (TiO_2-Ag) nanoparticles. This initial modification increased the flux recovery ratio from 68.61% to 83.57% and reduced the flux decline ratio from 38.21% to 25.54%. The DMAEMA-modified membrane exhibited significantly higher sterilisation ratios than the unmodified membrane, demonstrating enhanced antibiofouling properties against *E. coli*, with a maximum sterilisation ratio of 76.8%. Pure water flux tests further confirmed the improved performance, with the flux decline decreasing from 46.0% for the unmodified membrane to 37.3% after DMAEMA modification.

Subsequently, surface modification with varying concentrations of ADMH was carried out to further minimise biofouling. ADMH adhered to the membrane surface via graft polymerisation, as confirmed by SEM, FTIR, and NMR analyses. *E. coli* and *S. aureus*. The membranes were tested with *E. coli* and *S. aureus,* and, furthermore, with organic and inorganic foulant solutions, thus mimicking the microbial and fouling activity of municipal wastewater secondary effluent. Biofouling tests using *E. coli* and *S. aureus* demonstrated improved mortality ratios of 58.9% and 37.4%, respectively, along with reduced fouling decline (3.7-8.9%) and enhanced flux recovery ratios (69.2-96.9%). Although surface hydrophilicity increased with ADMH concentration, optimal fouling resistance was achieved

at moderate ADMH concentration, while resistance to organic and inorganic foulants showed limited improvement, highlighting the role of foulant type in defining membrane performance.

Finally, a hybrid modification involving ADMH, TiO_2, and Ag was investigated to simultaneously enhance the thin-film composite (TFC) RO membrane surface hydrophilicity and antibacterial activity, while maintaining salt rejection. The ADMH\TiO_2-Ag modified membrane maintained both thermal and mechanical stability, as confirmed by TGA analysis and a long-term filtration test. This hybrid modification produced the strongest antibacterial response, with mortality rates of 94.64% for *E. coli* and 90.13% for *S. aureus*. Contact angle was significantly reduced, indicating enhanced water affinity.

The findings showed that the combination of ADMH with Ag-TiO_2 provides a synergistic effect, improving the membrane's resistance to microbial, organic and inorganic foulants. Long-term crossflow filtration using real secondary effluent further demonstrated improved fouling resistance, with the hybrid modified membrane (M-HTA) decreasing slightly from 32 $L.m^{-2}h^{-1}$ to 30.1 $L.m^{-2}h^{-1}$ after 72 h, compared to 27.7 $L.m^{-2}h^{-1}$ for the unmodified membrane. These findings support the potential of hybrid-modified membranes for long-term wastewater treatment applications. This work provides a practical, scalable membrane surface functionalization approach to improve polyamide RO membrane performance in wastewater reuse applications, effectively linking modification strategies with the fouling control requirements of real wastewater treatment applications.

ACKNOWLEDGEMENTS

I am grateful to **GOD,** my Creator King, for the strength given to me to pursue and complete the degree.

I want to express my gratitude to the following people:

My Supervisor, Professor Mujahid Aziz (Assistant Dean, Learning and Teaching; Faculty of Engineering and the Built Environment, CPUT). His support, encouragement and patience were instrumental to the success of this project. Beyond academic supervision, his mentorship extended to personal and professional development. Hence, my saying goes "*it takes a supervisor to guide a research project, but it takes an academic father to help one realise their full potential.*"

The technical staff of the Chemical Engineering Department, particularly Mrs Hannelene Small and Mr Alwyn Bester, whose readiness to assist and technical expertise were invaluable. My appreciation extends further to the Environmental Engineering Research Group (EERG), particularly Aude Minang Nkombe, Grace Makwela, and Apiwe Ntakana.

The technical staff at the Central Analytical Facilities (CAF) at Stellenbosch University, the Analytical Lab and the Electron Microscopy Unit (EMU) at the University of Cape Town (UCT), the Technology Station at the Clothing and Textiles Department (CPUT), are acknowledged for their professional support and access to specialised facilities.

The Centre for Postgraduate Studies at CPUT and the National Research Foundation (NRF) (funding reference: PMDS22060519016) are acknowledged for their financial support towards this research.

My parents, Mr Fred Kasongo, my source of inspiration, and Mrs Doris Kasongo, for their love, sacrifices and moral support. I also extend my heartfelt gratitude to my sisters, Paty Faila and her family, Aline Kasongo and her family, and Ange Kasongo, as well as to my brothers, Glory Kasongo and Victorin Kasongo, for their constant encouragement and support throughout this journey.

To my wife, Emmanuella Munyany, thank you for your patience, encouragement, love, support and for standing by me at every stage of this process. To my son Zion Kasongo, thank you for being my daily reminder that there is life beyond deadlines. Your smiles were often the best motivation of all.

I extend my gratitude to my extended family and friends for their continuous support and prayers.

DEDICATION

This thesis is dedicated to my Wife Emmanuella Munyany & my Son Zion Kasongo.

RESEARCH OUTPUTS

Aziz, M, & **Kasongo, G**. 2021. Improving resistance to fouling of aromatic polyamide thin-film composite reverse osmosis membrane by surface grafting of N, N′- dimethyl aminoethyl methacrylate (DMAEMA). *Journal of Water Chemistry and Technology* 43(4): 312-320. [ISSN 1063-455X]

Morris, B., Aziz, M., & **Kasongo, G**. 2022. Remediation of wastewater with a low-pressure aromatic polyamide thin-film composite reverse osmosis membrane for membrane fouling minimisation and reuse application. *Environment Protection Engineering,* 48(2): 43-57. [DOI: 10.37190/epe220204]

Kasongo, G., Aziz, M. & Nkombe, A. 2025. Biofouling Resistance Improvement in Membrane-Based Municipal Wastewater Treatment: A Focus on Membrane Surface Modification by Graft Polymerization with 3-allyl-5, 5-dimethyl hydantoin. *Membranes,* 15(10). 314. [DOI.org/10.3390/membranes15100314]

Kasongo, G. & Aziz, M. 2025. Current state of Surface modification techniques of Thin Film Composite Polyamide membrane to minimise Biofouling: A review. *Water Practice & Technology*. Submitted 19 November 2025 [Paper ID: WPT-S-25-00372]

Manilal, K., Makwela, G., **Kasongo, G**. & Aziz, M. 2025. Treatment Technologies for Municipal and Industrial Secondary Effluents: Current Approaches and Reuse-Oriented Assessment. *Journal of Water Process Engineering.* Submitted 11 December 2025 [Paper ID: JWPE-D-25-09498]

Kasongo, G., & Aziz, M. 2025. Synergistic Antimicrobial Nanocomposite–Hydrophilic Monomer Surface Functionalization for Enhanced Biofouling Resistance in PA RO Membranes. *Separation and Purification Technology.* Submitted 19 December 2025 [SEPPUR-D-25-16866]

Conference presentation:

Kasongo, G., Aziz, M., & Nkombe, A. 2024. Fouling Resistance Improvement in Membrane-Based Municipal Wastewater Treatment: A Focus on Surface Modifications. WISA Biennial National Conference [Durban, South Africa, 12-14 June 2024].

Kasongo, G. & Aziz, M. 2025. Enhancing fouling resistance of RO membranes through chemical grafting with 3-Allyl-5,5-Dimethyl Hydantoin (ADMH) and TiO_2-Ag nanoparticles. Biennial Interinstitutional Chemical Engineering (ICE) Postgraduate Symposium, [UCT, Cape Town, South Africa, 11 July 2025].

Kasongo, G., Aziz, M. 2025. Eliminating Biofouling on TFC Reverse Osmosis (RO) Membranes via Combined Surface Modification with 3-Allyl-5,5-dimethylhydantoin (ADMH) and Titanium Oxide (TiO_2). IWA Water Reuse Conference [Cape Town, South Africa, 16-20 March 2025]

TABLE OF CONTENT

DECLARATION i
ABSTRACT ii
ACKNOWLEDGEMENTS iv
DEDICATION v
RESEARCH OUTPUTS vi
TABLE OF CONTENT viii
LIST OF TABLES xiii
LIST OF FIGURES xiv
LIST OF SYMBOLS xvii
LIST OF ABBREVIATIONS xviii
Chapter 1 1
INTRODUCTION 1
1.1 Background 2
1.2 Problem statement 3
1.3 Research questions 4
1.4 Aim and objectives 4
1.5 Novelty and justification of the research project 5
1.6 Scope of study and delineation 5
1.7 Significance of the study 5
1.8 Thesis outline 6
1.9 References 7
Chapter 2 9
LITERATURE REVIEW 9
2.1 Introduction 10
2.2 Types and Characteristics of Secondary Effluent 11
2.3 Municipal Secondary Effluent 12
2.3.1 Conventional Activated Sludge Secondary Effluent 12
2.3.2 Biological Nutrient Removal Secondary Effluent 12

2.3.3 Membrane Bioreactor Secondary Effluent 12
2.4 Industrial Secondary Effluent 13
2.4.1 Biodiesel Secondary Effluent 13
2.4.2 Textile Secondary Effluent 13
2.4.3 Palm Oil Mill Effluent 14
2.5 Comparison of Secondary Effluent Parameters 14
2.6 Techniques Used for Treatment of Secondary Effluent 15
2.6.1 Adsorption 18
2.6.2 Coagulation - Flocculation 18
2.6.3 Advanced Oxidation Processes 18
2.6.4 Membrane Technology 19
(I) Nanofiltration membranes 20
(II) Reverse osmosis membranes 21
2.6.5 Fouling of polyamide reverse osmosis membranes 22
2.6.6 Biofouling of Polyamide Reverse Osmosis Membranes 23
2.6.7 Biofilm formation 25
2.6.8 Membrane biofouling mitigation techniques 25
2.6.9 Membrane surface modification techniques to minimise biofouling 26
2.6.10 Nano-structuring of RO membrane to minimise biofouling 30
2.6.11 Membrane surface properties characterisation 35
2.6.12 Membrane and nanocomposite characterisation 37
2.6.13 Membrane biofilm characterisation 38
(I) Challenges and Limitations of membrane surface modification 38
2.7 Summary 39
2.8 References 41
Chapter 3 54
METHODOLOGY 54
3.1 Introduction 55
3.2 Membrane surface modification using DMAEMA 55

3.2.1 Materials and methods 55
(I) Materials and reagents 55
3.2.2 Redox-initiated grafting of DMAEMA 55
3.2.3 Characterisation of the modified and unmodified membrane 56
3.2.4 Membrane performance and antifouling evaluations 56
3.2.5 Anti-biofouling evaluation 58
3.3 Membrane surface modification using ADMH 59
3.3.1 Materials and Reagents 59
3.3.2 Synthesis of 3-Allyl-5,5-Dimethylhydantoin (ADMH) 59
3.3.3 Membrane Surface Modification using ADMH 59
3.3.4 Membrane Characterisation 61
3.3.5 Fouling Experiments 62
3.3.6 Static Adhesion Test 62
3.3.7 Dynamic Adhesion Test 62
3.3.8 Membrane Performance Assessment 63
3.4 Membrane modification using ADMH\TiO_2-Ag 65
3.4.1 Materials and Reagents 65
3.4.2 Synthesis of TiO_2-Ag Nanocomposites 65
3.4.3 PA RO Membrane surface modification 66
3.4.4 TiO_2-Ag grafting 66
3.4.5 Grafting of ADMH\TiO_2-Ag 67
3.4.6 Membrane characterisation 68
3.4.7 Fouling experiments 69
3.4.8 Membrane performance assessment 70
3.5 Reference 72
Chapter 4 73
MEMBRANE SURFACE MODIFICATION THROUGH CHEMICAL GRAFTING USING N, N′-DIMETHYL AMINOETHYL METHACRYLATE (DMAEMA) 73
4.1 Introduction 74

4.2 Membrane surface modification using DMAEMA: Membrane characterisation 74
4.2.1 ATR-FTIR 74
4.2.2 SEM analysis 75
4.2.3 Membrane performance and antifouling properties 76
4.2.4 Anti-biofouling properties 78
4.3 Summary 79
4.4 References 80
Chapter 5 83
BIOFOULING RESISTANCE IMPROVEMENT OF PA RO MEMBRANES THROUGH CHEMICAL GRAFTING WITH 3-ALLYL-5, 5-DIMETHYL HYDANTOIN. 83
5.1 Introduction 84
5.2 Membrane surface modification using ADMH: Membrane characterisation 85
5.2.1 ADMH Characterisation 85
5.2.2 Membrane Surface Modification and Characterisation 85
5.2.3 Biofouling Resistance 90
5.2.4 Organic Fouling Resistance 94
5.2.5 Inorganic Fouling Resistance 95
5.3 Summary 96
5.4 References 97
Chapter 6 99
HYBRID MEMBRANE SURFACE MODIFICATION OF PA RO MEMBRANE TO ADDRESS BIOFOULING IN THE TREATMENT OF MUNICIPAL SECONDARY EFFLUENT 99
6.1 Introduction 100
6.1 Membrane surface modification using ADMH\ TiO_2-Ag 101
6.1.1 ADMH and TiO_2-Ag characterisation: PSD 101
6.1.2 ADMH and TiO_2-Ag characterisation: FTIR and XRD 102
6.1.3 Membrane surface characterisation: FTIR analysis 103
6.1.4 Membrane surface characterisation: Thermal stability TGA 105
6.1.5 Membrane surface characterisation: SEM-EDX and analysis 106

6.1.6 TEM analysis 108
6.1.7 Membrane surface characterisation: Contact angle and charge measurements 109
6.2 Membranes biofouling resistance and performance tests 110
6.2.1 Static adhesion tests 110
6.2.2 Microbial dynamic adhesion and membrane performance tests 111
6.2.3 Confocal Laser Scanning Microscopy (CLSM) 112
6.2.4 Organic and inorganic fouling tests 114
6.2.5 Membrane test using real secondary effluent 115
6.3 Summary 116
6.4 References 117
Chapter 7 122
CONCLUSION AND RECOMMENDATIONS 122
7.1 Conclusion 123
7.2 Recommendations 125
APPENDICES 126
APPENDIX A: sample calculations 127
Sample calculation of modifying solution (ADMH): 127
Sample calculation of RO performance indicators: 128
APPENDIX B: membrane surface modification data 130
Membrane surface modification using ADMH\TiO_2-Ag: Membrane characterization 130
APPENDIX C: Membrane performance assessment data 134
Membrane surface modification using ADMH\TiO_2-Ag: Batch Experimental Data of fouling tests 134
APPENDIX D: Lab-scale long term experimental tests using secondary effluent 140
APPENDIX E: Data recording sample for the lab-scale RO filtration tests 141

LIST OF TABLES

Table 1: Comparison of key wastewater quality parameters of major secondary effluent types 15
Table 2: TFC RO Membrane surface modification techniques using hydrophilic materials to minimise biofouling and reported main findings 28
Table 3: TFC RO Membrane surface modification techniques using nanoparticle additives to minimise biofouling and reported main findings 32
Table 4. Synthetic feed solution composition 57
Table 5: Feed and fouling solutions used in this study. 63
Table 6: Unmodified and 0.1 mol. L^{-1} DMAEMA modified membranes sterilisation ratios after contact time with E. coli of 1×10^{7} CFU. mL^{-1} initial concentration. 78
Table 7: Pure water flux of membranes before and after 30 hours contact with E. coli suspension of ~ 2×10^{8} CFU. mL^{-1} initial concentration 79
Table 8: Mortality Ratio, FDR, and FRR values of ADMH grafted membranes. 94
Table 9: Particles size distribution of nanoparticles presented in percentile 101
Table 10: Apparent concentration of elements on membranes obtained from EDX analysis 108
Table 11: Mortality Ratio, FDR, and FRR values of ADMH grafted membranes. 112
Table 12: Microorganisms cell count obtained using ImageJ software 114
Table 13: Table of concentration and mass labels 127
Table 14: The mass of polyamide TFC RO membranes before and after grafting with ADMH, TiO_2, TiO_2-Ag and ADMH\TiO_2-Ag 130
Table 15: membrane charge (Zeta Potential) tested at pH 7 130
Table 16: membrane contact angle measure with deionized water at ambient temperature 130
Table 17: E. Coli Mortality Ratio for tested membranes 134
Table 18: S. Aureus Mortality Ratio for tested membranes 135
Table 19: FDR of membranes after 8 hours of filtration with E. Coli 136
Table 20: FRR of membranes after 8 hours of filtration with E. Coli 136
Table 21: Salt Rejection of tested membranes with 2000 mg. L^{-1} of NaCl solution Feed 137
Table 22: Permeability of tested membranes with DI water 137
Table 23: Fouling test using the organic foulant (150 mg. L^{-1} HA): Permeate Flux Decline 138
Table 24: Fouling test using the inorganic foulant (150 mg. L^{-1} $NaHCO_3$): Permeate Flux Decline 139
Table 25: Long-term fouling test using municipal secondary: Flux Decline 140
Table 26: RO process operating conditions for membrane performance evaluation 141
Table 27: Process parameters recorded during the fouling test using the lab-scale RO membrane system 142

LIST OF FIGURES

Figure 1: Distribution of common non-biological foulant types identified on polyamide RO membranes from multiple membrane autopsy studies, illustrating the contribution of organic and inorganic fouling to membrane performance decline (Kucera, 2019). 3
Figure 2: Schematic illustration of fouling layer formation on the membrane during membrane cross-filtration 3
Figure 3. General flow of a municipal wastewater treatment process and the techniques used. Adapted from Kato & Kansha (2024). 11
Figure. 4. Description of different secondary effluent treatment techniques 17
Figure 5: Common foulant types of polyamide membranes registered from several membrane autopsies, including biofouling. Adapted from Komlenic (2010) and Kucera (2019). 23
Figure 6: Graphical illustration of membrane surface modification of a polyamide RO membrane with pSM-AgNPs. The RO membrane surface was first functionalized by poly (3-sulfopropyl methacrylate potassium salt) (pSM) via atom transfer radical polymerisation (ATRP), followed by the addition of Ag nanoparticles (Yang et al., 2021). 30
Figure 7: SEM images of a study conducted on TFC PA RO membrane modified SEM before modification (a) and after modification (b) with silica nanoparticles (SiO_2). Left: Top-view; Right: Cross-section view (Peyki et al., 2015). 35
Figure 8: ^1H NMR spectrum illustrating the structure of 2-carboxyethyl acrylate (CAA), [2-(acryloyloxy)ethyl] trimethyl ammonium chloride (TMA) and p(CAA-co-TMA) grafted on PA RO membranes. The p(CAA-co-TMA) was grafted onto the PA RO membranes with different ratios, denoted as C13T1, C6T1, C3T1, C1T1, and C1T3 (Yang et al., 2020). 36
Figure 9: Photo (up) and process flow diagram (down) of the lab-scale flat cell RO system used for membrane performance and antifouling capability tests. 57
Figure 10: Graphical illustration of the RO membrane surface modification process used in this study. 60
Figure 11: Schematic illustration of the experimental setup used for chemical grafting on the PA RO membrane. 61
Figure 12: Experimental timeline during membrane performance and antifouling capability tests. 64
Figure 13: Graphical illustration of the RO membrane surface modification process using ADMH\TiO_2-Ag. 67
Figure 14:. ATR-FTIR spectra of the unmodified membrane and DMAEMA modified membranes 75
Figure 15:. SEM images of virgin (unmodified) membrane (a) and DMAEMA modified membranes (top-view & cross section): (b) 0.02 mol. L^{-1} DMAEMA, (c) 0.05 mol. L^{-1} DMAEMA, (d) 0.075 mol. L^{-1} DMAEMA and (e) 0.1 mol. L^{-1} DMAEMA. 76

Figure 16: Pure water flux of membranes and the salt rejection during filtration of the synthetic feed solution 76
Figure 17: Normalized flux of unmodified and DMAEMA-modified membranes during filtration of the foulant model solution 77
Figure 18**:** FDR using the simulated feed solution and pure water FRR of membranes 78
Figure 19: Modifying agent ADMH FTIR characteristics after synthesis. 85
Figure 20: Grafting yield of ADMH on the RO membrane surface after modification 86
Figure 21: FTIR graphs for the Unmodified, M_0, $M_{0.2mol/L}$, $M_{0.4mol/L}$, $M_{0.6mol/L}$ and $M_{0.8mol/L}$ (modified membranes with 0.2 mol. L^{-1}, 0.4 mol. L^{-1}, 0.6 mol. L^{-1} and 0.8 mol. L^{-1} respectively) in the wavenumber range of 2780-3230 $cm-1$. 87
Figure 22: SEM images of the unmodified and ADMH grafted membranes (top-view & cross-section): (a) unmodified membrane, (b) 0.2 mol. L^{-1} ADMH, (c) 0.4 mol. L^{-1} ADMH, (d) 0.6 mol. L^{-1} ADMH, (e) 0.8 mol. L^{-1} ADMH. 88
Figure 23: Solid C^{13} CPMAS NMR results for unmodified and all ADMH-modified membranes 89
Figure 24: Contact angle measurements of unmodified and ADMH-modified RO membranes at different grafting concentrations (0.2 - 0.8 mol L^{-1}). 90
Figure 25: Static adhesion test results for unmodified and modified membranes against E. Coli (left) and S. Aureus (right). 91
Figure 26: Flux of ADMH grafted membranes compared to the unmodified membrane during dynamic fouling tests with E. coli solution using an RO system. 92
Figure 27: Flux of ADMH grafted membranes compared to the unmodified membrane during dynamic fouling tests with S. Aureus solution using a RO system. 93
Figure 28: Membranes' antifouling properties during fouling tests with organic foulant solutions. . 94
Figure 29: Membranes' antifouling properties during fouling tests with inorganic foulant solutions. 95
Figure 30: Zetasizer-derived particle size distribution of the nanoparticles 101
Figure 31: XRD (left) and FTIR (right) spectra of ADMH, the nanoparticles and nanocomposites used for the modification of the PA RO membrane in this work 103
Figure 32: FTIR spectra of unmodified (M-U) and surface-modified membranes (M-H, M-TA, M-HTA), showing changes in functional groups after grafting 104
Figure 33: TGA (top left) and DTG (top right) curves of unmodified and surface-modified membranes, showing thermal degradation behaviour. Insets provide zoomed views (DTG curves) of key decomposition regions for detailed comparison. 106
Figure 34: SEM images and corresponding EDX spectra of unmodified and surface-modified membranes, showing changes in surface morphology and elemental composition after grafting. 107
Figure 35: TEM cross-sectional images of unmodified and grafted membranes (cross-section), showing the membrane morphology and the distribution of nanoparticles within the active layer of the membranes 109

Figure 36: Contact angle (left) and zeta potential (right) of unmodified and surface-modified membranes, showing changes in surface hydrophilicity and surface charge after grafting and nanoparticle incorporation. 110
Figure 37: Mortality ratio and membrane antifouling efficiency obtained during the static adhesion test with *E. Coli* (left) and *S. Aureus* (right). 111
Figure 38: CLSM results of membranes after 8 hours of dynamic biofouling tests using Flux of modified membranes compared to the unmodified membrane during dynamic fouling tests with *E. Coli* and *S. Aureus* solution in the cross-filtration lab-scale RO system. 114
Figure 39: Membrane flux decline during fouling tests with the organic foulant humic acid (left) and inorganic foulant sodium bicarbonate (right) solutions. 115
Figure 40: Membranes flux profile of the M-U membrane and M-HTA membrane during RO filtration with secondary effluent from municipal wastewater treatment plant (left) & CLSM images (right) of the membranes obtained after the experimental tests with the secondary effluent. The flux was recorded over 72 hours (3 days) with interval periods of 2 hours during the day, and 10 hours at night 116
Figure 41: Contact angle cycles of membranes obtained in the analysis of membranes' hydrophilicity 131
Figure 42: TEM images of membranes (Raw data) 132
Figure 43: CLSM images of the M-U (left) and M-HTA (right) membranes after the long-term fouling test (dead bacteria) 133
Figure 44: CLSM images of M-U (left) and M-HTA (right) membrane after the long-term fouling test (live bacteria) 133

LIST OF SYMBOLS

A	Area (m^2)
C	Electrical Conductivity ($\mu S.cm^{-1}$)
J	Water flux ($L.m^{-2}\ hr^{-1}$)
Mw	Molecular weight (g/mol)
P	Pressure (bar)
R	Salt rejection (%)
T	Temperature (°C)
t	Time (hours)
Δt	Time interval (min)
V	Volume (L)

Subscripts

f	Feed
p	Permeate
f	Final
$i\ (0)$	Initial
t	Time dependent

LIST OF ABBREVIATIONS

AA: Acrylic acid

AC-HBPAE: Acrylated hyperbranched poly (amino ester)

AEMA: Amino ethyl methacrylate

AC: Activated carbon

ADMH: 3-allyl-5,5-dimethylhydantoin (modifying agent)

AFM: Atomic force microscopy

AgNPs: Silver nanoparticles

AIBA: 2,2-azobis (isobutyramidine) hydrochloride (initiator)

ANOVA: Analysis of Variance

AOP: Advanced Oxidation Process

AOPs: Advanced oxidation processes

ATRP: Atom transfer radical polymerization

AS: Activated sludge

BNR: Biological Nutrient Removal

BOD3: Biochemical Oxygen Demand after 3 days

BOD5: Biochemical Oxygen Demand after 5 days

CAS: Conventional activated sludge

C*f*: Feed electrical conductivity

CFV: Crossflow velocity

COD: Chemical Oxygen Demand

CP: Concentration polarisation

C*p*: Permeate electrical conductivity

CSD: Convective Sludge Drying

DEWATS: Decentralised Wastewater Treatment Systems

DNA: Deoxyribonucleic Acid

DOC: Dissolved Organic Carbon

EC: Electrical Conductivity

EfOM: Effluent organic matter

EPS: Extracellular polymeric substances

FDR: Flux decline ratio

FE-SEM: Field-emission scanning electron microscope

FO: Forward osmosis

FTIR: Fourier-transform infrared spectroscopy

FRR: Flux recovery ratio

HA: Humic acid

HRT: Hydraulic Retention Time

IP: Interfacial polymerization

MBR: Membrane bioreactor

MF: Microfiltration

MWCO: Molecular Weight Cut-Off

NF: Nanofiltration

NOM: Natural organic matter

NOx: Nitrogen oxides

NPs: Nanoparticles

PBC: Plant-based coagulants

PCBs: Polychlorinated biphenyls

PEG: Polyethene glycol

PES: Polyethersulfone

NTFC: Nanofiber TFC

PFAS: Perfluoroalkyl substance

POME: Palm oil mill effluent

POPs: Persistent organic pollutants

PSO: Persulphate oxidation

RO: Reverse osmosis

ROS: Reactive oxygen species

TDS: Total dissolved solids

TFC: Thin-film composite

TFN: Thin-Film Nanocomposite

TEM: Transmittance Electron Microscopy

TiO_2: Titanium dioxide

TMP: Transmembrane Pressure

TOC: Total Organic Carbon

TSS: Total Suspended Solids

SS: Suspended solids

UF: Ultrafiltration

UV: Ultraviolet (radiation)

WWTP: Wastewater treatment plant

XPS: X-ray photoelectron spectroscopy

XLE: Extra-low energy

XRD: X-ray Diffraction

Chapter 1

INTRODUCTION

1.1 Background

Membrane technology has proven to be one of the most effective technologies globally for treating wastewater from different sources (Pervez et al., 2020; Aziz & Kasongo, 2019). Fouling is a major concern, if not the top challenge, associated with the RO membrane process in the treatment of wastewater, causing membrane degradation and poor performance, which impedes membrane operation (Ponnusamy et al., 2013; Qasim et al., 2019). Membrane fouling is an inevitable phenomenon and represents an extreme operational and economic challenge in the RO process. It involves complex physical and chemical interactions between unwanted impurities (foulants) present in the feed and the membrane surface (Kasongo et al., 2019; Aziz & Kasongo, 2021). Generally, membrane fouling can be external or internal. In external (surface) fouling, the foulants accumulate on the membrane surface. In contrast, internal fouling involves fouling mechanisms occurring within the membrane pores. Owing to the compact and nonporous nature of RO membranes, external fouling is more frequent during the RO process (Qasim et al., 2019) Membrane fouling is recognised as a major obstacle to the smooth operation and widespread application of this technology (Kasongo et al., 2019; Aziz & Kasongo., 2019; Akther et al., 2020). Fouling, in turn, necessitates membrane cleaning, resulting in higher operating costs due to increased energy consumption, additional chemicals and system downtime. A review study conducted in 2016 (Jiang et al., 2017) showed a significant increase in the number of published papers addressing the issue of RO membrane fouling and predicted that by the year 2022, the cumulative number of papers published would double. This indicates a great interest among researchers in mitigating fouling. A variety of measures have been investigated for fouling control (Lau et al., 2012). Biofouling is particularly recognized as a contributing factor to more than 45% of all membrane fouling (Komlenic, 2010). Kucera, (2019) stated that biofouling control and prevention remain the most difficult challenge facing polyamide membrane systems operations, despite advances in membrane performance over the last 45 years. Figure 1 shows the average foulants distribution on polyamide membranes, excluding biofouling, obtained from several autopsies. All showed biofilm formation, and 33% of the membrane was biofouled, with biofouling as the primary cause of poor performance.

Biofouling cannot be significantly reduced by pretreating feed water due to the self-replicating nature of microbial cells. Furthermore, the degradation of polyamide thin film composite membranes through contact with the disinfectant chlorine is a key limitation to the commercial membrane as this affects membrane performance in long-term operations (Lau et al., 2012; Qasim et al., 2019). Hence, important attention must be directed to the interaction between the PA top active layer and the underlying supporting membrane for a better understanding of the impact of membrane substrate properties on the performance of the active layer.

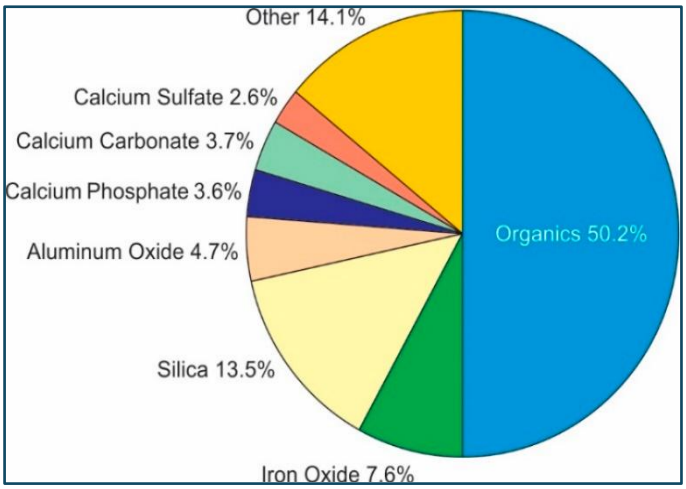


Figure 1: Distribution of common non-biological foulant types identified on polyamide RO membranes from multiple membrane autopsy studies, illustrating the contribution of organic and inorganic fouling to membrane performance decline (Kucera, 2019).

1.2 Problem statement

Fouling, and biofouling in particular, remains a major limitation in the application of PA RO membranes for wastewater treatment (Kucera, 2019). A variety of measures have been investigated for biofouling control, including pretreatment of feedwater and the use of disinfectants. However, biofouling of RO membranes cannot be significantly reduced by pre-treating the feed water due to the self-replicating nature of microbial cells. Additionally, the use of disinfectants such as chlorine degrades the membrane and affects its performance in long-term operations (Ansari et al., 2021). As a result, research efforts have increasingly focused on improving membrane surface properties through surface modification techniques. However, several suggested PA RO membrane modification methods have been reported to improve certain membrane properties, such as fouling resistance, at the disadvantage of membrane permeability or solute rejection. Consequently, there remains a need to develop PA RO membranes that exhibit enhanced biofouling resistance while maintaining or improving water flux and salt rejection, particularly under realistic wastewater treatment conditions. Figure 2 provides an overview of the fouling mechanisms occurring under crossflow operating conditions.

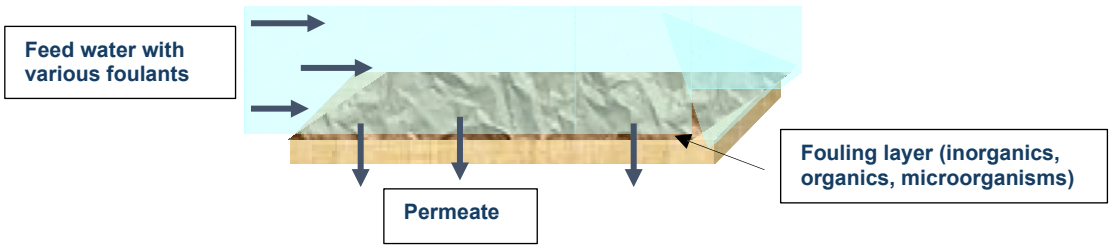


Figure 2: Schematic illustration of fouling layer formation on the membrane during membrane cross-filtration

1.3 Research questions

This study was guided by the following research questions:

1. Can the modification of the Polyamide (PA) Reverse Osmosis (RO) membrane surface with N, N′- dimethyl aminoethyl methacrylate (DMAEMA) improve membrane fouling resistance against selected model foulants in municipal secondary effluent?
2. Can the modification of the PA RO membrane using 3-Allyl-5,5-Dimethyl Hydantoin (ADMH) enhance membrane biofouling resistance against both gram-positive and gram-negative bacteria?
3. Does the modification of the PA RO membrane surface using ADMH and titanium dioxide (TiO_2) - silver (Ag) nanocomposite have an impact on the physico-chemical characteristics of the membrane?
4. Can the modification of the PA RO membrane using ADMH and TiO_2-Ag nanocomposite mitigate biofouling, organic fouling and inorganic fouling in the treatment of municipal secondary effluent?

1.4 Aim and objectives

In this project, a novel membrane surface modification approach was introduced to mitigate biofouling of Polyamide RO membranes in the treatment of municipal secondary effluent by hybrid chemical grafting of 3-Allyl-5,5-dimethylhydantoin (ADMH) and coating the membrane surface with a titanium dioxide (TiO2)- silver (Ag) nanocomposite.

The main objectives were:

- To modify the PA RO membrane surface through chemical grafting using N, N′- dimethyl aminoethyl methacrylate (DMAEMA) and assess its performance using synthetic secondary effluent.
- To graft different concentrations of 3-Allyl-5,5-dimethylhydantoin (ADMH) onto a PA RO membrane and evaluate the antibiofouling resistance of the membrane against gram-positive and gram-negative bacteria.
- To graft 3-Allyl-5,5-dimethylhydantoin (ADMH) and titanium dioxide (TiO_2) - silver (Ag) nanocomposite onto a PA RO membrane and evaluate the physico-chemical characteristics of the membranes through analytical analyses.

- To assess the effectiveness of ADMH and TiO_2-Ag nanocomposite surface modification in mitigating biofouling, organic fouling and inorganic fouling during the treatment of municipal secondary effluent using PA RO membranes.

1.5 Novelty and justification of the research project

Hybrid PA RO membrane surface modification using a hydrophilic monomer (ADMH) and biocidal nanoparticles (TiO_2-Ag) through chemical grafting and nanoparticle coating has not been reported and will be investigated for the first time in this study. Furthermore, this project evaluates the resistance of the modified membranes against both the positive and gram-negative bacteria, as well as organic and inorganic foulants. The project will impact and influence practices used in the synthesis and manufacturing of commercial membranes designed to minimise biofouling, as it presents a new viable option for the design and development of RO fouling-resistant membranes. The project will contribute to wastewater management and water reuse schemes.

1.6 Scope of study and delineation

This study focuses on enhancing the antimicrobial properties of RO membranes for treating MBR effluents. The study will be based on a comparison between modified and unmodified membranes. The antimicrobial abilities of the modified RO membranes will be assessed against two types of bacteria, gram-negative bacteria (*E. coli*) and gram-positive bacteria (*S. aureus*), as well as humic acid and sodium bicarbonate, which serve as the organic and inorganic foulants, respectively. Moreover, the study focuses on the effect of grafting concentration. Parameters such as pH, temperature, and initiator type were excluded to limit experimental complexity and isolate the effects of surface chemistry and nanoparticles used in this work. These parameters are recognised as influential and may be recommended for investigation in future work to further optimise membrane modification strategies.

1.7 Significance of the study

This project enhances efforts to improve RO membrane performance and resistance to fouling in the treatment of municipal wastewater, thereby contributing to the body of knowledge in wastewater management and water reuse for various applications. The study will impact and influence practices

used in the synthesis and manufacturing of commercial membranes designed to minimise biofouling. The project is therefore significant for wastewater treatment as it presents a new viable option for the design and development of RO fouling-resistant membranes.

1.8 Thesis outline

This thesis is structured as follows:

Chapter 1 provides a detailed Introduction of the project, aim and objectives, delineation as well as the significance of the study.

Chapter 2 presents a detailed review of the literature and theory related to the research project's various topics.

Chapter 3 provides details on the membrane modification procedures, analyses, equipment, apparatus, and data analysis tools used in this research project.

Chapter 4 presents work on membrane surface modification via chemical grafting with N, N′-dimethylaminoethyl methacrylate (DMAEMA), tested with municipal secondary effluent.

Chapter 5 presents and discusses different results obtained from modifying the polyamide RO membrane via the grafting of 3-Allyl-5,5-dimethylhydantoin (ADMH) to minimise fouling.

Chapter 6 presents and discusses the different results obtained from modifying the polyamide RO membrane using 3-Allyl-5,5-dimethylhydantoin (ADMH) and TiO_2-Ag NPs to enhance fouling resistance and improve membrane performance.

Chapter 7 presents the conclusion and recommendations.

1.9 References

Akther, N., Ali, S.M., Phuntsho, S. & Shon, H. 2020. Surface modification of thin-film composite forward osmosis membranes with polyvinyl alcohol–graphene oxide composite hydrogels for antifouling properties. *Desalination*, 491(April): 114591. https://doi.org/10.1016/j.desal.2020.114591.

Ansari, A., Peña-Bahamonde, J., Wang, M., Shaffer, D.L., Hu, Y. & Rodrigues, D.F. 2021. Polyacrylic acid-brushes tethered to graphene oxide membrane coating for scaling and biofouling mitigation on reverse osmosis membranes. *Journal of Membrane Science*, 630(December 2020).

Aziz, M. & Kasongo, G. 2019. Scaling prevention of thin film composite polyamide Reverse Osmosis membranes by Zn ions. *Desalination*, 464(April): 76–83. https://doi.org/10.1016/j.desal.2019.04.021.

Aziz, M. & Kasongo, G. 2021. The removal of selected inorganics from municipal membrane bioreactor wastewater using UF/NF/RO membranes for water reuse application: A pilot-scale study. *Membranes*, 11(2): 1–14.

Jiang, S., Li, Y. & Ladewig, B.P. 2017. A review of reverse osmosis membrane fouling and control strategies. *Science of the Total Environment*, 595: 567–583. http://dx.doi.org/10.1016/j.scitotenv.2017.03.235.

Kasongo, Godwill, Steenberg, C., Morris, B., Kapenda, G., Jacobs, N. & Aziz, M. 2019. Surface grafting of polyvinyl alcohol (PVA) cross-linked with glutaraldehyde (GA) to improve resistance to fouling of aromatic polyamide thin film composite reverse osmosis membranes using municipal membrane bioreactor effluent. *Water Practice and Technology*, 14(3): 614–624.

Komlenic, R. 2010. Rethinking the causes of membrane biofouling. *Filtration and Separation*, 47(5): 26–28. http://dx.doi.org/10.1016/S0015-1882(10)70211-1.

Kucera, J. 2019. Biofouling of polyamide membranes: Fouling mechanisms, current mitigation and cleaning strategies, and future prospects. *Membranes*, 9(9).

Lau, W.J., Ismail, A.F., Misdan, N. & Kassim, M.A. 2012. A recent progress in thin fi lm composite membrane : A review. *DES*, 287: 190–199. http://dx.doi.org/10.1016/j.desal.2011.04.004.

Pervez, M.N., Balakrishnan, M., Hasan, S.W., Choo, K.H., Zhao, Y., Cai, Y., Zarra, T., Belgiorno, V. & Naddeo, V. 2020. A critical review on nanomaterials membrane bioreactor (NMS-MBR) for wastewater treatment. *npj Clean Water*, 3(1).

Ponnusamy, K., Kappachery, S., Thekeettle, M., Song, J.H. & Kweon, J.H. 2013. Anti-biofouling property of vanillin on Aeromonas hydrophila initial biofilm on various membrane surfaces. *World Journal of Microbiology and Biotechnology*, 29(9): 1695–1703.

Qasim, M., Badrelzaman, M., Darwish, N.N., Darwish, N.A. & Hilal, N. 2019. Reverse osmosis desalination: A state-of-the-art review. *Desalination*, 459: 59–104.

Chapter 2

LITERATURE REVIEW

2.1 Introduction

The escalating global demand for freshwater, driven by rapid urbanisation, climate change, and population increase, has placed pressure on conventional water resources (Borah, 2025). Urbanisation and rapid population growth are primary drivers of water scarcity, as the global population has doubled since 1950, while water consumption has increased sixfold (Islam, 2025). Wastewater treatment typically involves a sequence of processes, with each stage designed to target specific contaminants. In most systems, treatment progresses through four stages: preliminary, primary, secondary, and tertiary (Joshi & Soni, 2025), as shown in Figure 3. Preliminary treatment removes large debris and inorganic particles that could hinder operations, while primary treatment eliminates most settleable solids, leaving colloidal and dissolved organics. Secondary treatment utilises biological processes to further break down the remaining organic matter. When the effluent still contains residual solids, nutrients, or micropollutants that prevent safe discharge or reuse, tertiary treatment is employed to achieve the required water quality (Shoba Vincent & Ramadoss, 2025).

The reuse of secondary effluent is increasingly recognised as a sustainable and reliable alternative to conventional freshwater sources (Diallo et al., 2024; Aziz & Kasongo, 2021; Kasongo et al., 2025). It is important to treat secondary effluent for the micropollutants, endocrine-disrupting chemicals, hormones, pathogens, and other contaminants that are not completely removed by conventional municipal wastewater treatment processes (Aziz & Ojumu, 2020). Municipal secondary effluent, in particular, the outflow from conventional biological wastewater treatment processes, often contains trace organic compounds, pathogenic microorganisms, including enteric viruses that are resistant to treatment (Gao et al., 2016; Kasongo et al., 2019), that can pose risks to human health and the environment if not adequately treated before reuse or discharge (Wu et al., 2025). Trace organic pollutants include persistent organic pollutants (POPs), such as polycyclic aromatic hydrocarbons (PAHs) and polychlorinated biphenyls (PCBs), as well as emerging contaminants like perfluoroalkyl substances (PFASs), pharmaceuticals, antibiotics, plasticisers, and flame retardants. These compounds are often long-lasting, bio-accumulative, and highly toxic. Secondary effluent can also harbour microplastics and compounds with genotoxic, cytotoxic properties, posing risks to human health, aquatic ecosystems, and soil quality if not adequately treated before reuse or discharge (Thushari et al., 2025). For example, residual pollutants in secondary effluent have been shown to induce cytotoxicity, oxidative stress, and genotoxicity in human mesenchymal stem cell models, thereby disrupting osteogenic and neurogenic differentiation by activating endocrine receptors (Yang et al., 2024). Because they are not completely removed by conventional wastewater treatment, they can pose significant risks when effluents are reused for irrigation or discharged into sensitive water bodies (Liu et al., 2024). The persistence and potential for bioaccumulation of these substances

underscore the need for advanced treatment processes and robust monitoring strategies to ensure the safety and sustainability of water resource management (Tripathy et al., 2025). Secondary wastewater effluent treatment relies on biological and advanced tertiary processes to meet environmental standards and the desired quality for water reuse (Ezugbe & Rathilal, 2020).

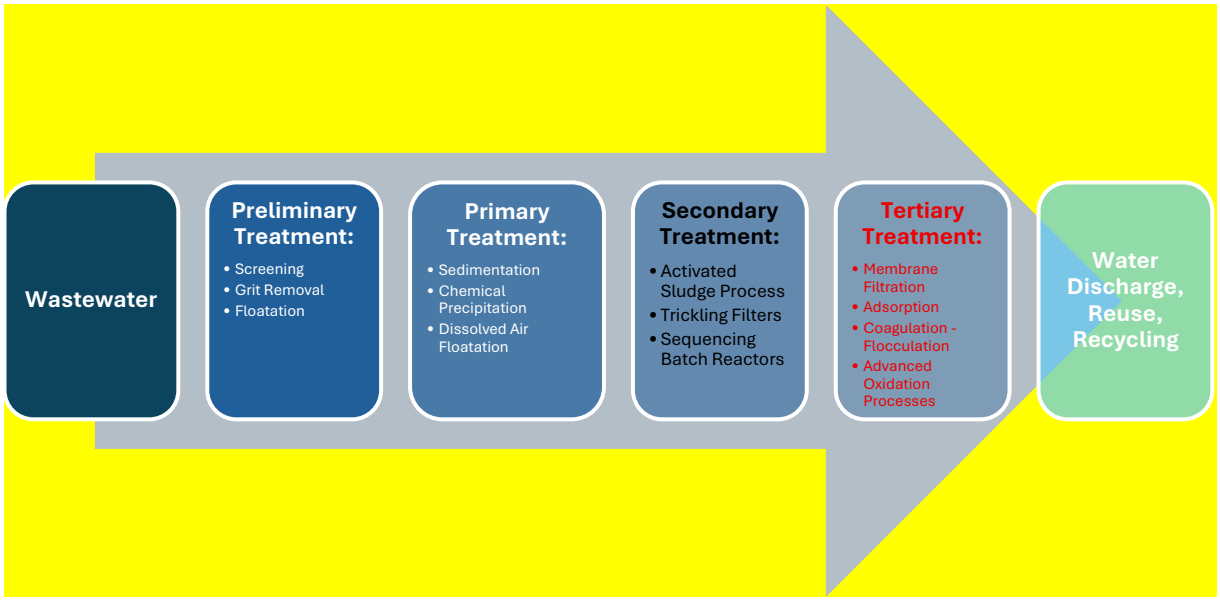


Figure 3. General flow of a municipal wastewater treatment process and the techniques used. Adapted from Kato & Kansha (2024).

2.2 Types and Characteristics of Secondary Effluent

Secondary effluent is the liquid stream that exits the secondary treatment step of a wastewater treatment plant (WWTP), after primary sedimentation. While most biodegradable organic matter is removed at this stage, the effluent still contains suspended solids, phosphorus, nitrogen, and various trace contaminants (Donald et al., 2022). Its quality depends strongly on the upstream biological process, and challenges remain in reducing residual nitrogen and phosphorus, managing surplus sludge, and mitigating gaseous by-products such as CO_2 and NO_X, which can contribute to environmental pollution and health risks. For this reason, many regions enforce strict discharge standards before secondary effluent can be released or reused (Wang et al., 2023). Given the increasing global demand for water reuse and the tightening of environmental regulations, it is crucial to focus on secondary effluents, which are most widely generated and pose significant treatment challenges today.

2.3 Municipal Secondary Effluent

Municipal secondary effluent refers to the treated water that exits the biological (secondary) stage of municipal WWTPs, and its characteristics can vary depending on the specific treatment processes and operational conditions used (Zhou et al., 2022). Municipal sectors generate vast quantities of secondary effluent, with municipal sources primarily utilising CAS, biological nutrient removal (BNR), and MBR systems (Rahman et al., 2023). These effluent types are highly relevant because they represent some of the largest and most persistent sources of wastewater requiring advanced treatment for safe discharge or reuse. Municipal WWTPs not only produce large volumes of secondary effluent but also generate significant quantities of sludge with high water content, reflecting the scale and complexity of municipal wastewater management (Abrahams et al., 2021). The prevalence of MBR and CAS systems in both municipal and industrial settings is driven by their ability to handle large volumes and diverse contaminant loads.

2.3.1 Conventional Activated Sludge Secondary Effluent

One major type is the effluent from CAS systems. These systems face challenges such as sludge bulking, poor floc formation during treatment of low-strength wastewater, and reduced removal efficiency due to low biomass concentration. In addition, the continuous increase in incoming flow contributes to the gradual deterioration of effluent quality from these plants (Latif, 2022).

2.3.2 Biological Nutrient Removal Secondary Effluent

Another type is effluent from advanced BNR systems, which are specifically designed to reduce nitrogen and phosphorus levels more effectively. These systems may employ processes such as enhanced denitrifying phosphorus removal, pyrite-based autotrophic denitrification, or microalgae-based treatments, each offering distinct efficiencies and operational characteristics for nutrient removal (Zhou et al., 2022).

2.3.3 Membrane Bioreactor Secondary Effluent

Effluent from MBR systems is another type, where membranes are integrated with activated sludge to allow higher biomass concentrations and longer sludge retention times. This results in improved effluent quality, reduced sludge production, and a smaller footprint compared to CAS. MBRs also enhance micropollutant removal, although their effectiveness against certain hydrophilic and persistent compounds remains limited (Liu et al., 2022). The improved quality and consistency of MBR effluent, with lower suspended solids and more concentrations of nutrients and organics, make

it suitable for safe discharge into sensitive water bodies or for potential non-potable reuse (Aziz & Ojumu, 2020).

2.4 Industrial Secondary Effluent

Industrial sectors are among the largest consumers of water, producing correspondingly high volumes of secondary effluent. Effective management of these effluents is therefore critical to achieving sustainable water use and pollution control (Chakawa & Aziz, 2021). Industrial secondary effluent is the liquid waste discharged from industrial facilities after biological (secondary) treatment. Although this process removes a significant portion of biodegradable organic matter, the resulting effluent often still contains nutrients, heavy metals, and refractory or toxic organic compounds. As such, further treatment is typically required to comply with environmental discharge standards or enable safe reuse. The composition and characteristics of industrial secondary effluents vary greatly depending on the type of industry and the nature of the raw wastewater (Selvasembian et al., 2022). This variability, coupled with the presence of complex chemical constituents, poses significant challenges for effective treatment and reuse. Consequently, the implementation of well-designed tertiary treatment strategies becomes essential (Morris et al., 2022). Notable contributors include industries such as biodiesel production (Torres et al., 2021), textile manufacturing (Sathya et al., 2022), and palm oil milling (Kacaribu et al., 2025), all of which generate effluents rich in complex, high-strength pollutants that are difficult to treat using conventional methods. Addressing these challenging waste streams is vital to developing scalable, sustainable tertiary treatment solutions that meet current and future water quality standards.

2.4.1 Biodiesel Secondary Effluent

Biodiesel effluent is generated during the refining stage of biodiesel production, where warm water is used to wash and remove unreacted methanol, glycerol, fatty acid soaps, and catalyst residues. It is characterised by very high pollutant loads, with COD up to 600,000 mg/L, BOD up to 200,000 mg/L, variable pH, and high oil and grease (Torres et al., 2021). Conventional treatment processes are often insufficient to reduce the high COD, BOD, and fats, grease, and oil concentrations in biodiesel effluent to acceptable levels, making advanced treatment approaches necessary to comply with environmental standards (Myburgh et al., 2019).

2.4.2 Textile Secondary Effluent

Textile industry effluent is generated from industrial textile production and is typically contaminated with high concentrations of dyes, heavy metals, and other hazardous chemicals. These components make the effluent toxic and potentially carcinogenic to living organisms. Secondary effluent may still

be toxic and coloured, requiring further treatment such as algal remediation for safe reuse or discharge (Waqas et al., 2022).

2.4.3 Palm Oil Mill Effluent

Palm oil mill effluent (POME) is the wastewater generated during the processing of palm oil. Once subjected to secondary treatment, POME effluent retains high concentrations of organic matter, including BOD, COD, and oils and greases, as well as minor hazardous compounds like siloxanes and phenolic compounds. Careful management is required to comply with environmental standards (Meena et al., 2023).

2.5 Comparison of Secondary Effluent Parameters

Table 1 presents a comparison of key physicochemical and organic parameters in municipal and industrial secondary effluents, including those from CAS, BNR, MBR, biodiesel, textile, and POME treatment processes. Each effluent type represents a different treatment process with specific operating conditions. These differences in treatment strategy and operating parameters account for the variation in effluent quality observed across the sources.

Dimane & El Hammoudani, (2021) evaluated CAS from a WWTP in Al-Hoceima, Morocco. The treatment plant consists of pretreatment (screening, grit removal, and de-oiling), secondary biological treatment (aeration and clarification tanks), tertiary treatment (microfiltration and UV disinfection), sludge treatment (rotary filters, dehydration, and chemical stabilisation), and odour treatment. Hu et al., (2020) investigated a BNR process treating municipal wastewater with no external carbon, sodium acetate, and sludge alkaline fermentation liquid (SAFL) as carbon sources. Table 1 reports values from the reactor with no external carbon, representing conventional BNR effluent. Plevri et al., (2021) evaluated a combined anaerobic biological treatment with membrane filtration to treat municipal wastewater under three sets of operating conditions. In Table 1, results from the first set of conditions (HRT = 2 d, Q = 20 L. d^{-1}, flux = 1.6 $L.m^{-2}$ h^{-1}, T = 18-23 °C) are reported.

Jayaramaiah & Dawn (2025) investigated the use of Nanochloropsis microalgae for treating biodiesel wastewater and producing biomass and lipids. Table 1 reflects the effluent after 25 days of cultivation. Hossain et al., (2022) evaluated the treatment of textile wastewater using a mixed aerobic bacterial consortium and compared it with a Fenton process with sand filtration. Values reported in Table 1 correspond to the biological treatment after 96 h of aeration, representing the most complete removal of pollutants. Ahmad Farid et al., (2019) evaluated convective sludge drying (CSD) for treating POME. The CSD process uses low-grade mill steam, produces nutrient-rich dewatered solids, and a decoction that is suitable for reuse.

Table 1: Comparison of key wastewater quality parameters of major secondary effluent types

Wastewater Parameters	Municipal Secondary Effluent			Industrial Secondary Effluent		
	CAS [1]	BNR [2]	MBR [3]	Biodiesel [4]	Textile [5]	POME [6]
COD (mg/L)	35	20.69	105	200	160	67.5
BOD (mg/L)	11 (BOD_5)	-	-	11.3	50	2 (BOD_3)
EC (µS/cm)	2241	-	560[7]	3000	900	-
pH	7.33-8.53	-	6.5[7]	7.01	6.7	6.5
TSS	19 mg/L	-	-	0.03 ppm	-	-
TDS	-	-	360	184 ppm	290 mg/L	-
TN (mg/L)	0.12	14.71	-	-	-	5.0
DON (mg/L)	-	55.07	-	-	-	-

[1] Dimane & El Hammoudani, 2021

[2] Hu et al., 2020

[3] Plevri et al., 2021

[4] Jayaramaiah & Dawn, 2025

[5] Hossain et al., 2022

[6] Ahmad Farid et al., 2019

[7] Aziz & Kasongo, 2021

2.6 Techniques Used for Treatment of Secondary Effluent

Tertiary wastewater treatment encompasses a diverse set of advanced processes designed to improve effluent quality after primary and secondary treatment, enabling water reuse and compliance with increasingly stringent environmental standards, and mainly focuses on the removal of nutrients such as nitrogen and phosphorus, while also incorporating advanced techniques for targeting persistent pollutants and emerging organic micropollutants (Solcova et al., 2024). Among the wide range of tertiary treatment technologies, adsorption (Tran, 2023), coagulation-flocculation (Loh et al., 2022), advanced oxidation processes (AOPs) (Manna & Sen, 2023), and membrane technology (Mortula et al., 2022) have been widely investigated and applied. The selection and combination of these technologies depend on the specific contaminants present, desired effluent quality, and operational considerations, as no single method is universally optimal (de Boer et al., 2022). Some processes, such as coagulation-flocculation, are frequently employed as pretreatment steps to enhance the efficiency of subsequent tertiary treatments by removing suspended solids and colloidal particles, thereby reducing fouling and improving the performance of downstream units such as membranes or adsorption beds (Aragaw & Bogale, 2023). The integration of multiple techniques,

often referred to as a multi-barrier approach, maximises contaminant removal and ensures robust treatment outcomes (de Boer et al., 2022). As research and technology advance, the complementarity and adaptability of tertiary treatment methods continue to play a crucial role in safeguarding water quality and supporting sustainable water management. Figure 4 presents and describes the different secondary effluent treatment techniques discussed in this review article.

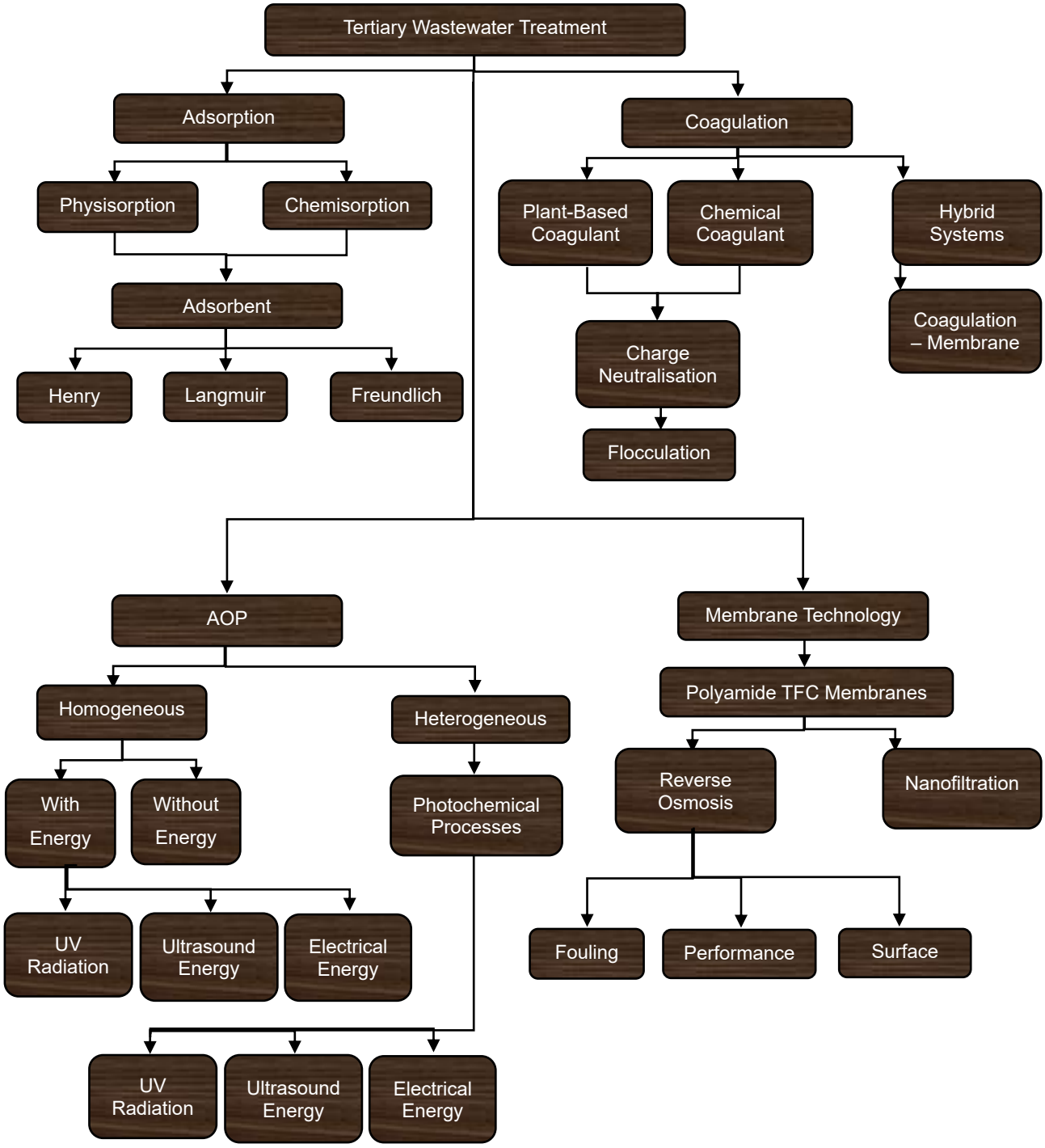


Figure. 4. Description of different secondary effluent treatment techniques

2.6.1 Adsorption

Adsorption is a process in which a substance accumulates at the interface between phases, such as solid-liquid or liquid-gas systems (Alaqarbeh, 2021). It is widely used in wastewater treatment due to its simplicity and efficiency in removing residual pollutants, including organic compounds, nutrients, and heavy metals. Its effectiveness depends on several parameters, including solution pH, adsorbent dose, temperature, and contact time (Sukmana et al., 2021). Adsorption can also be applied in combination with other treatment processes, such as chemical coagulation, to enhance the removal of organic pollutants, fats, oils, and surfactants from complex wastewater streams (Roman & Aziz, 2021). Adsorption behaviour can be described using adsorption isotherms, which describe how pollutants interact with adsorbents at equilibrium. Henry's isotherm represents a linear relationship between the adsorbed amount and the adsorbate concentration, typically valid at low concentrations. The Langmuir isotherm assumes monolayer adsorption on a homogeneous surface with a finite number of adsorption sites. The Freundlich isotherm describes multilayer adsorption on heterogeneous surfaces (Kalam et al., 2021).

2.6.2 Coagulation - Flocculation

Coagulation is a widely used wastewater treatment process that removes chemical pollutants, such as BOD and COD, and physical impurities, including suspended solids and turbidity, using chemical coagulants (alum, ferric chloride, and polyaluminum chloride) or natural coagulants (chitosan and seed extracts). Coagulants form larger, denser flocs that settle efficiently, and the process effectiveness depends on factors such as coagulant dosage, mixing time, and temperature (Sukmana et al., 2021). Flocculation is the process of aggregating suspended particulate matter into larger flocs while allowing controlled breakage of flocs into smaller units or primary particles (Ho et al., 2022). Coagulation and flocculation are often applied sequentially to maximise the removal of suspended and colloidal particles from wastewater.

During coagulation, colloids are destabilised primarily through charge neutralisation. Flocculation follows, promoting aggregation of these destabilised particles, forming larger, denser flocs that settle efficiently (Beyene et al., 2016; Zaki et al., 2023). Together, coagulation and flocculation help remove colloidal impurities and reduce turbidity in the water, preparing it for subsequent treatment steps (Mohamed Noor et al., 2022).

2.6.3 Advanced Oxidation Processes

AOPs are used to degrade persistent micropollutants in wastewater. Their effectiveness stems from the generation of reactive oxygen species (ROS), particularly hydroxyl radicals (•OH), which possess very high redox potential and non-selective reactivity. These radicals initiate oxidation pathways, such as hydrogen abstraction and electron transfer, leading to the breakdown of complex contaminants into carbon dioxide, inorganic acids, or other harmless end products (Saravanan et

al., 2022). They are commonly classified by the source of •OH radicals' production, including UV/H_2O_2, Fenton reactions, and ozone-based oxidation. Hybrid or combined AOPs can further enhance treatment performance, making them a key option for advanced water purification and reuse (Pandis et al., 2022). UV/H_2O_2 systems combine UV light with hydrogen peroxide to generate OH radicals, effectively degrading organic micropollutants and inactivating bacteria. (Wang & Zhuan, 2020)

Fenton reactions involve hydrogen peroxide activated by iron salts (Fe^{2+}), producing highly reactive OH radicals that break down persistent organics and inactivate pathogens (Wang & Zhuan, 2020; Odabasi & Buyukgungor, 2024). Ozone-based processes, such as O_3/UV or O_3/H_2O_2/UV, produce hydroxyl radicals, enabling the removal of recalcitrant compounds. These AOPs can be used individually or in combination to enhance pollutant removal efficiency and adapt to specific wastewater characteristics (Bermúdez et al., 2021). Diverse AOPs that rely on OH generation as the primary mechanism for pollutant degradation.

The reviewed studies demonstrate that AOPs, whether applied alone or in combination with biological or chemical treatments, can achieve substantial reductions in key wastewater quality parameters. AOPs consistently remove significant amounts of organic pollutants and solids, while also effectively targeting specific contaminants. In most cases, pH and turbidity tend to increase slightly following treatment, highlighting the need for post-treatment adjustments if required. The choice of AOP type and operational conditions can be tailored to the wastewater characteristics to maximise pollutant removal. These results collectively indicate that by selecting an appropriate AOP system and optimising process parameters, significant improvement in effluent quality can be achieved, making the treated water suitable for non-potable reuse.

2.6.4 Membrane Technology

The separation of contaminants from water is dependent on semi-permeable barriers to achieve selective mass transfer based on molecular size, charge, and relative physicochemical properties (Çankaya, 2023). Water molecules pass through the membrane while dissolved solids, suspended particles, and other pollutants are retained on the feed side. The process can be characterised by the pressure difference (reverse osmosis (RO), nanofiltration (NF), ultrafiltration (UF), microfiltration (MF), and forward osmosis (FO)). RO and NF membrane technologies are effective in removing a variety of contaminants, including heavy metals, organic micropollutants, pharmaceuticals, and persistent chemicals (Chang et al., 2022). They operate on size exclusion and charge interactions, making them relevant to selective mass transfer (Maroufi & Hajilary, 2023). In comparison, MF and UF are less efficient due to large pore sizes.

(I) Nanofiltration membranes

NF has its roots in research conducted over 15 years, beginning in the 1960s, originating as a variant of RO and UF (Maroufi & Hajilary, 2023). Initially, NF was termed “open RO” or “tight UF” due to its intermediate properties (Covaliu-Mierlă et al., 2023). Due to limitations in membrane material (cellulose acetate), research has shifted towards alternative materials, such as polymers. Advances in membrane technology have since led to the development of composite and ceramic NF membranes, which leveraged interfacial polymerisation to form specialised layers that enhance mass transfer and selectivity (Namla et al., 2025).

NF membranes provide a unique combination of relatively high flux and low operating pressure, making them ideal for removing pollutants such as dyes, soil leaching, and arsenic. They can filter out divalent ions and small organic matter with pore sizes ranging from $(1 - 10nm)$ (Namla et al., 2025). Pilot-scale research conducted by Aziz & Kasongo, (2021) compared the performance of RO, NF, and UF technologies in treating membrane bioreactor (MBR) effluent. As the UF presented a removal efficiency of approximately 40%, RO and NF achieved superior inorganic removal rates exceeding 90% for $COD, NH_4{}^+, PO_4^{3-};\ and\ NO_3^-$.

NF technology proved to be viable, as RO effectiveness came at the cost of energy consumption 1.4 times higher than that of NF. While all three technologies relied on high pressure to operate, NF offers high selectivity, primarily attributed to steric hindrance and charge interactions (Maroufi & Hajilary, 2023). The narrow pore-size distribution enables effective selective separation based on ion valence and size, which can be further enhanced by manipulating surface charge and leveraging the Gibbs-Donna effect (Namla et al., 2025). Total dissolved solids (TDS) and pH of feed wastewater significantly influence the performance of NF and RO technologies by affecting surface charge and osmotic pressure.

Osmotic pressure increases with TDS concentration, requiring higher operating pressures for both NF and RO technologies. This affects RO membranes more due to their very narrow pore size. In a study conducted by Aziz & Kasongo, (2021), the RO membrane achieved high salt rejection, ranging from 94% to 97% at a controlled pH of 6.5 and 89% to 94% with the pH uncontrolled. This shows that, when pH is varied, electrostatic interactions between the charged membrane surface and ionic species alter rejection rates. NF membranes, being particularly sensitive, rely on charge-based repulsion mechanisms in addition to size exclusion for pollutant removal (Namla et al., 2025). NF and RO are intrinsically linked and use a similar thin-film composite (TFC) structure.

Saravanan et al., (2023) investigated the treatment of leather industry wastewater using RO and hybrid organic polyamide NF membranes to achieve significant pollutant reduction. The process, optimised using Taguchi analysis, achieved 89% reductions in total COD and total wastewater

hardness, while sulphate was reduced to 88%. As a result, the proposed technology improved filtration efficiency for wastewater treatment. NF membranes offer versatile applications, ranging from water purification to disease prevention and desalinating seawater to recover valuable compounds. Extending its effectiveness in the pharmaceutical industry by separating and concentrating active ingredients and removing impurities. However, fouling tends to clog pores, reducing their selectivity.

(II) Reverse osmosis membranes

Similar to NF, reverse osmosis (RO) membranes have even narrower pore sizes, enabling them to retain virtually all ions while allowing water molecules to pass. Due to size exclusion, monovalent ions tend to pass through the membranes more easily than divalent ions (Kasongo et al., 2019; Aziz & Kasongo, 2021). RO's pore size makes it more effective than NF in desalination applications. According to a scientific study, cellulose acetate membranes demonstrated approximately 98% NaCl retention rates, albeit at the expense of limited permeability and thermal stability. Currently, polyamide thin-film composite (TFC) membranes are predominantly used in RO due to their high permeability, stability, and excellent NaCl retention rates.

A comprehensive review of RO desalination by Shabib et al., (2025) revealed significant advancements in addressing global water scarcity. While RO technologies demonstrate excellent performance, integrating renewable energy has reduced greenhouse gas emissions by up to 90%. Li et al., (2025) focused on developing high-rejection seawater RO membranes for enhanced desalination performance. Fabricated polyamide TFC membranes achieved an excellent rejection rate of 99.90% $NaCl$ and 92.39% boron, with a flux of 37.85 $L.m^{-2}h^{-1}$ under standard test conditions. Al-Hobaib et al., (2016) developed high-performance polyamide TFC RO membranes via interfacial polymerisation using dodecane solvent mixed with co-solvents. The addition of co-solvents decreased membrane roughness, pore size, and thickness. However, with a concentration ranging from $0{,}5 - 5wt\%$, the results showed that the contact angle increased with co-solvent concentration.

TFC membrane's structure consists of a porous support layer and a dense polyamide film (Al Mayyahi, 2018). The polyamide film contains functional groups that control water and solute transport. Their functional groups control water and solute transport. Although polyamide membranes are highly recommended, they suffer from chlorine attack and fouling, which stands as a critical gap in the literature. The problem statement can be verified through membrane autopsy analysis. Identifying the causes and failures of the membrane. Over 600 autopsies indicated fouling as the major cause. In 75% of cases, and 63% of cases for seawater desalination membranes, fouling was indicated as the primary failure for RO technologies (Namla et al., 2025).

2.6.5 Fouling of polyamide reverse osmosis membranes

The effect of membrane fouling includes reduced membrane permeability caused by clogging (Bai et al., 2023). Fouling can alter solute retention, with a tendency to increase for MF and UF, and decrease for RO and NF. Feed water characteristics, hydrodynamic circumstances, temperature, and pH all have an impact on fouling formation and development (Çankaya, 2023). Commonly, membrane fouling is defined as a “flux decline with time”. Maeda, (2024) quotes that fouling not only compromises membrane flux and lifespan, but it concurrently rises differential and feed pressure. Water quality deteriorates as energy consumption and operational costs increase, ultimately hindering the widespread adoption of membrane technology.

Understanding the spatial distribution of fouling within membrane systems is essential to comprehending its impact on performance. Fouling can occur internally (inside membrane pores) or externally (on the membrane surface) (Li et al., 2025). External fouling accumulates bigger entities, whereas internal fouling occurs when small particles and macromolecules accumulate within the pore’s walls, damaging the membrane structure.

The mechanisms underlying membrane fouling are multifaceted and have been extensively investigated by various researchers. It can be categorised into various forms, such as adsorption, pore blocking, deposition, and cake formation (Chang et al., 2022). A characteristic flux decline behaviour associated with fouling has been observed, comprising three stages: an initial rapid drop, a gradual long-term decline, and eventual attainment of a steady-state flux. This decline is influenced by particle size and shape. The type of foulants encountered varies depending on the membrane process, configuration, material, and application. Foulants can be broadly classified into four categories: biofouling, inorganic (scaling), colloidal fouling, and organic fouling (Çankaya, 2023). Smaller molecules, such as polypropylene glycol, can act as organic foulants, providing a framework for understanding the complex interactions between foulants and membrane surfaces.

Natural organic matter (NOM) is a primary cause of organic fouling in both surface and groundwater, with effluent organic matter (EfOM) being a significant concern for municipal wastewater reuse (Maeda, 2024). Slowing the flow of permeate through the membrane over time. Among the four, organic fouling, along with biofouling, has been considered a major contributor to fouling in RO and NF membranes. Unlike MF and UF membranes, which can be mitigated by chlorine backwashing to control biofouling, RO and NF membranes, particularly those made of polyamide, are susceptible to biofouling due to their low chlorine tolerance (Bai et al., 2023). The shift from cellulose acetate to TFC RO membranes has also altered fouling patterns, with TFC RO membranes being more prone to biofouling (Duan et al., 2024). Biofouling enables the adhesion and accumulation of living microorganisms, leading to the development of biofilms on the membrane and/or feed spacer (Chang et al., 2022). Biofilms consisting primarily of extracellular polymeric substances (EPS) and microbial cells (Ezugbe & Rathilal, 2020) form when microorganisms attach to moist surfaces and multiply by

feeding on accumulated nutrients. Thus, eventually clog membrane pores and increase resistance to permeate flow (Bera et al., 2022). Crossflow velocity (CFV) can either increase or decrease biofilm accumulation, while high flux rates can accelerate biofilm development (Maeda, 2024).

2.6.6 Biofouling of Polyamide Reverse Osmosis Membranes

Biofouling is the process of microorganism adhesion and proliferation on the membrane surface. In other words, it is the formation of biofilm to an unacceptable degree that could cause substantial operational costs. (Jiang et al., 2017; Hu et al., 2016). A variety of measures have been investigated for fouling control (Lau et al., 2012). Biofouling is notably a contributing factor to more than 45% of all membrane fouling (Komlenic, 2010). Kucera (2019) stated that biofouling control and prevention remain the most significant challenge facing the operation of polyamide membrane systems, despite advances in membrane performance over the last 45 years. Figure 5 shows the average distribution of foulants on reverse osmosis membranes obtained from several autopsies, including biofouling. All membranes showed biofilm formation, and 33% had biofouling as the leading cause of poor performance.

The pretreatment of feed water cannot significantly reduce biofouling because of the self-replicating nature of microbial cells. Furthermore, the degradation of polyamide thin film composite membranes through contact with the disinfectant chlorine is a critical limitation to commercializing membranes, as this affects membrane performance in long-term operations (Lau et al., 2012; Qasim et al., 2019; Miyoshi et al., 2024). Hence, significant attention must be paid to the interaction between the PA top active layer and the underlying supporting membrane to better understand the impact of membrane substrate properties on the active layer's performance.

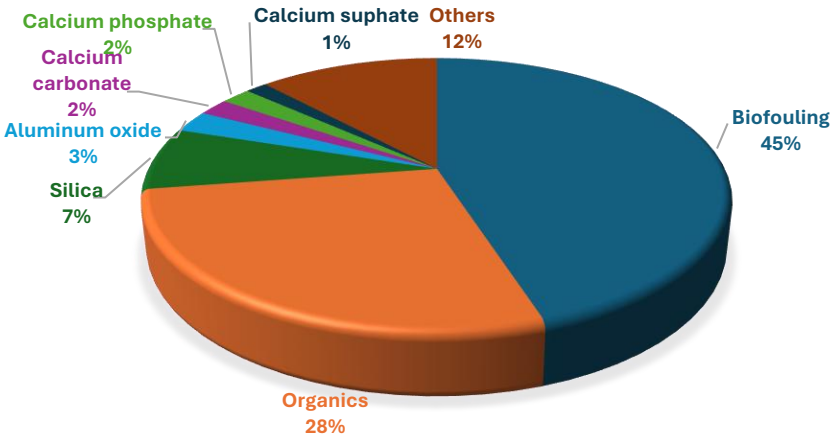


Figure 5: Common foulant types of polyamide membranes registered from several membrane autopsies, including biofouling. Adapted from Komlenic (2010) and Kucera (2019).

Extensive studies on membrane surface properties have focused on controlling biofilm growth. Efforts have focused on increasing the hydrophilic character of the membrane surface to make it less susceptible to organic and biofouling: for example, redox-initiated graft polymerisation of hydrophilic monomers (Herzberg et al., 2011) and nanoparticles integration onto RO membranes (Ansari et al., 2021; Armendáriz-Ontiveros et al., 2020; Jeon et al., 2021), which has resulted in improved resistance to biofouling.

Bacteria and other microorganisms naturally adhere to surfaces to survive. In nearly all water systems, microorganisms can colonise almost any surface. Biofouling is more complex than different fouling types (Kasongo, 2018). A pipe system's dead or low-flux zone could also affect bacteria growth (Jiang et al., 2017). Other factors could also affect this process, which could be classified into microbial properties, membrane surface characteristics, surface-bacteria interactions, and operational conditions. Membrane characteristics include surface hydrophobicity, surface charge, chemical compositions, roughness and surface morphology (Al-Juboori & Yusaf, 2012; Kasongo, 2018). Recent studies have also shown that the support layer of the RO membrane significantly affects the properties of the resulting PA active layer. It has been demonstrated that the thickness, roughness, and cross-linking degree of the PA layer are dependent on the surface properties of the support layer, including its porosity and hydrophilicity (Sharabati et al., 2019). Thus, further studies to comprehend the relation between the support layer and the PA active layer may be necessary to minimise membrane PA surface biofouling.

Operating conditions include permeating flux, crossflow velocity, temperature, pressure, pH, salt concentration, presence of specific molecules, and feed spacer (Wang et al., 2015a; Suwarno et al., 2016; Jiang et al., 2017). Usually, bacterial adhesion is promoted by the prior adsorption of organic materials onto the surface (the conditioning film). Within seconds, surfaces immersed in water become covered with a so-called conditioning film consisting of organic macromolecules (humic substances, polysaccharides and proteins) and inorganic compounds. This substrate conditioning is suggested to enhance the attachment of cells to the surface (Kochkodan & Hilal, 2015). The general outcome of bacterial colonisation of surfaces is the formation of biofilms. It was shown that the biofouling process occurs through a cascade of events, including cell transport, deposition and adhesion, exopolymer production and cell growth and proliferation (Kochkodan & Hilal, 2015; Nagaraj et al., 2018). Hence, there are two key components of biofilms: the bacteria and the extracellular polymeric substances (EPS), which are excreted by bacteria during the metabolism process (Jiang et al., 2017). As analysed, microorganisms can form biofouling that can grow and multiply. As a result, unless pretreatment removes 100% of the bacteria, the remaining bacteria can gradually grow on the membrane surface, leading to membrane biofouling.

2.6.7 Biofilm formation

For the biofilm to form, two conditions are essential: bacteria and nutrients. Therefore, if all the nutrients are removed from the water through pretreatment technologies, the remaining cells cannot increase due to a lack of food sources. Based on this principle, researchers have investigated the relationship between membrane fouling rate and assimilable organic carbon (bacterial nutrient) content. By observing operational changes such as increased differential pressure and decreased permeate flux, they found that membrane biofouling was more serious when the nutrient level was higher (Jiang et al., 2017; Weinrich et al., 2016). Previous researchers have used several strategies to prevent biofilm formation on membranes or disperse and remove mature biofilms. Some methods to alleviate biofouling on RO membranes include physical flushing or cleaning of membranes, adding chemical compounds targeting the bacterial cells and/or extracellular matrix, and modifying the membrane surface and structure (J. Xu et al., 2013a; G. R. Xu et al., 2013; Nagaraj et al., 2018).

2.6.8 Membrane biofouling mitigation techniques

Researchers have employed various techniques to mitigate the issue of biofouling in RO membrane systems. These include physical disruption of biofilm matrices, control by biocides, and chemically modifying the anti-fouling behaviour of RO membranes (Shahzad et al., 2021; J. Wang et al., 2024). A recent study by Song et al., (2020) used a pretreatment strategy for controlling biofouling in seawater treatment with RO membrane processes by applying the disinfectants Cl_2 and ClO_2. The required concentration of Cl_2 was 2.5 times higher than that of ClO_2. It was reported that the ClO_2 disinfection process had better disinfection efficiency than Cl_2 under the same conditions and was preferred for suppressing the regrowth of microorganisms to the greatest extent. ClO_2 was considered more economical than the Cl_2 process for seawater desalination plants. However, further studies have reported that the self-replicating nature of most microorganisms significantly impairs and limits the effectiveness of fouling control strategies in pretreatment processes (Choi et al., 2020). Wang et al., (2019) have reported that fouling became more severe after chlorine dosage in the Membrane bioreactor (MBR) effluent from a full-scale municipal wastewater treatment plant. As a result, the thickness of the foulants increased significantly with the chlorine dosage. The authors identified microorganisms resistant to chlorine dosage, including Methylobacterium, Pseudomonas, Sphingomonas and Acinetobacter. Jung et al., (2018) used a Nisin solution to prevent biofouling of RO membranes. Nisin solution was added to the feed solution. It was found that the use of nisin solution had a slight effect on the permeate water flux and salt rejection of the polyamide thin film RO membrane. An increase in salt rejection was observed, accompanied by a slight decline in water flux. This could be due to the temporary adhesion of nisin to the polyamide layer of the RO membrane, which may occur because of the electrostatic attraction between the negatively charged surface of the membrane and the positively charged nisin solution. Moreover, the Nisin solution did

not affect the growth of P. aeruginosa bacteria but only showed antimicrobial activity against Bacillus sp.

Several studies have reported the shortcomings of most of the techniques above (Nagaraj et al., 2018). The clean-in-place (CIP) practices are often ineffective due to incorrect chemical selection; incomplete penetration of biofilm layers, poor cleaning practices regarding pH, temperature, and contact time, improper recirculation flow rates, and incomplete removal of biomass (Matin et al., 2011; Armstrong et al., 2011). The repeated use of biocides may also cause bacterial resistance by modifying the bacterial cell envelope, reducing biocide permeability, producing enzymes to degrade the biocides, or acquiring other biocide resistance genes (Nagaraj et al., 2018). Biofilm control strategies using enzymes to degrade the EPS matrix include glycosidases, proteases and deoxyribonucleases. Still, such enzymes target specific strains, and their efficacy in complex multi-species biofilms has not been established. In addition, enzymes are typically expensive, and there are other practical difficulties associated with treating and flushing membranes on an industrial scale (Armstrong et al., 2011; Nagaraj et al., 2018).

It is, therefore, crucial to develop more efficient and cost-effective methods for removing biofilms and alleviating biofouling. The surface modification of RO membranes is a promising method for preventing bacterial adsorption and biofouling (Kasongo et al., 2025). TFC Membrane surface modification techniques provide sustainable and environmentally friendly methods without releasing extra chemicals in RO systems, compared to chemical cleaning (Kim et al., 2019).

2.6.9 Membrane surface modification techniques to minimise biofouling

The formation of biofouling on the RO membrane can be mitigated by modifying the properties of the RO membrane surface using several techniques, including grafting and physical coating (Al-Juboori & Yusaf, 2012). Grafting of the membrane surface can be conducted through several techniques, including photochemical, free radical, radiation, plasma-induced and redox-induced (Bet-Moushoul et al., 2016). Surface modification techniques are applied to enhance certain membrane characteristics that mitigate membrane fouling, including roughness, surface charge, and membrane hydrophilicity. The hydrophobic interaction between bacteria and membrane surfaces is one of the leading causes of bacterial adhesion (Cheng et al., 2013; Wang et al., 2015; Liu et al., 2015; Aziz & Kasongo, 2021). Therefore, the hydrophilic treatment of RO membranes using hydrophilic polymers has been investigated to prevent the adsorption of organic foulants. Various hydrophilic polymers have been reported; especially, zwitterionic polymers, hydroxylated polymers, and polyethene glycol (PEG) are frequently used due to their high anti-adsorption properties. Realised by different functional groups, treatment of RO membranes using hydrophilic polymers has been investigated to prevent the adsorption of organic foulants (Saeki et al., 2021). Surfaces modified by zwitterionic polymers, particularly, exhibit high anti-adsorption properties against organic

foulants, including cells and bacteria, as well as anti-biofouling properties. Due to its relatively high hydration capacity, simple molecular structure, and cost efficiency, 2-hydroxyethyl methacrylate (HEMA) is frequently used as a hydrophilic polymer. Surface modification using HEMA effectively prevents the adsorption of foulants (Saeki et al., 2021). Table 2 summarises commonly reported hydrophilic surface modification approaches for TFC RO membranes and their key outcomes.

Table 2: TFC RO Membrane surface modification techniques using hydrophilic materials to minimise biofouling and reported main findings

Modifying agent	Modification method	Effect on membrane performance and anti-biofouling properties	Ref.
MEDSAH; HEMA and PEGMA	*Interfacial polymerisation (IP) method and surface-initiated atom transfer radical polymerisation (SI-ATRP)*	- MEDSAH had superior anti-biofouling properties compared to the other two hydrophilic polymers - HEMA-modified membrane adsorbed a considerably larger amount of bacteria than the virgin membrane - The PEGMA-modified membrane had a lower water permeability than the virgin PA membrane	(Saeki et al., 2021)
Zwitterionic sulfobetaine silane (EPBS; MPPS)	*Coating*	- The flux value of the pristine membrane decreased by 38% after biofouling of marine bacteria, while the flux reduction was 16% and 20% for the EPBS and MPPS modified membranes - No membrane pure water flux and salt rejection data were reported after the modification	(Saffarimiandoab et al., 2019)
Polyampholyte (CAA/ TMA)	*Surface-initiated atom transfer radical polymerisation (Grafting)*	- Modified membrane with 1:1 CAA/TMA surface ratio had nearly zero net surface charge (positive charge) and showed an excellent anti-biofouling performance in the presence of S. paucimobilis bacteria - The surface modification at different ratios of modifying agents affected both water permeability and salt rejection: Water permeability increased with the increase of TMA portion, while the salt rejection decreased.	(Yang et al., 2020)
Chlorhexidine (CH.)	*Interfacial polymerisation (IP)/immobilisation*	- The surface roughness of the membrane measured by AFM slightly decreased as the CH layer was increased (membrane became smoother). - Biofouling experimental tests with P. aeruginosa showed that the modified membranes inhibited biofilm formation by their vigorous anti-bacterial activity	(Kim et al., 2019)

ATRP initiator/Zwitterionic polymer (pMEDSAH)	*Surface-initiated atom transfer radical polymerisation (SI-ATRP)*	- Bacterial adhesion onto the membrane surface decreased with the increasing polymerisation time of modified membranes - After 20 h filtration time with bacterial solution, the water permeability of the pMEDSAH-grafted membranes was higher than that of the virgin membrane, which decreased to values below 40% - No significant changes in the salt rejection - The RO membrane surface became more hydrophilic after modification	(Yang et al., 2018)
Glycerol and dimethyldimethoxysilane (DMDMS)	*Chemical grafting and self-crossing*	- Membranes demonstrated simultaneous 30 % flux gain and 70 % reduction in protein fouling; this illustrates a synergistic graft/coat hybrid approach	(Jia et al., 2025)
hyperbranched polyglycerol (hPG)	*Graft polyerization*	- RO membranes reached a high water permeance of 3.27 ± 0.17 $L.m^{-2}\,h^{-1}$ bar while maintaining an excellent NaCl rejection (99.30 ± 0.15%). - improved chlorine-resistance with the maximum exposure of 20,000 ppm·h where the NaCl rejection of the membrane was still 98.69 ± 0.39%,	(Wang et al., 2024)

2.6.10 Nano-structuring of RO membrane to minimise biofouling

Membrane surface modification is a widely researched technique to prevent scaling and biofouling. Among different materials used for surface modification, nanoparticle addition has shown great promise in preventing scaling and biofouling. Recent studies have shown that adding nanoparticles improves surface antimicrobial properties and prevents polymers' biodegradation (Kochkodan et al., 2014; Yang et al., 2021; Dolina et al., 2015). Advanced nanomaterials are being developed for surface functionalisation as adsorption materials, nanocatalysts, coatings, and membrane fabrication (Shahzad et al., 2021). Figure 6 outlines a hybrid polymer-nanoparticle surface modification approach for polyamide RO membranes.

The incorporated nanomaterials, such as zeolite, silica, and multiwalled carbon nanotubes (Ong et al., 2016), Silver nanoparticles (Ag NPs), copper nanoparticles (Cu NPs), TiO_2 nanoparticles, and graphene oxide (GO) nanosheets have been demonstrated to not only prohibit the growth of microorganisms effectively but also have little effect on the membrane permeability and selectivity (Liu et al., 2017). More nanomaterials, including zinc oxide (ZnO) and carbon nanotube, have been introduced into the PA layer to improve the biofouling resistance of the membrane (Jeon & Lee, 2020; Jeon et al., 2021; Shen et al., 2020; Ngo et al., 2020; Ashfaq et al., 2020).

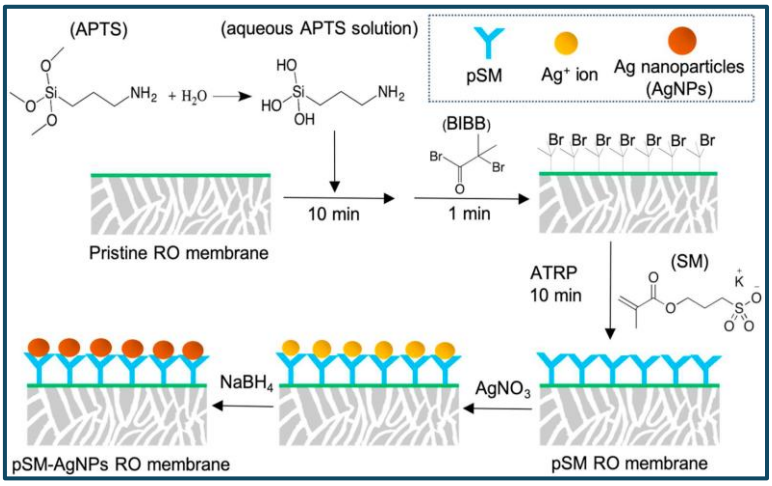


Figure 6: Graphical illustration of membrane surface modification of a polyamide RO membrane with pSM-AgNPs. The RO membrane surface was first functionalized by poly (3-sulfopropyl methacrylate potassium salt) (pSM) via atom transfer radical polymerisation (ATRP), followed by the addition of Ag nanoparticles (Yang et al., 2021).

Related studies have reported two principal approaches to preparing nanoparticle-incorporated membranes. The two approaches are the phase inversion method and the immersion method. The former involves adding the nanoparticles to a casting solution, while the latter consists of soaking the membrane in an aqueous suspension of nanoparticles. (Bet-Moushoul et al., 2016). The

nanomaterial-incorporated TFC membrane, referred to as thin film nanocomposite (TFN), has received significant interest because its separation performance and durability (fouling and oxidation resistance) can be effectively enhanced depending on the properties of the incorporated nanomaterials.

Table 3 compiles reported nanoparticle-based surface modification strategies for improving the biofouling resistance of TFC RO membranes. Based on extensive literature, titanium dioxide (TiO_2) nanocomposite-based polymeric membranes have been well-studied and reviewed. Meanwhile, several research articles have demonstrated that zinc oxide (ZnO) nanoparticles exhibit comparable physical and chemical properties to those of titanium dioxide (TiO_2). Therefore, ZnO nanoparticles are believed to be a competitive alternative to TiO_2 nanoparticles in forming anti-fouling organic-inorganic composite membranes (Shen et al., 2020). It has also been reported that Silver and titanium dioxide have strong antimicrobial properties and can be included in RO membranes to reduce biofouling (Giwa et al., 2016). Copper-based nanoparticles have been incorporated into RO membrane surface and performance, particularly CuO-NPs, which could improve the hydrophilic property of RO membranes. Cu-NPs have been incorporated onto the RO membrane surface through the grafting and coating approaches. RO membrane grafted with Cu-NPs promoted by GO linker was reported to present better anti-bacterial properties when exposed to synthetic wastewater of *E. coli* bacteria for 7 days (García et al., 2021).

Graphene oxide (GO) nanoparticles have also been used as anti-biofouling membrane coatings due to their antimicrobial properties and, in most cases, an observed increase in flux in modified membranes. A study has reported that a PA membrane was functionalized with GO, and the membrane showed a 65% reduction in *E. coli* without affecting water flux performance (Perreault et al., 2014). It has also been reported that coated GO and silver (Ag) nanoparticles on cellulose acetate showed inactivation of cells (*E. coli*) by 86% after 2h contact time, and a higher water flux performance (Armendáriz-Ontiveros et al., 2020). Egorova et al., (2024) also reported a significant improvement in biofouling resistance of the membrane after coating a PA RO membrane with Iron nanoparticles coupled with plasma-activated water cleaning.

Table 3: TFC RO Membrane surface modification techniques using nanoparticle additives to minimise biofouling and reported main findings

Agent/Additives (Nanoparticles)	Modification method / Synthesis	Main findings	Ref.
polyacrylic acid (PAA)/ GO NPs	Coating	- Membrane surface charge decreased - PAA and GO coating on the RO membrane did not improve the anti-scaling property of the membrane. - PAA and GO coating on the RO membrane harmed the anti-biofouling property of the membrane	(Ansari et al., 2021)
Green TiO_2 NPs	Coating	- Fouling resistance to BSA solution improved by 21.5%. The *E. coli* sterilization ratio of 99.9% obtained. - Increased water permeability by 40.9%. - Slight decrease in NaCl rejection 6.3%	(Abu-Dalo et al., 2023)
GO NPs	Coating	- The membrane showed better anti-scaling properties in the presence of $CaSO_4$ solution after modification - Coating of GO on the membrane inhibited microbial (H. aquamarine) growth by 81.7% - No significant reduction in permeability was noted, while the salt rejection (with NaCl solution) of the membrane increased	(Ashfaq et al., 2020)
BSA/Ag NPs	layer-by-layer interfacial polymerisation (LBL-IP)	- The incorporation of Ag NPs affected the surface roughness and charge of the PA layer very little. - A clear growth profile and inhibition zone of *E. coli* bacteria: BSA/Ag NPs modified membranes exhibited an 8.38% water flux decline, while the	(Liu et al., 2017)

		unmodified membrane declined by 31.7% after the biofouling experimental tests.	
Ag-ZnO	interfacial polymerisation (IP) method	- Improved membrane permeability after modification from 0.9 to 1.9 ($L.m^{-2}h^{-1}bar^{-1}$) - Rejection of Chlorophenol (2,4-DCP) improved from 58% to 85% - No biofouling experimental data provided	(Kotlhao et al., 2019)
Poly(acryloyl hydrazide)/Ag NPs	Layered IP (LIP) method	- Water permeance and NaCl salt rejection were enhanced - Membrane surface roughness decreased - The modified membrane showed better anti-biofouling performance (in the presence of gram-positive *S. aureus*, gram-negative *E. coli* and *P. aeruginosa*) and rinsing efficiency (41% flux recovery vs 12%)	(Jeon et al., 2021)
Fe NPs	Coating	- Increases in T, DO (Dissolved Oxygen), and pH improve the efficacy of the FeNP coating - The fluxes for the FeNP-coated membrane were 50% to 65% lower than the new membrane; a 43% increase in contact angle was noted after modification. - A reduction of 38% of biofouling by Bacillus from the Chilean site was noted after FeNP coating	(Armendáriz-Ontiveros et al., 2020)
Poly (3-sulfopropyl methacrylate potassium salt) (pSM) /Ag NPs	Atom transfer radical polymerisation (ATRP)	- pSM-AgNPs RO membrane reached 95% reduction of S. paucimobilis and B. subtilis bacterial adhesion compared to that of the virgin PA RO membrane	(Yang et al., 2021)

		- The water permeability of the pSM-AgNPs modified RO membrane increased while the salt rejection remained comparable to that of the virgin membrane - The chlorine tolerance of the RO membrane was not found to improve	
rGO/TiO_2 NPs	Interfacial polymerisation (IP) of	- The modified membranes had a rough surface - High salt rejection of the membrane was still retained, while the water permeability of the membrane increased due to the presence of GO NPs - rGO/TiO_2 modified membrane was more resistant to chlorine than the virgin membrane - 0.02 wt.% rGO/TiO_2 membrane had the best anti-fouling ability when tested with BSA.	(Safarpour et al., 2015)
β-cyclodextrin GO NPs	interfacial polymerisation method adopted	- The water permeation flux and anti-bacterial activity of the β-CD-f-GO modified membrane showed an improvement by approximately 38% and 45.9%, respectively - Modified membrane showed improved stability and resistance to chlorine - The modified membrane showed better anti-bacterial properties, estimated at 45.9%, while the unmodified RO membrane bacterial resistance was 23% when tested with *E.coli* bacteria.	(Matshetshe et al., 2022)

2.6.11 Membrane surface properties characterisation

The effect of functionalisation on membrane surface properties has been investigated through contact angle measurements, scanning electron microscopy-energy dispersive X-ray spectroscopy (SEM-EDX), Atomic force microscopy (AFM), Fourier Transform infrared (FTIR) and Raman Spectroscopic (RS) techniques, as well as Nuclear magnetic resonance (NMR) by many researchers (Ong et al., 2016; Kim et al., 2021).

Research conducted by Gayed et al., (2019) used x-ray diffraction (XRD) to complement FTIR and thermal gravimetric analysis (TGA) to evaluate the thermal stability of nanoparticles after being introduced onto the surface of a PA RO membrane. Ngo et al., (2020) used Electron microscopy (SEM-EDX) to evaluate the surface morphology, size, and elemental mapping after modification of a PA RO membrane with graphene oxide - Titanium dioxide nanoparticles (GO-TiO_2). The researchers determined the components in the GO-TiO_2 mixture on the membrane surface. Figure 7 illustrates the SEM analysis highlighting structural changes on the membrane surface and cross-section following SiO_2 nanoparticle incorporation, in a study conducted by Peyki et al., (2015).

On the other hand, Yang et al., (2021) used TEM to observe the surface of the pristine PA RO membrane and the modified silver nanoparticles incorporated membrane (AgNPs) and study the size distribution of AgNPs by image analysis of the corresponding TEM images. The mean particle size was calculated from a sample size of 100 particles. ATR-FTIR has been widely employed in membrane surface modification studies to analyse the functional groups of active membrane layers (Shafi et al., 2017; Mushtaq et al., 2021).

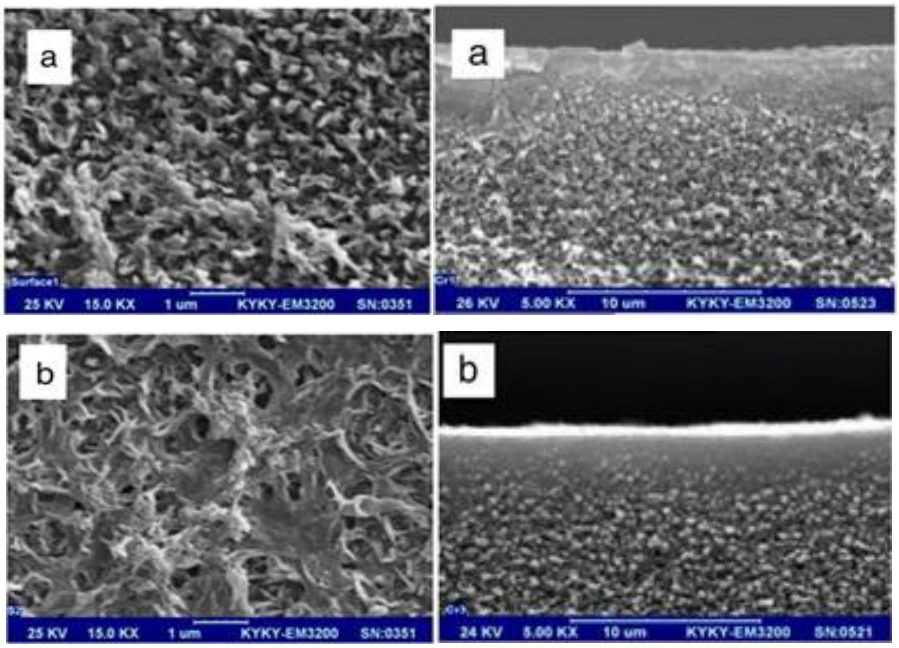


Figure 7: SEM images of a study conducted on TFC PA RO membrane modified SEM before modification (a) and after modification (b) with silica nanoparticles (SiO_2). Left: Top-view; Right: Cross-section view (Peyki et al., 2015).

Similar to ATR-FTIR, NMR is used to describe the structure of the chemical compound after functionalisation of the membrane surface. Figure 8 shows an illustration of the ^{1}H NMR analysis used to verify the successful grafting of modifying agents at varying ratios onto the PA RO membrane surface.

The use of NMR in characterising the PA RO membrane surface appears to be currently limited. This is due to the disadvantages associated with the analysis when characterising the membrane (Al-Juboori & Yusaf, 2012). However, studies reported successfully using the analysis to confirm changes observed on the membrane surface after modification (Jeon & Lee, 2020; Jeon et al., 2021). Wei et al., (2010) used NMR to depict the structure of an RO membrane synthesised by free-radical graft polymerisation of 3-allyl-5,5-dimethylhydantoin (ADMH). They confirmed the chemical structure of ADMH featuring a hydantoin ring and an allyl functional group on the membrane surface, through ^{1}H NMR spectroscopy, which showed the characteristic peaks of ADMH. In a new in situ hybridisation strategy for the synthesis of silver-incorporated reverse osmosis (RO) membranes, Jeon et al., (2021) also confirmed the structure of the chemical compound at each synthesis step by gel permeation chromatography, ^{1}H NMR.

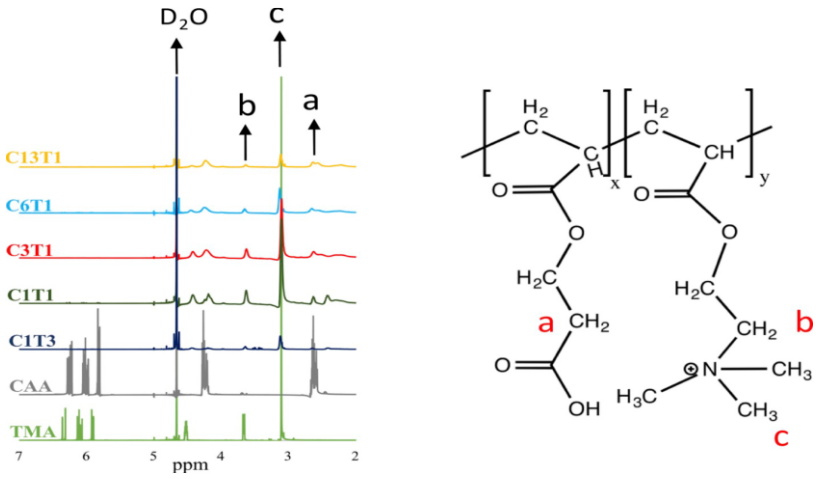


Figure 8: ^{1}H NMR spectrum illustrating the structure of 2-carboxyethyl acrylate (CAA), [2-(acryloyloxy)ethyl] trimethyl ammonium chloride (TMA) and p(CAA-co-TMA) grafted on PA RO membranes. The p(CAA-co-TMA) was grafted onto the PA RO membranes with different ratios, denoted as C13T1, C6T1, C3T1, C1T1, and C1T3 (Yang et al., 2020).

A study conducted by Perreault et al. (2014) used AFM imaging and successfully evaluated the size and thickness (1.7 nm thick) of graphene oxide sheets impregnated on the surface of the PA RO membrane were evaluated by atomic. Although limited, the characterisation of membrane surfaces after modification through Raman spectroscopy has also been exploited. RS has been primarily used to study the polymer chain's orientation and the polymer's degree of crystallinity in the membrane (Qasim et al., 2019). A recent study by Ansari et al., (2021) evaluated the stability of polyacrylic acid (PAA) and graphene oxide (GO) coatings on the membranes by collecting Raman mapping before

and after using the membranes in the RO system. The RS spectroscopy showed the characteristic peaks corresponding to the symmetric C-O-C stretching. The phenyl ring vibration of the polyamide membranes at two characteristic broad peaks, 1147 cm^{-1} and 1585 cm^{-1}, respectively, indicates the combined presence of the phenyl ring vibration and the G band of G.O. Perreault et al., (2014) used RS. It successfully demonstrated the binding of graphene oxide to the TFC membrane. The Raman spectrum of the TFC membrane was mainly characterised by the signal of its thick polysulfone layer.

2.6.12 Membrane and nanocomposite characterisation

Understanding the materials' structure, characteristics, and performance is important, particularly in secondary wastewater treatment, where efficient pollutant removal is paramount (Li et al., 2025). Various techniques are used to analyse materials, providing insights into their morphology, chemical structure, and surface properties. This includes Fourier-transform infrared spectroscopy (FTIR), X-ray photoelectron spectroscopy (XPS), Field-emission scanning electron microscope (FE-SEM), and atomic force microscopy (AFM). FTIR is used for analysing the chemical structure of materials by measuring the absorption of infrared radiation, which helps identify functional groups. El-Fattah et al., (2025) reported FTIR spectra presenting medium-to-strong lines, which indicate the existence of specific functional groups in the PES molecules.TiO_2 FTIR spectra and TiO_2\AgBr samples with $Ti-O-Ti$ show stretches at $500-800\,cm^{-1}$, while the $O-H$ group bending and stretching at $1632\,cm^{-1}$ and $3300-3600\,cm^{-1}$, respectively (Vatanpour et al., 2024).

A non-destructive technique, XRD characterisation, was used for determining the atomic and molecular structure of a crystalline substance. XRD patterns of TiO_2 and TiO_2\AgBr materials disclose their phase composition and crystal structure (Vatanpour et al., 2024). The diffraction peaks in TiO_2 indicate a two-phase structure consisting of anatase and rutile phases. With TiO_2\AgBr nanocomposites presenting diffraction peaks that correspond to the cubic phase of AgBr, and the tetragonal phase for TiO_2 (Vatanpour et al., 2024). The surface and cross-sectional morphology of the membranes are analysed by FE-SEM. The micrographs reveal structural insights and alter the texture of the structure due to nanoparticle incorporation, which may increase surface roughness (Li et al., 2025). Consequently, surface roughness is assessed using AFM, which provides an indication of the complexity of nanomaterial enhancement. According to Vatanpour et al., (2024) the incorporation of $AgBr$ nanoparticles on the surface of TiO_2 resulted in a more porous structure. El-Fattah et al., (2025) used AFM and FE-SEM to analyse the surface roughness and morphology of PES-NTFC membranes, finding that the incorporation of the nanoparticles increased surface roughness and complexity.

2.6.13 Membrane biofilm characterisation

Some of the techniques described in **Sections 2.6.11 and 2.6.12** have been further utilised to evaluate the extent of biofouling. The use of electron microscopic techniques to study biofilms formed on surfaces began in the 1980s. Two types of electron microscopy have been extensively used: scanning electron microscopy (SEM) and transmission electron microscopy (TEM). The researchers could accurately identify the constituents of biofilm due to the high magnification of the analyses (Al-Juboori & Yusaf, 2012). SEM and TEM techniques facilitate the study of different aspects of biofilms in RO systems. These two microscopic techniques can produce high-resolution images, image surfaces with complex topological structures, and provide cross-sectional details of the biofilm, which in turn allows for visualising the spatial distribution of microorganisms in the biofilm matrix. However, using SEM and TEM for biofilm studies is associated with some drawbacks, such as slow analysis and complex sample preparation that requires desiccation and fixation, which may damage the biofilm. Al-Juboori & Yusaf, (2012) reported that ATR-FTIR is one of the common spectroscopies used for studying the characterisation of the developed biofilm on solid surfaces and pointed out the advantages, which include the speediness of the analysis, the accuracy of the wavenumber, the availability of FTIR and its compatible software, etc. However, disadvantages such as the influence of the refractive index of the surrounding environment on the analyses, the overlapping in the spectra of FTIR in the complex mixture of microorganisms, the need for a complete library of the spectra for each microorganism for an accurate analysis, and the limitation of the investigation into detecting thin biofilm have also been reported (Davis & Mauer, 2010; Al-Juboori & Yusaf, 2012). NMR has also been applied in analysing the performance of various chemical treatments in removing biofilm from RO membranes (Creber et al., 2010). A study reported on the use of NMR to describe the biofilm of Pseudomonas aeruginosa by analysing the molecular motility of the biofilm components (Al-Juboori & Yusaf, 2012). A previous study showed that the combination of 13C NMR and confocal laser scanning microscopy (CLSM) could be an essential technique to evaluate the growth of microorganisms in biofilm, the architecture of the biofilm and the detachment rate of the biofilm under starvation conditions (Garny et al., 2010). NMR has further been used to attain information concerning substrate consumption, intracellular metabolites in biofilms and the effect of biofilm on the hydrodynamics of the surrounding liquid and to obtain information about the spatial distribution of biofilm built on RO membrane (Al-Juboori & Yusaf, 2012).

(I) Challenges and Limitations of membrane surface modification

The long-term stability of materials introduced to the surface of the membrane remains inadequately documented, with only a few studies investigating long-term application of modified membranes. There is a gap in the literature concerning post-fouling autopsy analyses of RO membrane surfaces to assess surface condition, specifically regarding the distribution of modifying agents and the

accumulation of foulants, which would enable a more direct evaluation of fouling severity. Additionally, the economic ramifications of scaling production of modified membrane processes have not been thoroughly examined, highlighting the need for in-depth techno-economic analysis. Furthermore, there is a gap in comprehensive evaluations of the environmental implications of coatings containing nanomaterials.

2.7 Summary

This section of the thesis showed the need for tertiary treatment of secondary effluent, contributing to sustainable water resource management. Tertiary treatment has emerged as a crucial component in the pursuit of sustainable water management, addressing the pressing need to conserve and protect this valuable resource. Several important conclusions are drawn from a detailed evaluation of the four main tertiary treatment technologies identified: Moderate-to-high pollutant removal efficiencies (55-95% for COD, TSS, and turbidity) are demonstrated, and performance can be significantly improved when integrating the processes discussed, where applicable.

Across a variety of wastewater treatment, coagulation-flocculation produces remarkable removal rates (up to 100% turbidity reduction, 86-92% COD removal), with both chemical coagulants $FeCl_3$, and PACl and plant-based substitutes that demonstrate significant performance. Higher contaminant rejection (>90% for the majority of inorganics) is provided by membrane technologies, especially NF and RO. NF offers a good compromise between energy economy and selectivity, while RO appears to be more effective in terms of removal but requires more energy. Fouling remains a significant concern in all membrane-based systems. Despite advancements in membrane surface modification for improved performance, the following gaps and challenges remain: the long-term stability of surface-modified membranes has yet to be well demonstrated. The combination of membrane surface characterisation techniques has proven crucial for understanding membrane material performance and treatment mechanisms.

This section also presented research on TFC PA RO membranes aimed at minimising biofouling through surface modification. The nano-structuring of PA TFC RO membranes shows great promise in preventing bacterial activity and biofouling. However, as illustrated in this study, the modification techniques used thus far to incorporate nanomaterials onto the membrane surface appear to have minimal adverse effects, particularly in terms of membrane salt rejection and permeability. Future efforts should focus on identifying appropriate methods for functionalizing the PA RO membrane before incorporating targeted nanomaterials. The successful nano-structuring of functionalized PA membranes will impact the practices involved in the synthesis and manufacturing of commercial PA membranes designed to minimise biofouling.

Moving forward, the successful implementation of tertiary treatment systems for safe water reuse will depend on the strategic selection and optimisation of treatment methods tailored to specific effluent characteristics, as well as ongoing innovation in membrane materials, fouling mitigation strategies, and process integration.

2.8 References

Abrahams, M., Aziz, M. & Kasongo, G. 2021. Investigating the effects of different cationic charge flocculation polymers on municipal wastewater sludge dewatering. Water Practice and Technology, 16(3).

Abu-Dalo, M.A., Bozeya, A., Sawalmeh, Z., Albiss, B., Alnairat, N. & Abu-Zurayk, R. 2023. Antifouling polymeric nanocomposite membrane based on interfacial polymerization of polyamide enhanced with green TiO_2 nanoparticles for water desalination. PeerJ Analytical Chemistry, 5: 26.

Ahmad Farid, M.A., Roslan, A.M., Hassan, M.A., Aziz Ujang, F., Mohamad, Z., Hasan, M.Y. & Yoshihito, S. 2019. Convective sludge drying by rotary drum dryer using waste steam for palm oil mill effluent treatment. Journal of Cleaner Production, 240.

Akther, N., Ali, S.M., Phuntsho, S. & Shon, H. 2020. Surface modification of thin-film composite forward osmosis membranes with polyvinyl alcohol–graphene oxide composite hydrogels for antifouling properties. Desalination, 491(April): 114591. https://doi.org/10.1016/j.desal.2020.114591.

Alaqarbeh, M. 2021. Adsorption Phenomena: Definition, Mechanisms, and Adsorption Types: Short Review. RHAZES: Green and Applied Chemistry, 13: 43–51.

Al-Hobaib, A.S., Al-Suhybani, M.S., Al-Sheetan, K.M., Mousa, H. & Shaik, M.R. 2016. New RO TFC membranes by interfacial polymerization in n-Dodecane with various co-solvents. Membranes, 6(2).

Al-Juboori, R.A. & Yusaf, T. 2012. Biofouling in RO system: Mechanisms, monitoring and controlling. Desalination, 302: 1–23. http://dx.doi.org/10.1016/j.desal.2012.06.016.

Ansari, A., Peña-Bahamonde, J., Wang, M., Shaffer, D.L., Hu, Y. & Rodrigues, D.F. 2021. Polyacrylic acid-brushes tethered to graphene oxide membrane coating for scaling and biofouling mitigation on reverse osmosis membranes. Journal of Membrane Science, 630(2020).

Aragaw, T.A. & Bogale, F.M. 2023. Role of coagulation/flocculation as a pretreatment option to reduce colloidal/bio-colloidal fouling in tertiary filtration of textile wastewater: A review and future outlooks. Frontiers in Environmental Science, 11.

Armendáriz-Ontiveros, M.M., Álvarez-Sánchez, J., Dévora-Isiordia, G.E., García, A. & Fimbres Weihs, G.A. 2020. Effect of seawater variability on endemic bacterial biofouling of a reverse osmosis membrane coated with iron nanoparticles (FeNPs). Chemical Engineering Science, 223: 1–10.

Armstrong, M.W., Gallego, S. & Chesters, S.P. 2011. Removing biofilm from membranes--a practical approach. In Qingdao International Conference on Desalination and Water Reuse, Qingdao, China.

Ashfaq, M.Y., Al-Ghouti, M.A. & Zouari, N. 2020. Functionalization of reverse osmosis membrane with graphene oxide to reduce both membrane scaling and biofouling. Carbon, 166: 374–387. https://doi.org/10.1016/j.carbon.2020.05.017.

Aziz, M. & Kasongo, G. 2019. Scaling prevention of thin film composite polyamide Reverse Osmosis membranes by Zn ions. Desalination, 464(April): 76–83. https://doi.org/10.1016/j.desal.2019.04.021.

Aziz, M. & Kasongo, G. 2021. The removal of selected inorganics from municipal membrane bioreactor wastewater using UF/NF/RO membranes for water reuse application: A pilot-scale study. Membranes, 11(2): 1–14.

Aziz, M. & Ojumu, T. 2020. Exclusion of estrogenic and androgenic steroid hormones from municipal membrane bioreactor wastewater using UF/NF/RO membranes for water reuse application. Membranes, 10(3).

Bai, W., Samineni, L., Chirontoni, P., Krupa, I., Kasak, P., Popelka, A., Saleh, N.B. & Kumar, M. 2023. Quantifying and reducing concentration polarization in reverse osmosis systems. Desalination, 554.

Bera, S.P., Godhaniya, M. & Kothari, C. 2022. Emerging and advanced membrane technology for wastewater treatment: A review. Journal of Basic Microbiology, 62(3–4): 245–259.

Bermúdez, L.A., Pascual, J.M., Martínez, M.D.M.M. & Capilla, J.M.P. 2021. Effectiveness of advanced oxidation processes in wastewater treatment: State of the art. Water (Switzerland), 13(15).

Bet-Moushoul, E., Mansourpanah, Y., Farhadi, K. & Tabatabaei, M. 2016. TiO_2 nanocomposite based polymeric membranes: A review on performance improvement for various applications in chemical engineering processes. Chemical Engineering Journal, 283: 29–46. http://dx.doi.org/10.1016/j.cej.2015.06.124.

Beyene, H.D., Hailegebrial, T.D. & Direrssa, W.B. 2016. Investigation of Coagulation Activity of Cactus Powder in Water Treatment. Journal of Applied Chemistry, 2016.

de Boer, S., González-Rodríguez, J., Conde, J.J. & Moreira, M.T. 2022. Benchmarking tertiary water treatments for the removal of micropollutants and pathogens based on operational and sustainability criteria. Journal of Water Process Engineering, 46.

Borah, G. 2025. Urban Water Stress: Climate Change Implications for Water Supply in Cities. Water Conservation Science and Engineering, 10(1): 20.

Çankaya, S. 2023. Evaluation of the impact of water reclamation on blue and grey water footprint in a municipal wastewater treatment plant. Science of the Total Environment, 903.

Chakawa, S. & Aziz, M. 2021. Investigating the result of current density, temperature, and electrolyte concentration on cod: Subtraction of petroleum refinery wastewater using response surface methodology. Water (Switzerland), 13(6).

Chang, C., Yu, X., Guo, W., Guo, C., Guo, X., Li, Q. & Zhu, Y. 2022. Bacteriophage-Mediated Control of Biofilm: A Promising New Dawn for the Future. Frontiers in Microbiology, 13.

Cheng, Q., Zheng, Y., Yu, S., Zhu, H., Peng, X., Liu, Jia, Liu, Jingqun, Liu, M. & Gao, C. 2013. Surface modification of a commercial thin-film composite polyamide reverse osmosis membrane through graft polymerization of N-isopropylacrylamide followed by acrylic acid. Journal of Membrane Science, 447: 236–245. http://dx.doi.org/10.1016/j.memsci.2013.07.025.

Choi, W., Lee, C., Yoo, C.H., Shin, M.G., Lee, G.W., Kim, T.S., Jung, H.W., Lee, J.S. & Lee, J.H. 2020. Structural tailoring of sharkskin-mimetic patterned reverse osmosis membranes for optimizing biofouling resistance. Journal of Membrane Science, 595(August 2019): 117602. https://doi.org/10.1016/j.memsci.2019.117602.

Covaliu-Mierlă, C.I., Păunescu, O. & Iovu, H. 2023. Recent Advances in Membranes Used for Nanofiltration to Remove Heavy Metals from Wastewater: A Review. Membranes, 13(7).

Creber, S.A., Vrouwenvelder, J.S., van Loosdrecht, M.C.M. & Johns, M.L. 2010. Chemical cleaning of biofouling in reverse osmosis membranes evaluated using magnetic resonance imaging. Journal of Membrane Science, 362(1–2): 202–210. http://dx.doi.org/10.1016/j.memsci.2010.06.052.

Davis, R. & Mauer, L. 2010. Fourier transform infrared (FT-IR) spectroscopy: a rapid tool for detection and analysis of foodborne pathogenic bacteria. Current Research, Technology and Education Topics in Applied Microbiology and Microbial Biotechnology. A. Méndez-Vilas (Ed.), (1): 1582–1594. http://www.formatex.info/microbiology2/1582-1594.pdf.

Diallo, H.M., Ayyoub, H., Elazhar, F., Tahaikt, M., Elmidaoui, A. & Taky, M. 2024. Evaluation of the potential ultrafiltration to improve the quality of secondary effluents in tertiary treatment and reuse. Physics and Chemistry of the Earth, Parts A/B/C, 135: 103672.

Dimane, F. & El Hammoudani, Y. 2021. Assessment of quality and potential reuse of wastewater treated with conventional activated sludge. In Materials Today: Proceedings.

Dolina, J., Dlask, O., Lederer, T. & Dvořák, L. 2015. Mitigation of membrane biofouling through surface modification with different forms of nanosilver. Chemical Engineering Journal, 275: 125–133.

Donald, A.N., Asif, M., Felicien, S. & Ali, S. 2022. A review on the centralised municipal sewage and wastewater treatment unit processes. MOJ Ecology & Environmental Sciences, 7(2).

Duan, L., Yun, Q., Jiang, G., Teng, D., Zhou, G. & Cao, Y. 2024. A review of chloride ions removal from high chloride industrial wastewater: Sources, hazards, and mechanisms. Journal of Environmental Management, 353.

Egorova, A., Xia, B., Vyas, H.K.N., Armendáriz-Ontiveros, M.M., Lin, Y.-C., Garcia-Garcia, A., Wang, D.K., Cullen, P.J., Fimbres Weihs, G. & Mai-Prochnow, A. 2024. Iron nanoparticle coating and plasma-activated water cleaning as a biofouling removal method for reverse osmosis membranes suitable for desalination. Journal of Water Process Engineering, 59: 105043. https://linkinghub.elsevier.com/retrieve/pii/S2214714424002757.

El-Fattah, W.A., Guesmi, A., Ben Hamadi, N., Alzahrani, A., Hosni, M. & Shahat, A. 2025. Graphene oxide-modified thin-film composite membranes for sustainable petroleum refinery

wastewater treatment via an integrated biological/forward osmosis system. Process Safety and Environmental Protection, 200.

Ezugbe, E.O. & Rathilal, S. 2020. Membrane technologies in wastewater treatment: A review. Membranes, 10(5).

Gao, F., Li, C., Yang, Z.H., Zeng, G.M., Mu, J., Liu, M. & Cui, W. 2016. Removal of nutrients, organic matter, and metal from domestic secondary effluent through microalgae cultivation in a membrane photobioreactor. Journal of Chemical Technology and Biotechnology, 91(10): 2713–2719.

Gao, Q., Duan, L., Jia, Y., Zhang, H., Liu, J. & Yang, W. 2023. A Comprehensive Analysis of the Impact of Inorganic Matter on Membrane Organic Fouling: A Mini Review. Membranes, 13(10).

García, A., Rodríguez, B., Giraldo, H., Quintero, Y., Quezada, R., Hassan, N. & Estay, H. 2021. Copper-modified polymeric membranes for water treatment: A comprehensive review. Membranes, 11(2): 1–47.

Garny, K., Neu, T.R., Horn, H., Volke, F. & Manz, B. 2010. Combined application of 13C NMR spectroscopy and confocal laser scanning microscopy-Investigation on biofilm structure and physico-chemical properties. Chemical Engineering Science, 65(16): 4691–4700. http://dx.doi.org/10.1016/j.ces.2010.05.013.

Gayed, H.M., El Fadl, F.I.A., Maziad, N.A., El-Aassar, A.H.M. & Abdel-Mottaleb, M.S.A. 2019. Surface modification of composite polyamide reverse osmosis membrane by irradiated chitosan and TiO_2 nanoparticles. Desalination and Water Treatment, 160: 32–40.

Giwa, A., Akther, N., Dufour, V. & Hasan, S.W. 2016. A critical review on recent polymeric and nano-enhanced membranes for reverse osmosis. RSC Advances, 6(10): 8134–8163.

Herzberg, M., Sweity, A., Brami, M., Kaufman, Y., Freger, V., Oron, G., Belfer, S. & Kasher, R. 2011. Surface properties and reduced biofouling of graft-copolymers that possess oppositely charged groups. Biomacromolecules, 12(4): 1169–1177.

Ho, Q.N., Fettweis, M., Spencer, K.L. & Lee, B.J. 2022. Flocculation with heterogeneous composition in water environments: A review. Water Research, 213.

Hossain, M.S., Sarker, P., Rahaman, M.S., Ahmed, F.F., Shaibur, M.R. & Khabir Uddin, M. 2022. Biological Treatment of Textile Wastewater by Total Aerobic Mixed Bacteria and Comparison with Chemical Fenton Process. Pollution, 8(4).

Hu, H., Ma, S., Zhang, X. & Ren, H. 2020. Characteristics of dissolved organic nitrogen in effluent from a biological nitrogen removal process using sludge alkaline fermentation liquid as an external carbon source. Water Research, 176.

Hu, Y., Lu, K., Yan, F., Shi, Y., Yu, P., Yu, S. & Li, S. 2016. Enhancing the performance of aromatic polyamide reverse osmosis membrane by surface modi fi cation via covalent attachment of polyvinyl alcohol (PVA). , 501: 209–219.

Islam, F.A.S. 2025. Advanced Wastewater Treatment Technologies in Addressing Future Water Scarcity through Resource Recovery and Reuse. Journal of Engineering Research and Reports, 27(5): 370–398.

Jayaramaiah, S. & Dawn, S. 2025. Preliminary evaluation of biomass and lipid production potential of Nannochloropsis sp. under optimal conditions with different wastewater samples for Exopolymeric substances (EPS) production. BIO Web of Conferences, 172: 01003.

Jeon, S. & Lee, J.H. 2020. Rationally designed in-situ fabrication of thin film nanocomposite membranes with enhanced desalination and anti-biofouling performance. Journal of Membrane Science, 615(July): 118542. https://doi.org/10.1016/j.memsci.2020.118542.

Jeon, S., Shin, S.S., Park, C.H. & Lee, J.H. 2021. Star polymer-mediated in-situ synthesis of silver-incorporated reverse osmosis membranes with excellent and durable biofouling resistance. Journal of Membrane Science, 639(August): 119778. https://doi.org/10.1016/j.memsci.2021.119778.

Jia, H., Zhao, Q., Zhang, D., Shi, W., Gong, G. & Hu, Y. 2025. Designing high flux and antifouling PA RO membrane based on the surface modification with glycerol and dimethyldimethoxysilane. Desalination, 600.

Jiang, S., Li, Y. & Ladewig, B.P. 2017. A review of reverse osmosis membrane fouling and control strategies. Science of the Total Environment, 595: 567–583. http://dx.doi.org/10.1016/j.scitotenv.2017.03.235.

Joshi, K.K. & Soni, H.B. 2025. Genomic insights into chlorination effects on the development of bacterial antibiotic resistance during wastewater treatment – a review. Life Science Leaflets, 185: 19–28.

Jung, Y., Alayande, A.B., Chae, S. & Kim, I.S. 2018. Applications of nisin for biofouling mitigation of reverse osmosis membranes. Desalination, 429(June 2017): 52–59. https://doi.org/10.1016/j.desal.2017.12.003.

Kacaribu, A.A., Aisyah, Y., Febriani & Darwin. 2025. Development of wastewater treatment methods for palm oil mill effluent (POME): A comprehensive review. Resources Chemicals and Materials, 4(4): 100130.

Kalam, S., Abu-Khamsin, S.A., Kamal, M.S. & Patil, S. 2021. Surfactant Adsorption Isotherms: A Review. ACS Omega, 6(48).

Kasongo, G., Nkombe, A.M. & Aziz, M. 2025. Biofouling Resistance Improvement in Membrane-Based Secondary Effluent Treatment: A Focus on Membrane Surface Modification by Graft Polymerization with 3-Allyl-5, 5-Dimethyl Hydantoin. Membranes, 15(10).

Kasongo, G., Steenberg, C., Morris, B., Kapenda, G., Jacobs, N. & Aziz, M. 2019. Surface grafting of polyvinyl alcohol (PVA) cross-linked with glutaraldehyde (GA) to improve resistance to fouling of aromatic polyamide thin film composite reverse osmosis membranes using municipal membrane bioreactor effluent. Water Practice and Technology, 14(3): 614–624.

Kasongo Wa Kasongo, G. 2018. Enhancement of membrane surface characteristics to improve membrane performance and durability in the treatment of municipal MBR effluent. Cape Peninsula University of Technology.

Kim, J., Shin, M.G., Song, W.J., Park, S.H., Ryu, J., Jung, J., Choi, S.Y., Yu, Y., Kweon, J. & Lee, J.H. 2021. Application of quorum sensing inhibitors for improving anti-biofouling of polyamide reverse osmosis membranes: Direct injection versus surface modification. Separation and Purification Technology, 255(May 2020): 117736. https://doi.org/10.1016/j.seppur.2020.117736.

Kim, T.S., Park, S.H., Park, D., Lee, J.H. & Kang, S. 2019. Surface immobilization of chlorhexidine on a reverse osmosis membrane for in-situ biofouling control. Journal of Membrane Science, 576(October 2018): 17–25. https://doi.org/10.1016/j.memsci.2019.01.030.

Kochkodan, V. & Hilal, N. 2015. A comprehensive review on surface modified polymer membranes for biofouling mitigation. Desalination, 356: 187–207. http://dx.doi.org/10.1016/j.desal.2014.09.015.

Kochkodan, V., Johnson, D.J. & Hilal, N. 2014. Polymeric membranes: Surface modification for minimizing (bio)colloidal fouling. Advances in Colloid and Interface Science, 206: 116–140. http://dx.doi.org/10.1016/j.cis.2013.05.005.

Komlenic, R. 2010. Rethinking the causes of membrane biofouling. Filtration and Separation, 47(5): 26–28. http://dx.doi.org/10.1016/S0015-1882(10)70211-1.

Kotlhao, K., Lawal, I.A., Moutloali, R.M. & Klink, M.J. 2019. Antifouling properties of silver-zinc oxide polyamide thin film composite membrane and rejection of 2-chlorophenol and 2,4-dichlorophenol. Membranes, 9(8).

Kucera, J. 2019. Biofouling of polyamide membranes: Fouling mechanisms, current mitigation and cleaning strategies, and future prospects. Membranes, 9(9).

Latif, E.F. 2022. Applying novel methods in conventional activated sludge plants to treat low-strength wastewater. Environmental Monitoring and Assessment, 194(4).

Lau, W.J., Ismail, A.F., Misdan, N. & Kassim, M.A. 2012. A recent progress in thin fi lm composite membrane : A review. DES, 287: 190–199. http://dx.doi.org/10.1016/j.desal.2011.04.004.

Li, Q., An, L., Shang, C. & Meng, J. 2025. High rejection seawater reverse osmosis TFC membranes with a polyamide-polysulfonamide interpenetrated functional layer. Journal of Membrane Science, 715.

Liu, J., Yang, F., Cai, Y., Lu, G., Li, Y., Li, M., Fan, L. & Gao, L. 2024. Unveiling the existence and ecological hazards of trace organic pollutants in wastewater treatment plant effluents across China. Eco-Environment and Health, 3(1).

Liu, M., Chen, Q., Wang, L., Yu, S. & Gao, C. 2015. Improving fouling resistance and chlorine stability of aromatic polyamide thin- fi lm composite RO membrane by surface grafting of polyvinyl alcohol (PVA). DES, 367: 11–20. http://dx.doi.org/10.1016/j.desal.2015.03.028.

Liu, W., Song, X., Na, Z., Li, G. & Luo, W. 2022. Strategies to enhance micropollutant removal from wastewater by membrane bioreactors: Recent advances and future perspectives. Bioresource Technology, 344.

Liu, Z., Qi, L., An, X., Liu, C. & Hu, Y. 2017. Surface Engineering of Thin Film Composite Polyamide Membranes with Silver Nanoparticles through Layer-by-Layer Interfacial Polymerization for Antibacterial Properties. ACS Applied Materials and Interfaces, 9(46): 40987–40997.

Loh, Z.Z., Zaidi, N.S., Yong, E.L., Anshori, M.Y., Al-Kahtani, A.A., Boopathy, R., Ratnasari, A. & Syafiuddin, A. 2022. Comparative assessments on wastewater treatment technologies for potential of wastewater recycling. Desalination and Water Treatment, 261.

Maeda, Y. 2024. Fouling of Reverse Osmosis (RO) and Nanofiltration (NF) Membranes by Low Molecular Weight Organic Compounds (LMWOCs), Part 1: Fundamentals and Mechanism. Membranes, 14(10).

Manna, M. & Sen, S. 2023. Advanced oxidation process: a sustainable technology for treating refractory organic compounds present in industrial wastewater. Environmental Science and Pollution Research, 30(10).

Maroufi, N. & Hajilary, N. 2023. Nanofiltration membranes types and application in water treatment: a review. Sustainable Water Resources Management, 9(5).

Matin, A., Khan, Z., Zaidi, S.M.J. & Boyce, M.C. 2011. Biofouling in reverse osmosis membranes for seawater desalination: Phenomena and prevention. Desalination, 281(1): 1–16.

Matshetshe, K., Sikhwivhilu, K., Ndlovu, G., Tetyana, P., Moloto, N. & Tetana, Z. 2022. Antifouling and antibacterial β-cyclodextrin decorated graphene oxide/polyamide thin-film nanocomposite reverse osmosis membranes for desalination applications. Separation and Purification Technology, 278(February 2021): 119594. https://doi.org/10.1016/j.seppur.2021.119594.

Al Mayyahi, A. 2018. Important approaches to enhance reverse osmosis (RO) thin film composite (TFC) membranes performance. Membranes, 8(3).

Meena R, A.A., J, M., Banu J, R., Bhatia, S.K., Kumar, V., Piechota, G. & Kumar, G. 2023. A review on the pollution assessment of hazardous materials and the resultant biorefinery products in Palm oil mill effluent. Environmental Pollution, 328.

Miyoshi, Y., Nakata, Y., Kitagawa, T., Matsuyama, H., Yoshioka, T. & Nakagawa, K. 2024. Effect of Surface Modification of Polyamide-Based Reverse Osmosis Membranes by Glycerol Monoacrylate–Butyl Acrylate Copolymers on Antifouling. Industrial & Engineering Chemistry Research. https://pubs.acs.org/doi/10.1021/acs.iecr.4c00153.

Mohamed Noor, M.H., Wong, S., Ngadi, N., Mohammed Inuwa, I. & Opotu, L.A. 2022. Assessing the effectiveness of magnetic nanoparticles coagulation/flocculation in water treatment: a systematic literature review. International Journal of Environmental Science and Technology, 19(7).

Morris, B.G., Aziz, M. & Kasongo, G. 2022. Remediation of laundry wastewater with a low-pressure aromatic polyamide thin-film composite reverse osmosis membrane for membrane fouling minimisation and reuse application. Environment Protection Engineering, 48(2).

Mortula, M.M., Abdelrahman, M. & Tatan, B. 2022. Comparative Evaluation of Membrane Filtration on the Tertiary Treatment of Synthetic Secondary Effluent. Separations, 9(3).

Mujahid Aziz & Godwill Kasongo. 2021. Improving Resistance to Fouling of Aromatic Polyamide Thin-Film Composite Reverse Osmosis Membrane by Surface Grafting of N,N'-Dimethyl Aminoethyl Methacrylate (DMAEMA). Journal of Water Chemistry and Technology, 43(4): 312–320.

Mushtaq, R., Abbas, M.A., Mushtaq, S., Ahmad, N.M., Khan, N.A., Khan, A.U., Hong, W., Sadiq, R. & Jiang, Z. 2021. Antifouling and flux enhancement of reverse osmosis membrane by grafting poly (3-sulfopropyl methacrylate) brushes. Membranes, 11(3): 1–16.

Myburgh, D.P., Aziz, M., Roman, F., Jardim, J. & Chakawa, S. 2019. Removal of COD from Industrial Biodiesel Wastewater Using an Integrated Process: Electrochemical-Oxidation with IrO2-Ta2O5/Ti Anodes and Chitosan Powder as an Adsorbent. Environmental Processes, 6(4).

Nagaraj, V., Skillman, L., Li, D. & Ho, G. 2018. Review – Bacteria and their extracellular polymeric substances causing biofouling on seawater reverse osmosis desalination membranes. Journal of Environmental Management, 223 (2017): 586–599. https://doi.org/10.1016/j.jenvman.2018.05.088.

Namla, D., Oves, M., Alshaeri, M.A., Al-Maaqar, S.M., Issa, H.N.Y. & Mangse, G. 2025. Nanofiltration as an advanced wastewater treatment technique: a comprehensive review. Discover Applied Sciences, 7(4).

Ngo, T.H.A., Nguyen, C.T.M., Do, K.D., Duong, Q.X., Tran, N.H., Nguyen, H.T.V. & Tran, D.T. 2020. Improvement of Hydrophilicity for Polyamide Composite Membrane by Incorporation of Graphene Oxide-Titanium Dioxide Nanoparticles. Journal of Analytical Methods in Chemistry, 2020.

Ong, C.S., Goh, P.S., Lau, W.J., Misdan, N. & Ismail, A.F. 2016. Nanomaterials for biofouling and scaling mitigation of thin film composite membrane: A review. Desalination, 393: 2–15. http://dx.doi.org/10.1016/j.desal.2016.01.007.

Pandis, P.K., Kalogirou, C., Kanellou, E., Vaitsis, C., Savvidou, M.G., Sourkouni, G., Zorpas, A.A. & Argirusis, C. 2022. Key Points of Advanced Oxidation Processes (AOPs) for Wastewater, Organic Pollutants and Pharmaceutical Waste Treatment: A Mini Review. ChemEngineering, 6(1).

Perreault, F., Tousley, M.E. & Elimelech, M. 2014. Thin-Film Composite Polyamide Membranes Functionalized with Biocidal Graphene Oxide Nanosheets Thin-Film Composite Polyamide Membranes Functionalized with Biocidal Graphene Oxide Nanosheets Environmental Science & Technology Letters. Environmental Science and Technology Letters, 1(1): 71–76.

Peyki, A., Rahimpour, A. & Jahanshahi, M. 2015. Preparation and characterization of thin film composite reverse osmosis membranes incorporated with hydrophilic SiO2 nanoparticles. Desalination, 368: 152–158. http://dx.doi.org/10.1016/j.desal.2014.05.025.

Plevri, A., Mamais, D. & Noutsopoulos, C. 2021. Anaerobic MBR technology for treating municipal wastewater at ambient temperatures. Chemosphere, 275.

Qasim, M., Badrelzaman, M., Darwish, N.N., Darwish, N.A. & Hilal, N. 2019. Reverse osmosis desalination: A state-of-the-art review. Desalination, 459: 59–104.

Rahman, T.U., Roy, H., Islam, M.R., Tahmid, M., Fariha, A., Mazumder, A., Tasnim, N., Pervez, M.N., Cai, Y., Naddeo, V. & Islam, M.S. 2023. The Advancement in Membrane Bioreactor (MBR) Technology toward Sustainable Industrial Wastewater Management. Membranes, 13(2).

Roman, F. & Aziz, M. 2021. The Remediation of Carwash Wastewater with Chemical Coagulation and Adsorption Process. South African Chemical Engineering Congress: 68–91.

Saeki, D., Yonamine, G. & Matsuyama, H. 2021. Effect of hydrophilic polymer modification of reverse osmosis membrane surfaces on organic adsorption and biofouling behavior. Colloids and Surfaces A: Physicochemical and Engineering Aspects, 609(October 2020): 125680. https://doi.org/10.1016/j.colsurfa.2020.125680.

Safarpour, M., Khataee, A. & Vatanpour, V. 2015. Thin film nanocomposite reverse osmosis membrane modified by reduced graphene oxide/TiO_2 with improved desalination performance. Journal of Membrane Science, 489: 43–54.

Saffarimiandoab, F., Yavuzturk Gul, B., Erkoc-Ilter, S., Guclu, S., Unal, S., Tunaboylu, B., Menceloglu, Y.Z. & Koyuncu, I. 2019. Evaluation of biofouling behavior of zwitterionic silane coated reverse osmosis membranes fouled by marine bacteria. Progress in Organic Coatings, 134(May): 303–311.

Saravanan, A., Deivayanai, V.C., Kumar, P.S., Rangasamy, G., Hemavathy, R. V., Harshana, T., Gayathri, N. & Alagumalai, K. 2022. A detailed review on advanced oxidation process in treatment of wastewater: Mechanism, challenges and future outlook. Chemosphere, 308.

Saravanan, R., Sathish, T., Sharma, K., Rao, A.V., Sathyamurthy, R., Panchal, H. & Abdul Zahra, M.M. 2023. Sustainable wastewater treatment by RO and hybrid organic polyamide membrane nanofiltration system for clean environment. Chemosphere, 337.

Sathya, K., Nagarajan, K., Carlin Geor Malar, G., Rajalakshmi, S. & Raja Lakshmi, P. 2022. A comprehensive review on comparison among effluent treatment methods and modern methods of treatment of industrial wastewater effluent from different sources. Applied Water Science, 12(4).

Selvasembian, R., Mal, J., Rani, R., Sinha, R., Agrahari, R., Joshua, I., Santhiagu, A. & Pradhan, N. 2022. Recent progress in microbial fuel cells for industrial effluent treatment and energy generation: Fundamentals to scale-up application and challenges. Bioresource Technology, 346.

Shabib, A., Tatan, B., Elbaz, Y., Aly Hassan, A., Hamouda, M.A. & Maraqa, M.A. 2025. Advancements in reverse osmosis desalination: Technology, environment, economy, and bibliometric insights. Desalination, 598.

Shafi, H.Z., Matin, A., Akhtar, S., Gleason, K.K., Zubair, S.M. & Khan, Z. 2017. Organic fouling in surface modified reverse osmosis membranes: Filtration studies and subsequent morphological

and compositional characterization. Journal of Membrane Science, 527(2017): 152–163. http://dx.doi.org/10.1016/j.memsci.2017.01.017.

Shahzad, A., Oh, J.M., Azam, M., Iqbal, J., Hussain, S., Miran, W. & Rasool, K. 2021. Advances in the synthesis and application of anti-fouling membranes using two-dimensional nanomaterials. Membranes, 11(8).

Sharabati, J.A.D., Guclu, S., Erkoc-Ilter, S., Koseoglu-Imer, D.Y., Unal, S., Menceloglu, Y.Z., Ozturk, I. & Koyuncu, I. 2019. Interfacially polymerized thin-film composite membranes: Impact of support layer pore size on active layer polymerization and seawater desalination performance. Separation and Purification Technology, 212(2018): 438–448. https://doi.org/10.1016/j.seppur.2018.11.047.

Shen, L., Huang, Z., Liu, Y., Li, R., Xu, Y., Jakaj, G. & Lin, H. 2020. Polymeric Membranes Incorporated With ZnO Nanoparticles for Membrane Fouling Mitigation: A Brief Review. Frontiers in Chemistry, 8(April): 1–9.

Shoba Vincent, A. & Ramadoss, R. 2025. Bioinformatics Revolution in Wastewater Treatment Process Optimization. In Wastewater Treatment - Current Insights. IntechOpen.

Solcova, O., Dlaskova, M. & Kastanek, F. 2024. Challenges and Advances in Tertiary Waste Water Treatment for Municipal Treatment Plants. Processes, 12(10): 2084.

Song, M., Im, S.J., Jeong, D. & Jang, A. 2020. Reduction of biofouling potential in cartridge filter by using chlorine dioxide for enhancing anti-biofouling of seawater reverse osmosis membrane. Environmental Research, 180(October 2019): 108866. https://doi.org/10.1016/j.envres.2019.108866.

Sukmana, H., Bellahsen, N., Pantoja, F. & Hodur, C. 2021. Adsorption and coagulation in wastewater treatment - Review. Progress in Agricultural Engineering Sciences, 17(1).

Suwarno, S.R., Hanada, S., Chong, T.H., Goto, S., Henmi, M. & Fane, A.G. 2016. The effect of different surface conditioning layers on bacterial adhesion on reverse osmosis membranes. DES, 387: 1–13. http://dx.doi.org/10.1016/j.desal.2016.02.029.

Tayeh, Y.A., Alazaiza, M.Y.D., Alzghoul, T.M. & Bashir, M.J. 2025. A comprehensive review of RO membrane fouling: Mechanisms, categories, cleaning methods and pretreatment technologies. Journal of Hazardous Materials Advances, 18.

Thushari, G.G.N., Guruge, K.P.G., Abeygunawardana, A.P. & Senevirathna, J.D.M. 2025. Wastewater as a Source of Microplastic Pollution: Fate and Risk on Biota. In Microplastics: Ecological and Food Security Implications. Cham: Springer Nature Switzerland: 89–157.

Torres, J.J., Cuello, M., Ochoa, N.A. & Pagliero, C. 2021. Biodiesel wastewater treatment using nanofiltration membranes. Process Safety and Environmental Protection, 148.

Tran, H.N. 2023. Adsorption Technology for Water and Wastewater Treatments. Water (Switzerland), 15(15).

Tripathy, S., Kar, O.P. & Pradhan, A. 2025. Challenges and Innovations in Industrial Wastewater Treatment: Safeguarding Water Resources and Promoting Sustainable Practices. Water, Air, & Soil Pollution, 236(2): 92.

Ustun Odabasi, S. & Buyukgungor, H. 2024. Comparative study of degradation of pharmaceutical and personal care products in wastewater by advanced oxidation processes: Fenton, UV/H2O2, UV/TiO_2. Clean - Soil, Air, Water, 52(2).

Vatanpour, V., Camadan, I., Kara, N., Naziri Mehrabani, S.A., Feizpoor, S., Habibi-Yangjeh, A. & Koyuncu, I. 2024. TiO_2/AgBr nanocomposite as a novel hydrophilic and photocatalytic modifier in the fabrication of polyethersulfone membrane for wastewater treatment. Separation and Purification Technology, 349.

Wang, J., Hao, S., Qi, P., Wang, W. & Hu, Y. 2024. Superior chlorine-resistance of hyperbranched polyglycerol (hPG) grafted polyamide reverse osmosis membrane and its chlorine-resistant mechanism. Journal of Membrane Science, 709.

Wang, J. & Zhuan, R. 2020. Degradation of antibiotics by advanced oxidation processes: An overview. Science of the Total Environment, 701.

Wang, Jing, Wang, Z., Wang, Jixiao & Wang, S. 2015. Improving the water flux and bio-fouling resistance of reverse osmosis (RO) membrane through surface modification by zwitterionic polymer. Journal of Membrane Science, 493: 188–199. http://dx.doi.org/10.1016/j.memsci.2015.06.036.

Wang, P., Shao, Y., Geng, Y., Mushtaq, R., Yang, W., Li, M., Sun, X., Wang, H. & Chen, G. 2023. Advanced treatment of secondary effluent from wastewater treatment plant by a newly isolated microalga Desmodesmus sp. SNN1. Frontiers in Microbiology, 14.

Wang, T., Hou, Z., Yang, H. & Hu, J. 2024. A PEGylated PVDF Antifouling Membrane Prepared by Grafting of Methoxypolyethylene Glycol Acrylate in Gama-Irradiated Homogeneous Solution. Materials, 17(4).

Wang, Y.H., Wu, Y.H., Tong, X., Yu, T., Peng, L., Bai, Y., Zhao, X.H., Huo, Z.Y., Ikuno, N. & Hu, H.Y. 2019. Chlorine disinfection significantly aggravated the biofouling of reverse osmosis membrane used for municipal wastewater reclamation. Water Research, 154: 246–257. https://doi.org/10.1016/j.watres.2019.02.008.

Waqas, M.R., Nadeem, S.M., Khan, M.Y., Ahmad, Z., Ali, L., Asghar, H.N. & Khalid, A. 2022. Phycoremediation of textile effluents with enhanced efficacy of biodiesel production by algae and potential use of remediated effluent for improving growth of wheat. Environmental Science and Pollution Research, 29(30).

Wei, X., Wang, Z., Zhang, Z., Wang, J. & Wang, S. 2010. Surface modification of commercial aromatic polyamide reverse osmosis membranes by graft polymerization of 3-allyl-5, 5-dimethylhydantoin. Journal of Membrane Science, 351(1–2): 222–233. http://dx.doi.org/10.1016/j.memsci.2010.01.054.

Weinrich, L., LeChevallier, M. & Haas, C.N. 2016. Contribution of assimilable organic carbon to biological fouling in seawater reverse osmosis membrane treatment. Water Research, 101: 203–213. http://dx.doi.org/10.1016/j.watres.2016.05.075.

Wu, H., Brighton, K., Chen, J., Shuai, D. & Aw, T.G. 2025. Quantification of Particle-Associated Viruses in Secondary Treated Wastewater Effluent. Food and Environmental Virology, 17(1): 19.

Xiao, J., Hao, S., Qin, Y., Qi, P., Zhang, Z. & Hu, Y. 2024. Fouling-resistant reverse osmosis membranes grafted with 2-aminoethanethiol having a low interaction energy with charged foulants. npj Clean Water, 7(1).

Xing, M., Zhang, H., Li, Z., Zhang, L. & Qian, W. 2024. Long-lasting renewable antibacterial N-halamine coating enable dental unit waterlines to prevention and control of contamination of dental treatment water. Frontiers in Materials, 11.

Xu, G.R., Wang, J.N. & Li, C.J. 2013. Strategies for improving the performance of the polyamide thin film composite (PA-TFC) reverse osmosis (RO) membranes: Surface modifications and nanoparticles incorporations. Desalination, 328: 83–100. http://dx.doi.org/10.1016/j.desal.2013.08.022.

Xu, J., Wang, Z., Yu, L., Wang, J. & Wang, S. 2013. A novel reverse osmosis membrane with regenerable anti-biofouling and chlorine resistant properties. Journal of Membrane Science, 435: 80–91. http://dx.doi.org/10.1016/j.memsci.2013.02.010.

Yang, J., Song, J., Gao, X., Li, M., Qin, H., Niu, Y., Luan, H., Chen, X., Guo, J., Yuan, T. & Liu, W. 2024. Integrated toxicity of secondary, tertiary, wetland effluents on human stem cells triggered by ERα and PPARγ agonists. Science of The Total Environment, 937: 173419.

Yang, Z., Saeki, D. & Matsuyama, H. 2018. Zwitterionic polymer modification of polyamide reverse-osmosis membranes via surface amination and atom transfer radical polymerization for anti-biofouling. Journal of Membrane Science, 550(2017): 332–339. https://doi.org/10.1016/j.memsci.2018.01.001.

Yang, Z., Saeki, D., Takagi, R. & Matsuyama, H. 2020. Improved anti-biofouling performance of polyamide reverse osmosis membranes modified with a polyampholyte with effective carboxyl anion and quaternary ammonium cation ratio. Journal of Membrane Science, 595(2019): 117529. https://doi.org/10.1016/j.memsci.2019.117529.

Yang, Z., Takagi, R., Zhang, X., Yasui, T., Zhang, L. & Matsuyama, H. 2021. Engineering a dual-functional sulfonated polyelectrolyte-silver nanoparticle complex on a polyamide reverse osmosis membrane for robust biofouling mitigation. Journal of Membrane Science, 618(2020): 118757. https://doi.org/10.1016/j.memsci.2020.118757.

Zaki, N., Hadoudi, N., Charki, A., Bensitel, N., Ouarghi, H. El, Amhamdi, H. & Ahari, M. 2023. Advancements in the chemical treatment of potable water and industrial wastewater using the coagulation–flocculation process. Separation Science and Technology, 58(15–16).

Zhang, R., Braeken, L., Liu, T., Luis, P., Wang, X. & Bruggen, B. Van Der. Remarkable Anti-Fouling Performance of TiO_2-Modified TFC Membranes with Mussel-Inspired Polydopamine Binding. *Applied Sciences*,*7*(1): 81. https://doi.org/10.3390/app7010081

Zhou, Q., Sun, H., Jia, L., Wu, W. & Wang, J. 2022. Simultaneous biological removal of nitrogen and phosphorus from secondary effluent of wastewater treatment plants by advanced treatment: A review. Chemosphere, 296: 134054.

Chapter 3

METHODOLOGY

3.1 Introduction

The different experimental phases of the project are presented in this section. The methodology has been divided into 3 sections as follows:

- Membrane surface modification using DMAEMA, surface characterisation and lab-scale fouling experimental tests
- Membrane surface modification using ADMH, surface characterisation, biofouling tests and lab-scale membrane performance tests.
- Membrane surface modification using ADMH\TiO_2-Ag, surface characterization, fouling and membrane performance tests.

3.2 Membrane surface modification using DMAEMA

3.2.1 Materials and methods

(I) Materials and reagents

A commercial spiral wound aromatic polyamide (PA) thin-film composite (TFC) extra-low energy (XLE) reverse osmosis (RO) membrane (Dow Filmtec XLE4040) was purchased from Water Components South Africa (Pty) Ltd. *Escherichia coli* ATCC 11303^{TM} strains were used for the biofouling tests and were obtained from LGC Standards, South Africa. Nutrient broth (NB), Nutrient agar (NA), and petri dishes were purchased from Lasec South Africa (Pty) Ltd. Ammonium phosphate ($(NH_4)_2PO_4$) and sodium metabisulfite ($Na_2S_2O_5$) were of laboratory grade and used without purification. Dimethyl amino ethyl methacrylate (DMAEMA), potassium persulfate ($K_2S_2O_8$), sodium chloride (NaCl), potassium chloride (KCl), sodium bicarbonate ($NaHCO_3$), magnesium sulphate ($MgSO_4$), calcium sulphate ($CaSO_4$), humic acid and sulfuric acid (H_2SO_4) were all obtained from Sigma Aldrich (Pty) Ltd, South Africa and were all analytical grade, used without further purification. Deionised (DI) water obtained from a Millipore water purification system is used to prepare solutions and for soaking and rinsing of membranes. DI water used for biofouling tests and solution preparation was further sterilised at 121 ºC in the autoclave.

3.2.2 Redox-initiated grafting of DMAEMA

Membrane samples were peeled and cut from the spiral wound module into a flat sheet of 18 cm length and 12 cm width. DI water was used to thoroughly rinse the membrane and remove preservatives before drying at room temperature (Kasongo et al., 2019). The membrane was then wrapped around a rectangular frame with the layer facing the inner part of the frame to allow complete contact with the modifying agent solution. The modifying solutions of fixed concentrations (0. 025 mol. L^{-1}, 0.05 mol. L^{-1}, 0.075 mol. L^{-1} and 0.1 mol. L^{-1} DMAEMA) contained sodium

metabisulfite (0.5 mol% of DMAEMA) and potassium persulfate (0.5 mol% of DMAEMA). The modification was conducted by pouring a DMAEMA solution onto the surface of the membrane, which was fixed around a rectangular frame and the oven's membrane, for an hour at 30 °C The modified membrane was then rinsed meticulously and preserved in DI water for experimental fouling test and structure analysis.

3.2.3 Characterisation of the modified and unmodified membrane

ATR-FTIR was conducted using a Thermo Scientific Nicolet iS10 spectrometer equipped with an internal reflecting diamond element to examine the chemical structure of the modified membranes. Spectra within the wavenumber range from 4000 to 650 cm^{-1} were composed by accruing 64 scans at a resolution of 4cm^{-1}. Spectra were corrected for atmospheric background and baseline. SEM images were obtained using the Nova NanoSEM instrument to study both unmodified and modified membranes' surface features. Top-view images of the surfaces were scanned at magnifications of 40 000, while cross-sections were scanned at magnifications of 1 000 times with a landing electron of 5.00 keV.

3.2.4 Membrane performance and antifouling evaluations

Membrane performance and antifouling experimental tests were conducted on a bench-scale RO system consisting of a cell (crossflow SEPA CF II RO unit) with a hydra-cell pump (model: G20BDSTHFECG), as shown in Figure 9. LabVIEW software was used to control and monitor the operating conditions of the RO systems. Membranes were flushed overnight with DI water (≈ 5 µS/cm) before fouling experiments. Fouling experiments were conducted for 42 hours at initial conditions of 5 bar feed pressure and 19 $cm.s^{-1}$ crossflow velocity at room temperature, while the transmembrane pressure was kept constant. The brine stream was recycled back to the feed tank to ensure a constant feed concentrate solution, thus mimicking high flux recovery in commercial applications (Zhao et al., 2010). Time-dependent flux and streams' electroconductivity (EC) and total dissolved solids were recorded at 45-minute intervals.

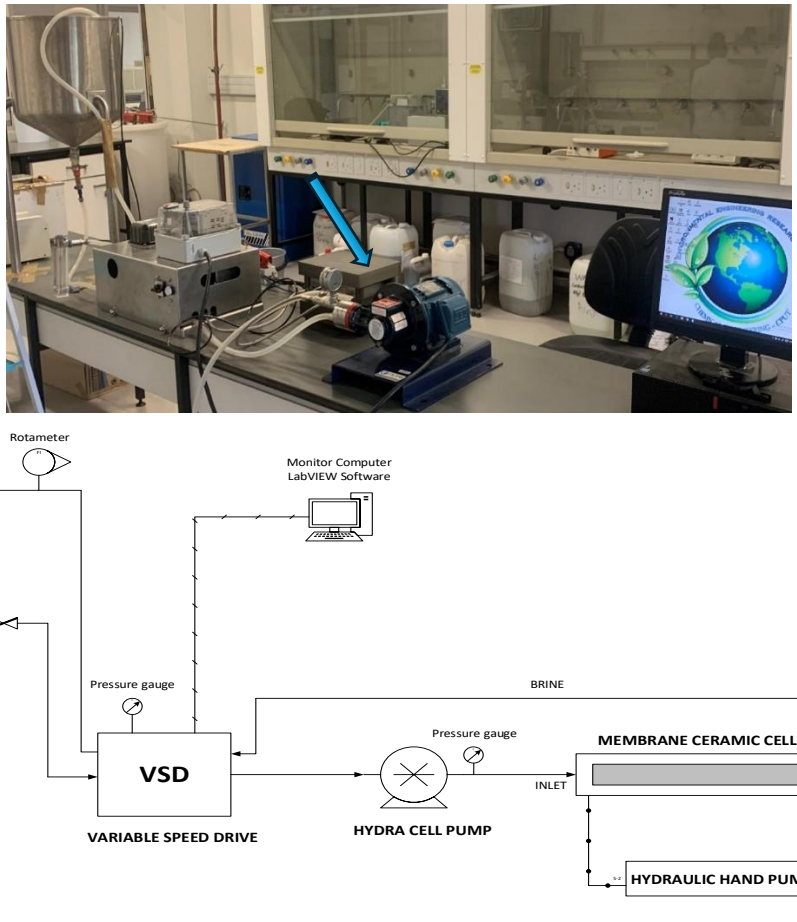


Figure 9: Photo (up) and process flow diagram (down) of the lab-scale flat cell RO system used for membrane performance and antifouling capability tests.

Table 4 shows the composition of the solution simulating the secondary effluent from an MBR municipal wastewater treatment plant (Giannakis et al., 2013; Rivas et al., 2015). The pH of the feed solution was approximately 6

Table 4. Synthetic feed solution composition

Chemical composition	Concentration (mg/L)
Potassium chloride	4
Dipotassium phosphate	7
Sodium chloride	7
Sodium bicarbonate	93
Magnesium sulphate	60
Ammonium sulphate	60
Calcium sulphate	60
Humic acid	5

The salt rejection, R (%) of the membrane was evaluated using the permeate conductivity, C_p (μScm^{-1}), and feed conductivity, C_f(μScm^{-1}), as shown in equation (1); The EC (Electric conductivity) was measured using a conductivity meter (YSI EcoSense EC300, YSI Inc., USA). The water flux (J) was evaluated using the permeate volume, V (m^3), collected for a given time, ΔT (hr), through the active surface area of the membrane, A (m^2), as shown in equation (2) (Aziz & Kasongo, 2019).

$$R = \frac{C_f - C_p}{C_f} \times 100 \quad (1)$$

$$J = \frac{V}{A \times \Delta T} \quad (2)$$

Fouled membranes were flushed with DI water after the experimental runs, at the same initial conditions, and the DI water flux was re-evaluated. Fouling was evaluated by measuring the flux decline ratio (FDR) and flux recovery ratio (FRR) of the membranes.

$$FDR = \left(1 - \frac{J_t}{J_0}\right) \times 100 \quad (3)$$

$$FRR = \left(\frac{J_{fw}}{J_{0w}}\right) \times 100 \quad (4)$$

The initial water flux, J_0 And the time-dependent water flux, J_t ($L.m^{-2}hr^{-1}$), were used to calculate the FDR (%), during the initial pure water flux, J_{0w} And the final pure water flux, J_{fw} ($L.m^{-2}hr^{-1}$) were used to calculate the FRR (%) (Kasongo et al., 2019).

3.2.5 Anti-biofouling evaluation

The anti-biofouling capacity of membranes was tested using *Escherichia Coli* suspensions. Membrane samples were placed under UV light for 30 minutes. Membranes were placed in contact with an *E. coli* suspension at a concentration of 1×10^7 10^8 $CFU.mL^{-1}$, prepared in nutrient broth (NB), for 3 hours. The membrane was then removed and rinsed with 10 mL of fresh nutrient broth. The collected solution was diluted in series (2-10-fold) with pure, sterile water, and 100 µL of each dilution was plated on Nutrient Agar (NA) medium in petri dishes. The petri dishes were then incubated at 37℃ for 24 hours. The same NB of *E. coli* suspension (~1×10^7 $CFU.mL^{-1}$), not being in contact with the membrane, was incubated at 37 ℃ for the same time with the inoculum on the surface of the membrane and diluted in series (2-10 folds) and plated on NA medium. The number of viable bacteria not in contact with the membrane surface, B, and the number of viable bacteria in contact with the membrane surface, A, were determined by manual counting to calculate the sterilisation ratio, R, as shown in equation (5). Biofouling was further evaluated through flux decline of pure water flux of 18 × 12 cm unmodified and DMAEMA-modified membranes before and after incubation with a constant volume of ~ 2 ×10^8 $CFU\ mL^{-1}$ *E. coli* suspension for 30 hours.

$$R = \left(\frac{B-A}{B}\right) \times 100 \qquad (5)$$

3.3 Membrane surface modification using ADMH

3.3.1 Materials and Reagents

The XLE-4040, a spiral-wound Thin Film Composite Polyamide RO membrane, was obtained from Dow Chemical Company. Sodium bicarbonate, humic acid, Potassium hydroxide (KOH), 5.5-dimethyl hydantoin (DMH), allyl bromide, methanol, initiator 2, 2-azobis (isobutyramidine) hydrochloride (AIBA), and glycerol were obtained from Sigma Aldrich (Pty) Ltd, South Africa. All chemicals were of analytical grade and used without further purification. Nutrient broth powder and nutrients were purchased from Lasec SA (Pty) Ltd. Deionised water with a conductivity of less than 5 µS. Cm^{-1}, obtained from a Millipore water purification system in the lab, was used for solution preparation, membrane rinsing, and conservation.

3.3.2 Synthesis of 3-Allyl-5,5-DimethylIhydantoin (ADMH)

The synthesis of ADMH was done according to the Gabriel reaction (Wei et al., 2010). A solution of 2.8g (0.05 mol) of KOH in 25 mL of deionised water was prepared, and 6.4g (0.05 mol) of DMH was added to the solution. Another solution, B, was prepared by mixing 4.4 mL (0.05 mol) of allyl bromide with 10 mL of methanol. Solution A and B were combined, and the mixture was stirred at 60 ◦C for 2 hours. The solution was cooled and dried under reduced pressure at approximately 25 ◦C. The resulting solid was recrystallized from petroleum, and multiple batches of ADMH were prepared to produce an aqueous solution for membrane modification.

3.3.3 Membrane Surface Modification using ADMH

The modification procedure was similar to the method employed by Wei et al., (2010) adapted to the procedure detailed below. Figure 10 illustrates the modification procedure graphically. A modifying apparatus was constructed with an inner frame and an outer frame, with solution circulation driven by a peristaltic pump, as shown in Figure 11. The membrane pieces were taped to the inner frame of the modifying apparatus to ensure the modifying agent solution was in direct contact with the membrane's active surface. The aqueous solution of the initiator AIBA was prepared at a mass concentration of 0.02 wt.% (i.e., a mass of 0.02g in 100mL), while the grafting monomer ADMH solutions were at different concentrations of 0.2 mol. L^{-1}; 0.4 mol. L^{-1}; 0.6 mol. L^{-1} and 0.8 mol. L^{-1}, prepared using 2.5g, 5g, 7.5g, and 10g dissolved in 100mL of water, respectively. The initiator solution was circulated through the membrane apparatus, and excess solution was removed by

gently drying the membrane under a lab-supplied nitrogen stream for 2 minutes. The apparatus was then flushed with deionised water for 15 minutes. The ADMH solution was pumped through the system for 20 minutes. Afterwards, the membrane was gently dried under a stream of laboratory nitrogen by sweeping the nozzle across the sample for 2 minutes. The membrane was then placed in a controlled-temperature oven at 60 °C for 20 minutes. The resulting membranes were then removed from the frames and thoroughly rinsed. The membrane samples were referred to $M_{0.2}$,$M_{0.4}$ $M_{0.6}$ and $M_{0.8}$ for the modified and M_0 for the unmodified membrane samples.

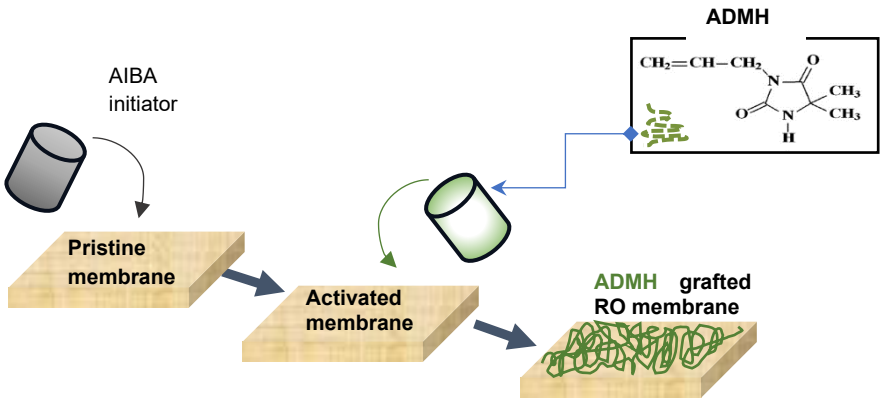


Figure 10: Graphical illustration of the RO membrane surface modification process used in this study.

The extent of polymerisation was first evaluated in terms of the degree of grafting yield *G*, using equation (1):

$$G = \left(\frac{w_1 - w_0}{w_0}\right) \times 100 \qquad (6)$$

Where w_0 is the weight of the membrane before modification, and w_1 is the weight of the membrane after modification.

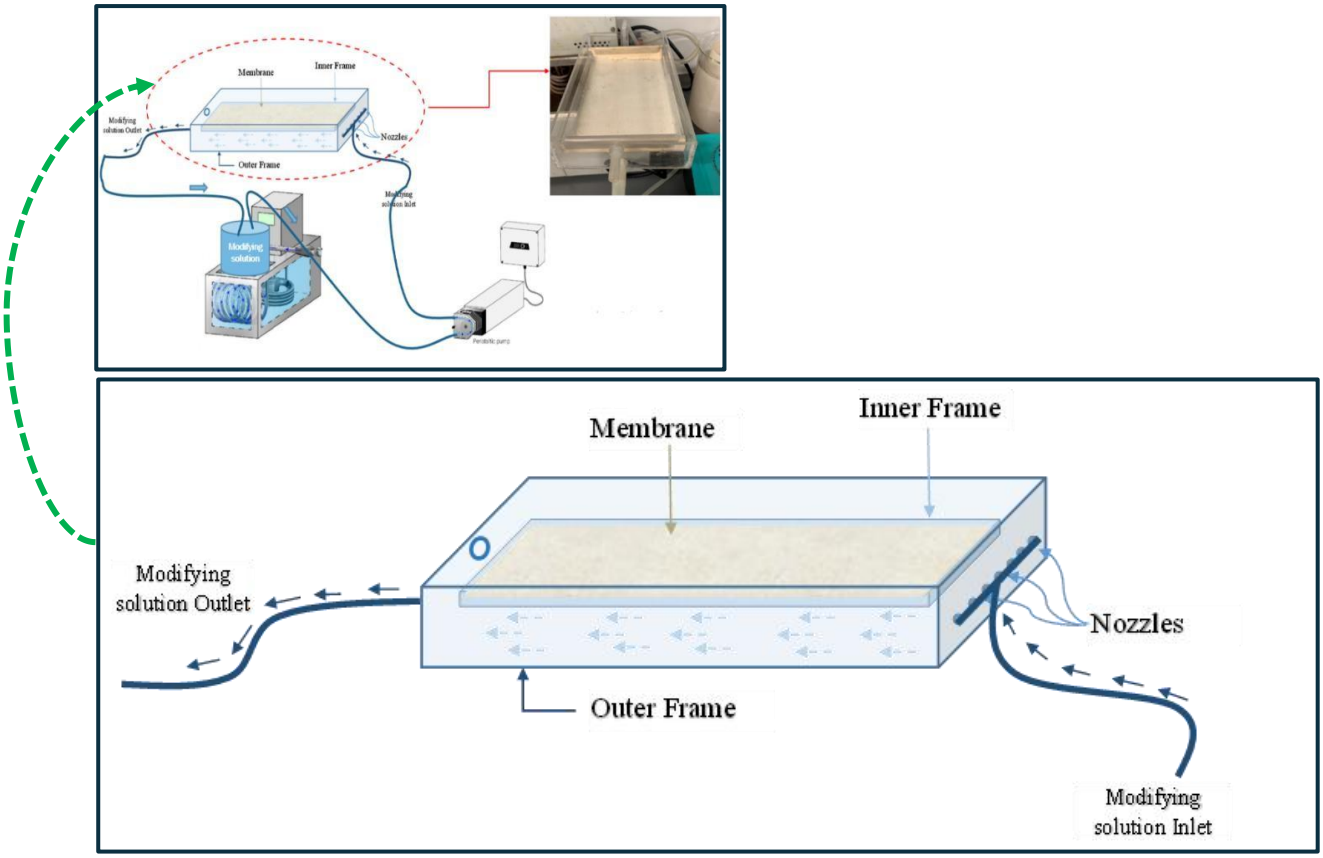


Figure 11: Schematic illustration of the experimental setup used for chemical grafting on the PA RO membrane.

3.3.4 Membrane Characterisation

The membrane samples were characterized by scanning electron microscopy (SEM), Fourier-transformed infrared spectroscopy (FTIR), and nuclear magnetic resonance (NMR) before and after modification. The SEM was performed using a FEI Nova Nano SEM with a magnification of 1200 at a 50-100 µm distance to assess the membrane's morphology. The FTIR analysis was performed using a PerkinElmer Spectrum Two FTIR spectrometer to determine the chemical composition of the membrane surface. The Solid state NMR experiments were carried out using 2.5 mm outer diameter zirconia rotors (Bruker, Karlsruhe, Germany); ^{13}C NMR spectra were obtained with a Bruker AVANCE III HD 500 MHz (11.1 Tesla) standard bore spectrometer and a triple channel broadband probe (Trigamma™ MAS probe), at a magic angle spinning rate of 10 kHz, frequencies of 500 MHz (^{1}H) and 125.8 MHz (^{13}C) and standard cross-polarization (CP) MAS techniques (^{1}H π/2 pulse length 3.4 µs and ^{13}C π/2 pulse length 4.0 µs, ^{1}H cross polarization field 120 kHz, ^{1}H–^{13}C cross polarization contact time 2.0 ms, broadband SPINAL64 decoupling during signal acquisition at a ^{1}H field strength of 120 kHz, recycle time 3 s, typical number of scans accumulated per spectrum *ca.* 10000). Chemical shifts were referenced to the downfield methylene signal from solid Glycine at 43.7 ppm. The contact angles of the membranes were measured to evaluate their hydrophilicity using a OneAttension tensiometer (Biolin Scientific) with pure water at ambient temperature. Five

measurement cycles were performed for each membrane, with the first cycle discarded to minimise artefacts; the average of cycles 2 to 5 and the average value ± standard deviation (n = 3 coupons per sample) is reported (Korhonen et al., 2013). Advancing contact angles are reported to reflect dynamic wettability by capturing the behaviour of the moving contact line, thereby providing more reliable insights than static measurements (Marmur et al., 2017).

3.3.5 Fouling Experiments

Solutions of the gram-negative *E. coli* and the gram-positive *S. aureus* bacteria were used as model microorganisms to assess the antibiofouling ability of the modified membranes. The bacterial culturing procedure was adapted from Wang et al., (2015). The highest-performing ADMH-modified membrane was then selected to evaluate the dynamic adhesion of microorganisms and to conduct organic and inorganic fouling tests in a crossflow filtration RO setup, as illustrated in Figure 9 (**section 3.2.4**). All dynamic adhesion and fouling experiments were performed under identical hydrodynamic conditions, maintaining an applied feed pressure of 15 bar and a cross-flow velocity of 19 cm s^{-1}.

3.3.6 Static Adhesion Test

The membrane was cut into circles 88 mm in diameter and placed under UV for 30 minutes. The pieces of modified and unmodified membranes were set for 3 hours in contact in the incubator at 37℃ with Nutrient broth (NB) containing *E. coli* or *S. aureus* suspension previously prepared, and a blank control contaminated broth solution that was not in contact with the membranes was also incubated for the same contact time for control. The membrane pieces were then removed and rinsed with saline water; the collected suspension solution (1 mL) was diluted in series (2-10-fold). 100 µL of diluent was plated onto nutrient agar (NA) in Petri dishes, labelled with a distinguishing pattern, and incubated at 37℃ for 20 hours. The same dilution process was used for the blank control and was plated on petri dishes. The Petri dishes were then removed, and the number of *E. coli* bacteria in contact with each membrane was determined using the plate count method. The same procedure was applied to *S. Aureus* bacteria for both the unmodified and modified membrane samples.

3.3.7 Dynamic Adhesion Test

The unmodified and ADMH-modified membranes were evaluated for their antibacterial potential through crossflow filtration of bacterial suspensions. The feed water was a synthetic solution that mimicked fouling in municipal secondary effluent, enabling an assessment of the membrane's performance against fouling. The water was pumped through the cell using a hydra-cell pump operating at 15 bar, with a velocity of 19 cm $s^{-1,}$ and an ambient temperature. The permeate water was discharged into a collecting beaker, and the retentate was recycled back to the feed tank. LabVIEW software was used to visualize every aspect of the setup and measurement data, including

conductivity, flow rate, and velocity. The pressure around the cell was monitored using a hydraulic pump. After the cell was secured, the feed solution was added, and the pump was switched on. The system was switched on, and the LabVIEW program was started to control the operating conditions. The flux was recorded every 30 minutes.

Table 5: Feed and fouling solutions used in this study.

Test type	Model solution/foulant	Concentration
Permeability	Deionized water	≈ 5 μS m^{-1}
Salt rejection	Sodium chloride	500 ppm
Organic fouling	Humic acid	100 mg L^{-1}
Inorganic fouling	Sodium bicarbonate	100 mg L^{-1}
Biofouling	Escherichia Coli	≈ 1.5 × 10^{8} CFU mL^{-1}
Biofouling	Staphylococcus aureus	≈ 8.1 × 10^{8} CFU mL^{-1}

3.3.8 Membrane Performance Assessment

Membrane performance was assessed by comparing the process parameters of the modified and unmodified membranes under identical operating conditions. Figure 12 outlines the sequence and duration used for the experimental tests to assess membrane performance and antifouling capability. Bacterial mortality on membranes was determined to evaluate their antibiofouling ability. The membrane water flux was assessed according to the method described by Kasongo et al., (2019). The following parameters were determined similarly as described in Chapter 3, Sections **3.2.4** and **3.2.5**.

- Permeate flux ($L.m^{-2}h^{-1}$)
- Flux decline ratio (FDR)
- Flux recovery ratio (FRR)
- Salt rejection
- Mortality ratio (R)

All statistical analyses were performed using Design Expert. For normally distributed data, differences between groups were assessed using one-way ANOVA. Results are presented as mean, and a *p*-value of less than 0.05 was considered statistically significant.

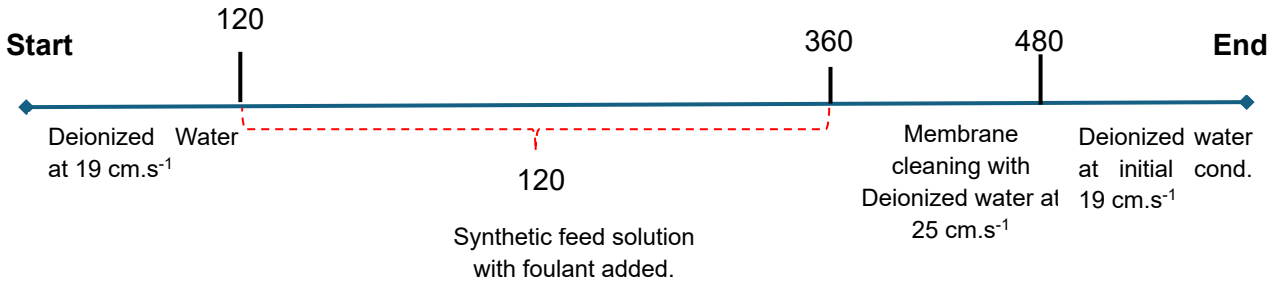


Figure 12: Experimental timeline during membrane performance and antifouling capability tests.

3.4 Membrane modification using ADMH\TiO_2-Ag

3.4.1 Materials and Reagents

A commercial spiral-wound polyamide thin-film composite (TFC) reverse osmosis (RO) membrane (XLE-RO-4040 model, FilmTec Membranes) was used for all modification experiments. Titanium dioxide (TiO_2) nanoparticles (anatase phase, particle size 20–30 nm) and initiator 2,2'-Azobis(2-Methyl-propionamide) dihydrochloride, sodium bicarbonate, humic acid, Potassium hydroxide (KOH), 5.5-dimethyl hydantoin (DMH), allyl bromide, methanol, initiator 2, 2-azobis (isobutyramidine) hydrochloride (AIBA), petroleum ether, L-ascorbic acid (AA, ≥99% purity), silver nitrate ($AgNO_3$), ammonium hydroxide (NH_4OH) and ethanol (≥99.8%) and glycerol were obtained from Sigma Aldrich (Pty) Ltd, South Africa. All chemicals were of analytical grade and used without further purification. Nutrient broth powder and nutrients were purchased from Lasec SA (Pty) Ltd. Deionised water with a conductivity of less than 5 µS/cm, obtained from a Millipore water purification system in the lab, was used for solution preparation, membrane rinsing, and conservation. A UV-B type spectrophotometer equipped with a 1000 W lamp (wavelength of 315 nm) was used for UV-initiated surface modification of the membrane.

3.4.2 Synthesis of TiO_2-Ag Nanocomposites

The synthesis of TiO_2-Ag nanocomposite was adapted from the method reported by Gogoi et al., (2020) and modified to achieve a 1:1 mass ratio of Ag^+ to TiO_2. Silver nitrate ($AgNO_3$) was used as the silver precursor, and L-ascorbic acid (AA) served as the reducing agent. First, 5 g of TiO_2 powder was added to 1000 mL of an aqueous $AgNO_3$ solution containing 7.88 g of $AgNO_3$. The solution was stirred vigorously at 500 rpm for 60 minutes at room temperature to ensure thorough mixing. The pH of the suspension was then adjusted to 7 by adding 0.1 M ammonium hydroxide (NH_4OH) to improve the adsorption of Ag^+ ions onto the TiO_2 support. Separately, a 25 mM aqueous solution of L-ascorbic acid was prepared and stirred for 30 minutes in a glass beaker. The TiO_2-Ag solution was then dispersed into the ascorbic acid solution and stirred continuously for another 30 minutes. During this step, the colour of the suspension changed from milky white to brown, indicating the reduction of silver ions (Ag^+) to metallic silver nanoparticles (Ag^0) on the TiO_2 surface. The resulting mixture was centrifuged at 4500 rpm for 20 minutes to separate the TiO_2 -Ag nanocomposite from the aqueous phase. The collected solid residue was washed four times with the ethanol-water mixture to remove any loosely bound or undoped silver ions. Finally, the purified TiO_2-Ag nanocomposite was dried in a hot air oven at 100 °C for 12 hours and stored in a vial before further use.

3.4.3 PA RO Membrane surface modification

Samples of commercial polyamide thin-film composite (TFC) RO membranes were cut to a measurement of 18cm × 12 cm, and each was weighed to measure the mass before the grafting process. The grafting of the ADMH onto the membrane prior to TiO_2-Ag grafting was conducted as described in **section 3.3.3**.

3.4.4 TiO_2-Ag grafting

The procedure for modifying commercial polyamide thin-film composite (TFC) reverse osmosis (RO) membranes with TiO_2-Ag nanoparticles was adapted from the method described by Asadollahi et al., (2020) with a few modifications. Before modification, each membrane sample was weighed and then wrapped securely around a modification frame, ensuring that the active (polyamide) side of the membrane faced the solution. During the grafting procedure, only the active layer of the RO membrane was exposed to the grafting solution, while the support layer was physically isolated and remained unmodified.

First, an initiator solution was prepared by dissolving 0.2 g of 2,2'-Azobis(2-Methyl-propionamide) dihydrochloride in 100 mL of DI water. The solution was stirred using a magnetic stirrer at 500 rpm until the initiator was completely dissolved, with no visible particles remaining. The initiator solution was then poured into the modification frame, with the clamped RO membrane set in such a way that only the active surface was fully in contact with the initiator solution. The membrane was exposed to UV light positioned 3 cm above the solution for 2 minutes. After UV exposure, the initiator solution was removed and stored in a glass beaker for potential reuse. The membrane was gently dried with nitrogen gas.

For the TiO_2-Ag grafting, a 0.4 $mol.L^{-1}$ TiO_2-Ag suspension was prepared by dispersing the calculated mass of TiO_2-Ag powder in 100 mL of DI water. The suspension was stirred at 500 rpm for 30 minutes to ensure a uniform and homogeneous mixture. The active side (polyamide) of the dried RO membrane was then put in contact with the TiO_2-Ag suspension for 30 minutes to allow adequate contact with the nanoparticles. After the contact time, the TiO_2-Ag suspension was removed, and the membrane was thoroughly rinsed with DI water to eliminate any loosely bound particles. Following rinsing, the membrane was exposed to UV light irradiation for 2 minutes to promote the grafting and stable attachment of TiO_2-Ag nanoparticles onto the membrane surface. Subsequently, the membrane was weighed to monitor any changes in mass due to grafting and then stored immersed in DI water for further analysis and biofouling testing.

3.4.5 Grafting of ADMH\TiO$_2$-Ag

Prior to nanoparticle grafting, the commercial polyamide TFC RO membrane was subjected to 3-allyl-5,5-dimethylhydantoin (ADMH) modification to introduce reactive allyl and hydantoin functional groups onto the surface.

The PA RO membrane was first weighed and then mounted on the modification frame illustrated in Figure 11 (**section 3.3.3**), ensuring contact between the active layer and the initiator solution. The initiator solution (0.2 g of 2,2'-Azobis(2-methyl-propionamide) dihydrochloride dissolved in 100 mL of DI water) circulated using a peristaltic pump at 65 rpm for 15 minutes at room temperature. Following this step, membranes were rinsed with DI water. For ADMH grafting, a concentration of 0.6 mol.L^{-1} ADMH was used, which was prepared by dissolving 30 g of ADMH in 400 mL of DI water. The solution was heated to 90 °C in a water bath to facilitate grafting at 60 °C under continuous circulation (65 rpm) in the modification frame. After 20 minutes, the ADMH-grafted membrane was dried under nitrogen gas, weighed, and stored in DI water. The ADMH-modified was treated with an initiator and placed in contact with the nanocomposites suspension (TiO$_2$-Ag) for 30 minutes. The resulting membrane was rinsed thoroughly with DI water, and irradiated with UV light for 2 minutes to stabilize nanocomposite attachment. Finally, the membranes were weighed and stored in DI water for further characterization and biofouling resistance testing. Figure 13 highlights the sequential modification of RO membranes with ADMH and TiO$_2$-Ag.

After modification, the membranes were denoted as follows:

- **M-U**: Pristine XLE PA membrane
- **M-H**: ADMH modified membrane
- **M-T**: TiO$_2$ modified membrane
- **M-TA**: TiO$_2$-Ag modified membrane
- **M-HTA**: ADMH\TiO$_2$-Ag modified membrane

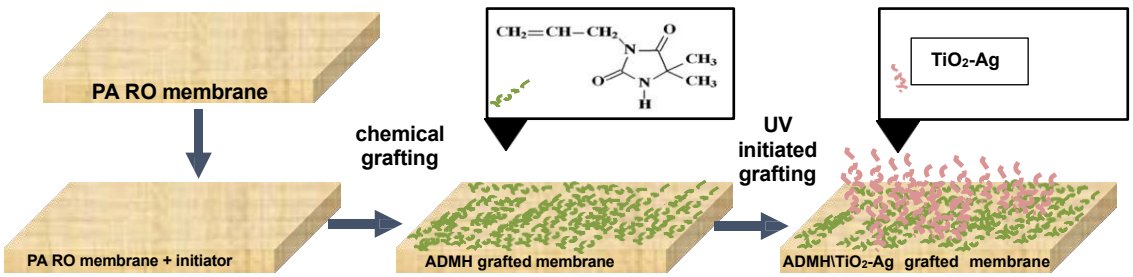


Figure 13: Graphical illustration of the RO membrane surface modification process using ADMH\TiO$_2$-Ag.

3.4.6 Membrane characterisation

(I) Particle size distribution (PSD) and X-ray diffraction (XRD)

The particle size distribution (PSD) of TiO_2 and Ag-TiO_2 nanoparticles was measured using a Mastersizer 3000 (Malvern Instruments, UK) equipped with a helium-neon laser operating at 632.8 nm. Crystalline phases were identified using X-ray diffraction (XRD) on a Bruker D8 Advance diffractometer with Cu Kα radiation (λ = 1.5406 Å).

(II) FTIR analysis

The chemical composition of membrane surfaces before and after modification was analysed using a PerkinElmer Spectrum Two FTIR spectrometer. Spectra were collected over the range of 4000-400 cm^{-1} with a resolution of 4 cm^{-1} to confirm the presence of functional groups and chemical changes induced by grafting and nanoparticle attachment. The FTIR was also used to characterise the nanocomposite (TiO_2-Ag) prepared.

(III) SEM-EDX

Membrane morphology and elemental distribution were examined using FEI Nova Nano SEM equipped with an energy-dispersive X-ray spectrometer (EDS). Samples were mounted on aluminium stubs and sputter-coated with a thin gold layer to enhance conductivity. EDS spectra were recorded at 15-20 kV to confirm the distribution of Ti and Ag on the modified surfaces.

(IV) TEM analysis

Cross-sectional images of membranes were obtained using an FEI Tecnai F20 TEM operated at 200 kV with a DE-16 direct detection camera. Samples were embedded in epoxy resin from equal masses of trimethylolpropane tri-glycidyl ether and 4,4′-methylenebis(2-methylcyclohexylamine) hardener, polymerised at 60 °C for 24 hours. Ultrathin sections (~100 nm) were cut with a Leica Ultracut S ultramicrotome, collected on carbon-coated grids, and imaged to visualise nanoparticle distribution through the membrane depth.

(V) Membrane thermal stability: TGA analysis

All thermogravimetric tests were carried out under identical experimental conditions to allow a fair comparison of the thermal behaviour of the membranes. The samples were placed in open Al_2O_3 crucibles and heated from 20 °C to 1025 °C at a constant rate of 20 $K.min^{-1}$. Nitrogen was used both as the purge and protective gas at 250 $mL.min^{-1}$ to maintain an inert atmosphere and prevent any oxidative effects that could alter the decomposition pathway. The reference and sample crucibles had nearly the same mass, which helped maintain a stable baseline during the run. Using the same

crucible type, gas flow, heating rate, and temperature range for every sample ensured that differences in mass-loss patterns were due to variations in membrane chemistry rather than differences testing conditions. This consistency is important in distinguishing true thermal decomposition from early losses associated with surface moisture or loosely bound organic groups.

(VI) Contact angle and membrane charge measurements

Surface wettability was quantified by advancing contact angle using a One Attension tensiometer (Biolin Scientific) with deionised water at room temperature. Five cycles were performed per sample, discarding the first to reduce artefacts. The mean and standard deviation from cycles 2-5 were reported, reflecting dynamic wettability behaviour.

Surface charge (zeta potential) of membranes and nanoparticle suspensions was measured using a Malvern Zeta analyser Nano ZS.

3.4.7 Fouling experiments

The gram-negative *E. coli* bacteria and gram-positive *S. aureus* bacteria solutions were used as model microorganisms to assess the antimicrobial ability of the modified membranes. The procedure for bacterial culturing described below was adapted from Wang et al., (2015) and Tuttle et al., (2021)

(I) Static adhesion test

The membrane was cut into small circles, 88 mm in diameter, and placed under UV for half an hour. The pieces of modified and unmodified membranes were set for 3 hours in contact in the incubator at 37 ℃ with Nutrient broth (NB) of approximately ± 0.47Abs (at 590 nm) containing *E. coli* suspension previously prepared, and a blank control contaminated broth solution that was not in contact with the membranes was also incubated for the same contact time for control. The membrane pieces were then removed and rinsed with saline water. The collected suspension solution (1 mL) was diluted in series (2-10-fold). 100 µL of diluents were plated on nutrient agar (NA) in Petri dishes, labelled with a distinguishing pattern and incubated at 37 ℃ for 20 hours. The same dilution process was used for the blank control, which was then plated on petri dishes. The Petri dishes were then removed, and the number of *E. coli* bacteria in contact with each membrane was determined using the plate count method. The same procedure was applied to *S. Aureus* bacteria for both the unmodified and modified membrane samples.

(II) Dynamic adhesion test

The unmodified and ADMH-modified membranes were evaluated for their antibacterial potential through crossflow filtration of bacterial suspensions. The feed water was a synthetic feed solution that mimicked fouling activities in municipal secondary effluent, to assess the membrane's

performance against fouling. The water was pumped through the cell using a hydra-cell pump. The permeate water was discharged into a collecting beaker, and the retentate was recycled back to the feed tank. LabVIEW software was used to visualise every aspect of the setup and measurement data, including conductivity, flow rate, and velocity. The pressure around the cell was monitored using a hydraulic pump. After the cell was secured, the feed solution was added, and the pump was switched on. The system was switched on, and the LabVIEW programme was started to control the operating conditions. The flux was recorded every 30 minutes for a duration of 10 hours. Organic fouling was simulated with humic acid at 150 mg·L^{-1} and inorganic fouling with sodium bicarbonate at 150 mg·L^{-1}. Dynamic bacterial adhesion tests were conducted with suspensions of *E. coli* (~8.5 × 10^{8} CFU·m L^{-1}) and *S. aureus* (~9.1 × 10^{8} CFU·m L^{-1}).

(III) Confocal Laser Scanning Microscopy (CLSM)
Biofilm formation after dynamic adhesion tests was examined by CLSM. Membrane samples (~1 × 0.5 cm) were stained with the live/dead backlight bacterial viability kit (Invitrogen; L7012) using a 1:1:1000 solution of PI:Syto9:PBS. After 10 minutes' incubation, samples were imaged on an Evident FV4000 confocal microscope with a UPLXAPO 40×/0.95 objective. Syto9 was excited at 488 nm and PI at 561 nm; emissions were collected at 500-540 nm and 570-620 nm, respectively. Z-stack images (0.7 µm steps) were acquired and processed with constrained iterative deconvolution.

3.4.8 Membrane performance assessment

Membrane performance was assessed by comparing the process parameters of the modified and unmodified membranes under identical operating conditions. The mortality ratio of the bacteria on membranes was determined to evaluate the antibiofouling ability of the membranes (Wang et al., 2015; Bian et al., 2022).
Pure water permeability was determined using deionised water of ~5 µS·cm^{-1}. Salt rejection was measured using a 2000 ppm NaCl solution.

The following parameters were determined as described in Chapter 3, **Sections 3.2.4** and **3.2.5**.

- Permeate flux ($L.m^{-2}h^{-1}$)
- Flux decline ratio (FDR)
- Flux recovery ratio (FRR)
- Salt rejection and
- Mortality ratio (R)

Furthermore, the antibacterial efficiency (A_e) of the pristine and surface-modified polyamide TFC RO membranes was quantitatively evaluated through the following expression (Nchoe et al., 2023).

$$A_e(\%) = \left(\frac{N_b - N_a}{N_b}\right) \times 100 \qquad (7)$$

Where N_b number of viable bacterial colonies recovered from the unmodified control membrane (pristine TFC-RO), and N_a number of viable bacterial colonies recovered from the modified membrane. This metric, expressed as a percentage, provides a direct measure of microbial growth inhibition induced by surface modification.

3.5 Reference

Bian, S., Wang, Y., Xiao, F., Tong, Y., Gao, C. & Zhu, G. 2022. Fabrication of polyamide thin-film nanocomposite reverse osmosis membrane with improved permeability and antibacterial performances using silver immobilized hollow polymer nanospheres. *Desalination*, 539: 115953. https://linkinghub.elsevier.com/retrieve/pii/S0011916422004088.

Gogoi, D., Namdeo, A., Golder, A.K. & Peela, N.R. 2020. Ag-doped TiO2 photocatalysts with effective charge transfer for highly efficient hydrogen production through water splitting. *International Journal of Hydrogen Energy*, 45(4): 2729–2744.

Kasongo, G., Steenberg, C., Morris, B., Kapenda, G., Jacobs, N. & Aziz, M. 2019. Surface grafting of polyvinyl alcohol (PVA) cross-linked with glutaraldehyde (GA) to improve resistance to fouling of aromatic polyamide thin film composite reverse osmosis membranes using municipal membrane bioreactor effluent. *Water Practice and Technology*, 14(3): 614–624.

Korhonen, J.T., Huhtamäki, T., Ikkala, O. & Ras, R.H.A. 2013. Reliable measurement of the receding contact angle. *Langmuir*, 29(12): 3858–3863.

Marmur, A., Volpe, C. Della, Siboni, S., Amirfazli, A. & Drelich, J.W. 2017. Contact angles and wettability: Towards common and accurate terminology. *Surface Innovations*, 5(1): 3–8.

Nchoe, O.B., Matshetshe, K., As' Ballim, M., Tetyana, P., Sikhwivhilu, K. & Moloto, N. 2023. Fabrication of Ag2S-incorporated polyamide thin film nanocomposite reverse osmosis membranes with antifouling properties. *Journal of Applied Polymer Science*, 140(41).

Tuttle, A., Trahan, N. & Son, M. 2021. Growth and Maintenance of Escherichia coli Laboratory Strains. *Current Protocols*, 1.

Wang, Jing, Wang, Z., Wang, Jixiao & Wang, S. 2015a. Improving the water fl ux and bio-fouling resistance of reverse osmosis (RO) membrane through surface modi fi cation by zwitterionic polymer. *Journal of Membrane Science*, 493: 188–199. http://dx.doi.org/10.1016/j.memsci.2015.06.036.

Wei, X., Wang, Z., Zhang, Z., Wang, J. & Wang, S. 2010. Surface modification of commercial aromatic polyamide reverse osmosis membranes by graft polymerization of 3-allyl-5 , 5-dimethylhydantoin. *Journal of Membrane Science*, 351(1–2): 222–233. http://dx.doi.org/10.1016/j.memsci.2010.01.054.

Chapter 4

MEMBRANE SURFACE MODIFICATION THROUGH CHEMICAL GRAFTING USING N, N′- DIMETHYL AMINOETHYL METHACRYLATE (DMAEMA)

This chapter has been published as:

Aziz, M, & **Kasongo, G**. 2021. Improving resistance to fouling of aromatic polyamide thin-film composite reverse osmosis membrane by surface grafting of N, N′- dimethyl aminoethyl methacrylate (DMAEMA). *Journal of Water Chemistry and Technology* 43(4): 312-320. [ISSN 1063-455X]

4.1 Introduction

Polymers are widely used for the preparation of membranes and may be altered to obtain the desired properties of the membrane (Rambabu & Velu, 2016). Various studies using different modification methods such as coating and graft polymerisation (Shafi et al., 2015; Wang et al., 2015; Kasongo et al., 2019) have improved antifouling properties of membranes after modifications using different model foulants. However, the surface coating's weakness is that the coated layer swept away over time due to its weak interaction with the membrane layer. Therefore, modification by surface grafting is favourable to alter membrane surfaces and minimise fouling (Wang et al., 2015) by changing the physicochemical properties of the membrane surface permanently (Sun et al., 2013; Asadollahi et al., 2017).

The purpose of this study was to improve the resistance to fouling of a low-pressure TFC RO membrane using a feed solution composition simulating secondary effluent from an MBR. DMAEMA grafting solutions were used as modifying agents. The graft polymerisation method applied in this study is not limited to experimental tests with a single foulants model. The method is extended to experimental tests involving a model foulant solution simulating natural wastewater from the municipal wastewater treatment plant MBR effluent, known to combine multiple foulants substances. Furthermore, the work suggests evaluating the membrane modification agent by altering its concentration to minimise the flux decline significantly, while also avoiding compromising the salt rejection.

4.2 Membrane surface modification using DMAEMA: Membrane characterisation

4.2.1 ATR-FTIR

Membrane surface functional groups were determined through ATR-FTIR spectra. showing that grafting thrived It can be seen from the spectra in Figure 14 that the functional amide I group (nitrogen C=O) and the carbonyl group were identified at wavenumbers of 1610 cm^{-1} and 1725 cm^{-1}, respectively and could be attributed to the polyamide layer present. Minor changes were observed for both unmodified and modified membranes. Similar observations were made at the absorption bands at 1480, 1510, and 1585 cm^{-1}, which could be attributed to the polysulfone layer. Wang et al., (2015) suggested that the peak at about 1240 cm^{-1} was ascribed to the membrane's aromatic structure.

According to Wei et al., (2010), the tiny volume of aromatic polyamide layer grafting sites may have caused the FTIR absorption bands to amalgamate with other bands, limiting their observation. It can be observed from the spectra that the wavenumbers intensified with an increase in DMAEMA concentration on the modified membranes. Therefore, it can be deduced that the DMAEMA solution was effectively grafted onto the top layer of the membrane. Cheng et al., (2013) investigated the graft polymerisation of N-isopropyl acrylamide on a TFC membrane and observed an increase in the

functional amide I group (nitrogen C=O) polysulfone. These results confirmed that the membranes' structure was not affected after modification (Lin et al., 2016).

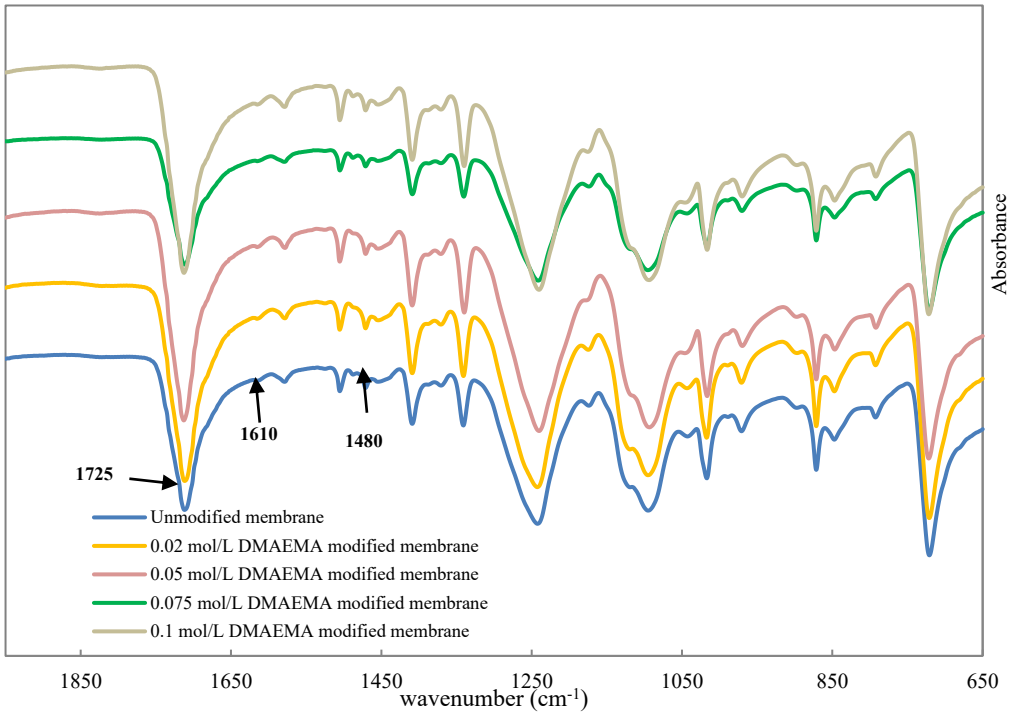


Figure 14:. ATR-FTIR spectra of the unmodified membrane and DMAEMA modified membranes

4.2.2 SEM analysis

SEM images revealed the morphological structure of the membranes, as shown in Figure 15, with the right images displaying the cross-sectional morphology at a magnification of 10,000. Unmodified and modified membranes presented a rigid and valley structure (Freger et al., 2002; Wang et al., 2015). The modified membranes exhibited a distinct morphology, with new structures appearing on their surfaces. These structures became more visible as the DMAEMA concentration increased, as observed by other researchers after graft polymerisation on the membrane surface (Mahdavi et al., 2017).

The thickness of the unmodified membrane was measured at 75 µm. It appears that the selective skin layer of the composite membrane condenses with an increase in the concentration of the DMAEMA-modifying solution. The newly formed skin layer showed a thickness of 77, 90, 92, and 93 µm as the DMAEMA solution increased from 0.02 to 0.1 mol.L^{-1}, causing a surface negative charge decrease (Yisong Hu et al., 2016). This may be related to the significant functional groups on DMAEMA, which increase the grafting yield and cause agglomerate structures on the TFC membrane surface. Mahdavi et al., (2017) investigated the grafting of AC-HBPAE on a TFC membrane and had similar observations regarding the increase in membrane thickness when increasing the modifying agent's concentration.

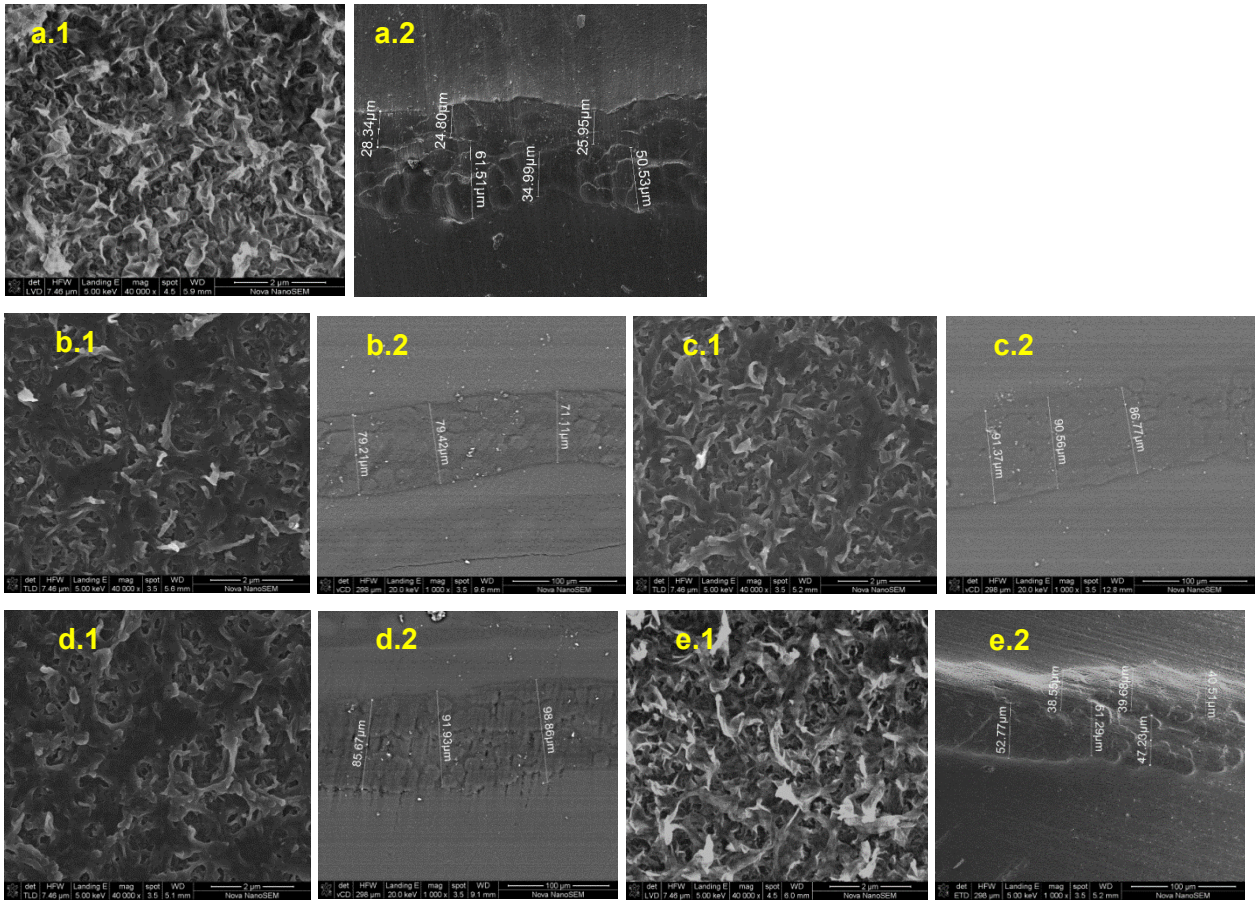


Figure 15:. SEM images of virgin (unmodified) membrane (a) and DMAEMA modified membranes (top-view & cross section): (b) 0.02 mol. L^{-1} DMAEMA, (c) 0.05 mol. L^{-1} DMAEMA, (d) 0.075 mol. L^{-1} DMAEMA and (e) 0.1 mol. L^{-1} DMAEMA.

4.2.3 Membrane performance and antifouling properties

The pure water flux of the membranes was measured to evaluate their permeability; the results are shown in Figure 16. The pure water flux of DMAEMA-modified membranes was higher than that of the unmodified membranes and increased with increased DMAEMA concentration. This may be attributed to the increase in membrane surface hydrophilicity after grafting the hydrophilic chains, enhancing water molecules (Wei et al., 2010).

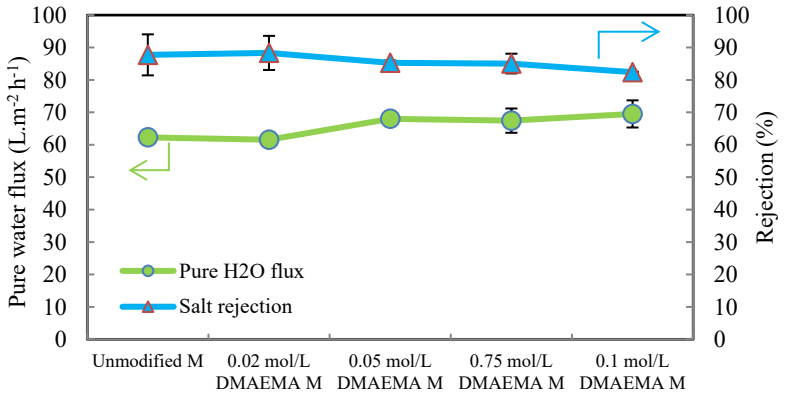


Figure 16: Pure water flux of membranes and the salt rejection during filtration of the synthetic feed solution

Membrane salt rejection was tested using the simulated secondary effluent from an MBR. The salt rejection decreased slightly, with an increase in DMAEMA concentration. A slight drop in salt rejection was observed with an increase in DMAEMA concentration. However, it was noted that up to the 0.02 $mol.L^{-1}$ DMAEMA modification, the salt rejection of the membrane was nearly the same as the unmodified membrane and slightly declined with the 0.05 $mol.L^{-1}$ DMAEMA modified membrane. This is explained by the interactions between the ions, foulants and the membrane surface charge after grafting (Wei et al., 2010). Donnan exclusion effects could also be liable for the decrease in salt rejection after modification (Cheng et al., 2013).

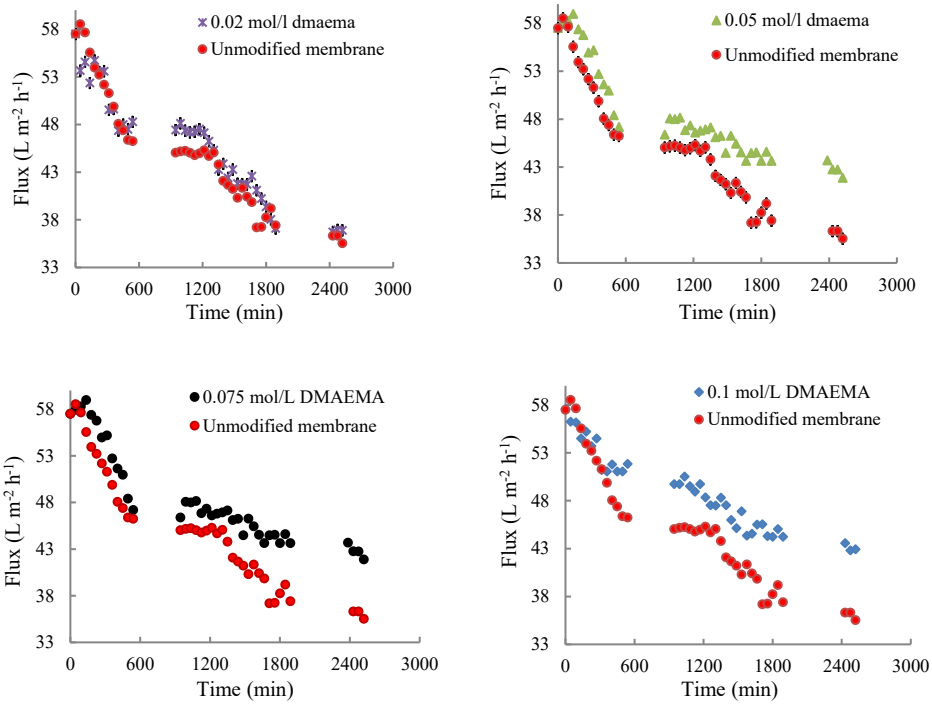


Figure 17: Normalized flux of unmodified and DMAEMA-modified membranes during filtration of the foulant model solution

Figure 17 displays the time-dependent flux of DMAEMA-modified membranes compared to that of the unmodified membrane at a crossflow velocity of 19 cm.s^{-1}, a pressure of 5 bar, and ambient temperature. The initial permeate flux was 57.5 L.m^{-2}.h$^{-1,}$ and the time-dependent flux was normalised at 25 ℃. The normalised flux, declining constantly, showed fouling of membranes (Cheng et al., 2013). The flux difference between the unmodified and the modified membranes increased with time. The unmodified membrane flux declined the most, while the 0.1mol/L DMAEMA membrane declined the least among DMAEMA-modified membranes. Figure 18 illustrates the flux decline ratio (FDR) and the flux recovery ratio (FRR), which were measured to evaluate the membranes' antifouling and cleaning properties, respectively. After the fouling test, the FDR decreased from

38.21% for the unmodified membrane to the lowest value of 25.5%, which was obtained among the DMAEMA-modified membranes. This showed that the membrane had better resistance to fouling.

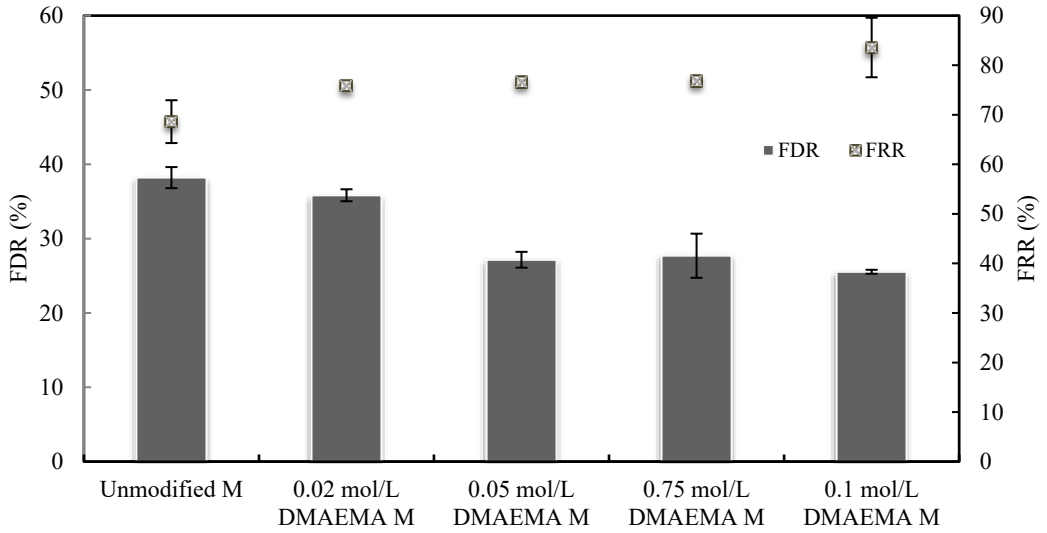


Figure 18: FDR using the simulated feed solution and pure water FRR of membranes

The pure water flux recovery of the unmodified membrane after fouling experiments was 68.61%, whereas the highest value of FRR obtained from DMAEMA-modified membranes was 83.57%. Higher flux recovery indicates the reversibility of fouling (Mahdavi et al., 2017). Thus, it can be said that the fouling of modified membranes was more reversible than that of the unmodified membrane.

4.2.4 Anti-biofouling properties

The 0.1 mol/L DMAEMA, together with the unmodified membrane, were selected for conducting a biofouling test to evaluate the membrane's anti-biofouling properties. Membrane sterilisation ratios are shown in Table 6. The 0.1 mol. L^{-1} DMAEMA-modified membrane provided the highest value of 76.8%, while the unmodified membrane yielded 33.8%. A higher sterilisation ratio indicates the extent to which the membrane possesses antimicrobial properties against the tested microorganism (Xu et al., 2013; Zhang et al., 2013). Thus, the DMAEMA-modified membrane possessed higher anti-microbial properties compared to the unmodified membrane.

Table 6: Unmodified and 0.1 mol. L^{-1} DMAEMA modified membranes sterilisation ratios after contact time with *E. coli* of 1×10^7 CFU. mL^{-1} initial concentration.

Membrane	A (CFU/mL)	B (CFU/mL)	Sterilization ratio, R (%)
Unmodified membrane	106 x 10^6	16x 10^7	33.75
0.1 DMAEMA mol/L modified M	37 x 10^6	16 x 10^7	76.80

DMAEMA-modified membranes were further evaluated in the RO process after exposure to an *E. coli* suspension for 30 hours and compared under the same initial conditions. The pure water fluxes of membranes are presented in Table 7.

Table 7: Pure water flux of membranes before and after 30 hours contact with *E. coli* suspension of ~ 2 ×10^8 CFU. mL^{-1} initial concentration

Membrane	Flux before contact (L. $m^{-2}h^{-1}$)	Flux after contact (L. $m^{-2}h^{-1}$)
Unmodified	62.07	33.49
0.05 DMAEMA mol/L modified	68.01	42.62

The water flux of the unmodified membrane decreased from 62.07 $L.m^{-2}hr^{-1}$ to 33.49 $L.m^{-2}hr^{-1}$; the DMAEMA modified membranes decreased from 68.01 $L.m^{-2}hr^{-1}$ to 42.62 $L.m^{-2}hr^{-1}$. Thus, the flux decline of the unmodified membrane after 30 hours of contact with the bacterial solution was 46.0% of the initial value, while the DMAEMA-modified membrane flux decline was 37.3%, indicating low biofouling of the modified membrane by *E. coli*.

4.3 Summary

The PA TFC RO membrane was modified through graft polymerisation of DMAEMA. ATR-FTIR spectra revealed an increase in the intensities of the peaks for the modified membranes. The chemical functional groups of unmodified and modified membranes, as observed through ATR-FTIR spectra, indicated a change in membrane structure after modification, characterised by an increase in the intensities of the peaks corresponding to these functional groups. SEM analysis also revealed a change in the morphology of the polyamide layer in the membrane, where the membrane density and thickness of the top layer varied with an increase in the DMAEMA solution concentration. The DMAEMA-modified membrane had a higher sterilisation ratio than the unmodified membrane, which showed better antimicrobial properties and the capacity to inhibit the growth and multiplication of the microorganism *E. coli*. This was further confirmed after evaluating pure water flux upon long contact time with, where the pure water flux of the unmodified and modified membranes could be recovered to 53.96 and 70.64%, respectively. Antifouling properties of the membranes tested using the simulated effluent indicated that the capacity to resist fouling increased with DMAEMA concentration. In conclusion, the grafting of DMAEMA enhanced the resistance to fouling and can be promising, especially for MBR secondary effluent from municipal wastewater plants.

4.4 References

Adewumi, J.R., Ilemobade, A.A. & Zyl, J.E. Van. 2010. Resources, Conservation and Recycling, Treated wastewater reuse in South Africa: Overview, potential and challenges. 'Resources, Conservation & Recycling', 55(2): 221–231.

Asadollahi, M., Bastani, D. & Musavi, S.A. 2017. Enhancement of surface properties and performance of reverse osmosis membranes after surface modification: A review. Desalination, 420(June): 330–383. http://dx.doi.org/10.1016/j.desal.2017.05.027.

Aziz, M. & Kasongo, G., 2019. Scaling prevention of thin-film composite polyamide Reverse Osmosis membranes by Zn ions. Desalination, 464(April): 76–83. https://doi.org/10.1016/j.desal.2019.04.021.

Aziz, M. & Kasongo, G., 2021. The Removal of Selected Inorganics from Municipal Membrane Bioreactor Wastewater Using UF/NF/RO Membranes for Water Reuse Application: A Pilot-Scale Study. Membranes, 11(2): 117.

Aziz, M. & Ojumu, T., 2020. Exclusion of estrogenic and androgenic steroid hormones from municipal membrane bioreactor wastewater using UF/NF/RO membranes for water reuse application. Membranes, 10(3).

Cheng, Q., Zheng, Y., Yu, S., Zhu, H., Peng, X., Liu, Jia, Liu, Jingqun, Liu, M. & Gao, C. 2013. Surface modification of a commercial thin-film composite polyamide reverse osmosis membrane through graft polymerisation of N-isopropyl acrylamide followed by acrylic acid. Journal of Membrane Science, 447: 236–245.

Giannakis, S., Isabel, A., Gamo, M., Darakas, E. & Escalas-can, A. 2013. Impact of different light intermittence regimes on bacteria during simulated solar treatment of secondary effluent : Implications of the inserted dark periods. Solar Energy, 98: 572–581.

Goh, P.S., Lau, W.J., Othman, M.H.D. & Ismail, A.F., 2018. Membrane fouling in desalination and its mitigation strategies. Desalination, 425(August): 130–155.

Goldie, I., Aziz, M., Petersen, M. & McLachlan, D. 2010. Evaluation of scaling prevention in reverse osmosis membranes by anodic zinc addition and magnetic fields. South African Water Research Commission.

Hu, Yisong, Wang, X.C., Yu, Z., Hao, H. & Sun, Q. 2016. New insight into fouling behaviour and foulants accumulation property of cake sludge in a full-scale membrane bioreactor. J. mem. Sci. 510: 10–17.

Ishigami, T., Amano, K., Fujii, A., Ohmukai, Y., Kamio, E., Maruyama, T. & Matsuyama, H. 2012. Fouling reduction of reverse osmosis membrane by surface modification via layer-by-layer assembly. Separation and purification technology, 99: 1–7.

Kasongo Wa Kasongo, G., 2018. Enhancement of membrane surface characteristics to improve membrane performance and durability in the treatment of municipal MBR effluent. (Master dissertation, Cape Peninsula University of Technology).

Kasongo, G., Steenberg, C., Morris, B., Kapenda, G., Jacobs, N. & Aziz, M. 2019. Surface grafting of polyvinyl alcohol (PVA) cross-linked with glutaraldehyde (GA) to improve resistance to fouling of aromatic polyamide thin-film composite reverse osmosis membranes using municipal membrane bioreactor effluent. Water Practice and Technology, 14(3): 614–624.

Lin, S., Huang, H., Zeng, Y. & Zhang, L. 2016. Facile surface modification by aldehydes to enhance chlorine resistance of polyamide thin-film composite membranes. Journal of Membrane Science, 518: 40–49.

Mahdavi, H., Hosseinzade, M.T. & Shahalizade, T. 2017. A polyamide thin-film composite membrane modified by Michael addition grafting of hyperbranched poly (amino ester). Journal of Polymer Research, 24(7): 1–11.

Mujtaba, IM, 2017. process : Model development based on experiment and simulation. Journal of Water Process Engineering, 18(February): 20–28.

Myburgh, D.P., Aziz, M., Roman, F., Jardim, J. & Chakawa, S. 2019. Removal of COD from Industrial Biodiesel Wastewater Using an Integrated Process: Electrochemical-Oxidation with IrO2-Ta2O/Ti Anodes and Chitosan Powder as an Adsorbent. Environmental Processes, 6(4): 819–840

Rambabu, K. & Velu, S., 2016. Modified polyethersulfone ultrafiltration membrane for the treatment of tannery wastewater. International Journal of Environmental Studies, 73(5): 819–826.

Rivas, G., Carra, I., Sánchez, J.L.G., López, J.L.C., Malato, S. & Pérez, J.A.S. 2015. Applied Catalysis B : Environmental Modelling of the operation of raceway pond reactors for micropollutant removal by solar photo-Fenton as a function of photon absorption. 'Applied Catalysis B, Environmental', 178: 210–217.

Shafi, H.Z., Matin, A., Khan, Z., Khalil, A. & Gleason, K.K. 2015. Surface modification of reverse osmosis membranes with zwitterionic coatings: A potential strategy for control of biofouling. Surface and Coatings Technology, 279: 171–179.

Wang, Jing, Wang, Z., Wang, Jixiao & Wang, S. 2015. Improving the water flux and bio-fouling resistance of reverse osmosis (RO) membrane through surface modification by zwitterionic polymer. Journal of Membrane Science, 493: 188–199.

Wei, X., Wang, Z., Zhang, Z., Wang, J. & Wang, S. 2010. Surface modification of commercial aromatic polyamide reverse osmosis membranes by graft polymerisation of 3-allyl-5, 5-dimethyl hydantoin. Journal of Membrane Science, 351(1–2): 222–233.

Wu, B., Kitade, T., Haur, T., Uemura, T. & Fane, A.G. 2013. Impact of membrane bioreactor operating conditions on fouling behaviour of reverse osmosis membranes in MBR – RO processes. Desalination. 311: 37–45.

You, M., Wang, P., Xu, M., Yuan, T. & Meng, J. 2016. Fouling resistance and cleaning efficiency of stimuli-responsive reverse osmosis (RO) membranes. Polymer (United Kingdom), 103: 457–467.

Zhang, Z., Wang, Z., Wang, J. & Wang, S. 2013. Enhancing chlorine resistances and anti-biofouling properties of commercial aromatic polyamide reverse osmosis membranes by grafting 3-allyl-5, 5-dimethyl hydantoin and N, N ′ -methylene bis (acrylamide). Desalination. 309: 187–196.

Zhao, Y., Song, L. & Leong, S. 2010. Fouling behaviour and foulant characteristics of reverse osmosis membranes for treated secondary effluent reclamation, Journal of Membrane Science, 349(1-2): 65–74.

Chapter 5

BIOFOULING RESISTANCE IMPROVEMENT OF PA RO MEMBRANES THROUGH CHEMICAL GRAFTING WITH 3-ALLYL-5, 5-DIMETHYL HYDANTOIN.

This chapter has been published as:

Kasongo, G., Aziz, M. & Nkombe, A. 2025. Biofouling Resistance Improvement in Membrane-Based Municipal Wastewater Treatment: A Focus on Membrane Surface Modification by Graft Polymerization with 3-allyl-5, 5-dimethyl hydantoin. *Membranes,* 15(10). 314. [DOI.org/10.3390/membranes15100314]

5.1 Introduction

Chemical grafting is a membrane surface modification technique that improves the performance of the membrane and its fouling resistance (Aziz & Kasongo, 2021; Kasongo et al., 2019). However, several proposed PA RO membrane modification methods have been reported to enhance specific properties, such as fouling resistance, however they also have drawbacks, including reduced permeability and solute rejection. Ansari et al., (2021) found that introducing both polyacrylic acid and graphene oxide to a RO membrane surface improved hydrophilicity; however, the modified membranes exhibited slightly lower resistance to microbial fouling. Yang et al., 2020) modified a polyamide RO membrane using 2-carboxyethyl acrylate (CAA) and cationic [2-(acryloyloxy)ethyl] trimethyl ammonium chloride (TMA). It was observed that the modification enhanced membrane biofouling resistance, while the salt rejection and permeability decreased by approximately 20% and 15% respectively. Recent studies have advanced antifouling membrane design through the use of PEG-based, zwitterionic, and N-halamine modifications. However, it's been reported that PEG layers are prone to oxidative degradation over time (T. Wang et al., 2024). High concentration zwitterionic coatings achieve excellent hydration and fouling resistance but often require complex synthesis and exhibit limited long-term stability (Zheng et al., 2025). In a recent study, N-halamine coatings demonstrated strong antibiofouling performance; however, their biocidal capacity declined after repeated recharging cycles (Xing et al., 2024).

Hence, there is a need to develop PA RO membranes with higher resistance to fouling, particularly biofouling, while maintaining or improving the membrane's water flux and salt rejection. On the other hand, the surface modification must be tailored to allow for selective targeting of specific foulants, as each type of foulant may require a different modification approach to mitigate fouling effectively.

This section of the project evaluates the biofouling resistance of a polyamide RO membrane by modifying its surface with 3-allyl-5,5-dimethyl hydantoin (ADMH). The application of the modified membranes is evaluated against model foulants that mimic fouling activities in the secondary effluent of municipal wastewater treatment plants.

Research on ADMH grafting for polyamide RO membranes has demonstrated its potential to enhance chlorine resistance and antibacterial activity (Wei et al., 2010; Zhang et al., 2013). However, the field lacks a comparative perspective, with many studies focusing on a single foulant type, leaving their performance against other prevalent foulants unexplored. The practical challenge, as discussed by Sisay et al., (2023), is that surface modifications typically create a complex interplay of properties, in which enhancing one characteristic, such as hydrophilicity, may inadvertently alter another, such as surface charge. This work systematically evaluates ADMH grafting across a range of concentrations (0.2–0.8 mol L^{-1}) against a panel of individual foulants encompassing organic, inorganic, Gram-positive, and Gram-negative bacterial foulants, providing a clearer insight into how biofouling benefits and fouling resistance correlate with membrane performance.

5.2 Membrane surface modification using ADMH: Membrane characterisation

5.2.1 ADMH Characterisation

The ADMH was characterised by FTIR using the PerkinElmer FTIR spectrum, two spectrometers with a scan range of 400-4000 cm^{-1} to confirm the chemical's purity. Figure 19 shows the FTIR results for ADMH after synthesis.

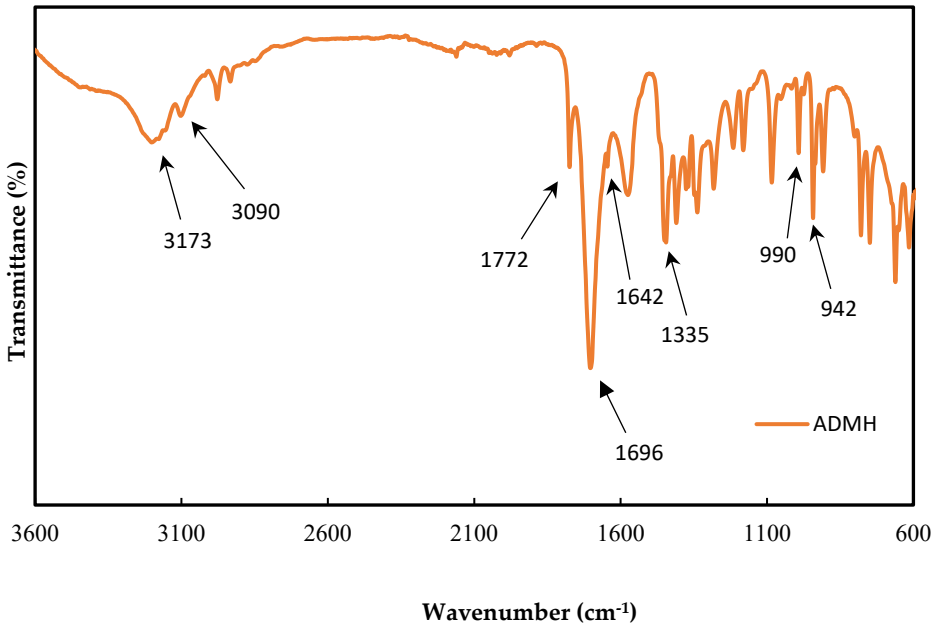


Figure 19: Modifying agent ADMH FTIR characteristics after synthesis.

An intense stretch at 73 cm^{-1} is due to the stretching vibration of $N-H$ bond and the strong pick at 1696cm^{-1} . This is due to the presence of a carbonyl group. The peak at 3090 cm^{-1} shows the strong stretching vibration of $=CH$ bond with a weak stretching vibration peak of $C=C$ bond at 1642 cm^{-1}. Also, the peak in 1772 cm^{-1} is due to stretching vibrations of the $C=O$ bond peak H. Moreover, the peak at 1335 cm^{-1} is due to the in-plane bending vibration of the $=CH$ bond, while the absorption peaks at 942 cm^{-1} and 990 cm^{-1} are present because of the out-of-plane bending of the $=CH_2$ bond (Wei et al., 2010).

5.2.2 Membrane Surface Modification and Characterisation

The degree of grafting was initially evaluated using the grafting yield. Figure 20 shows the grafting yield obtained with different ADMH concentrations. It is observed that the degree of grafting increases with the grafting concentration. This is due to the greater availability of monomer molecules at the membrane surface, which affects chain propagation during the graft polymerisation of the RO membrane. This implies a difference in the physicochemical properties of the modified membranes, as the properties of modified membranes are a function of the grafting yield, which is

highly dependent on the reaction conditions, such as the concentration of the modifying agent (Kasongo et al., 2019).

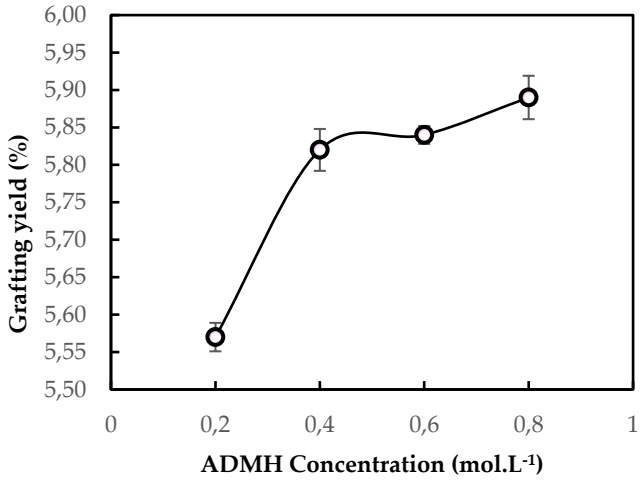


Figure 20: Grafting yield of ADMH on the RO membrane surface after modification.

The effect of surface-grafted ADMH on the membrane surface was investigated using FTIR, SEM, and NMR spectroscopy. Figure 21 shows the FTIR spectrum of the unmodified and ADMH-grafted membranes. The appearance of the characteristic peaks resembles those reported by Wei et al., (2010). The FTIR spectra of ADMH-grafted membranes clearly show the formation of a new band in the 3107 cm^{-1} which is a C=O bond in ADMH. The band becomes more visible as the ADMH concentration increases. Indeed, this observation suggests that ADMH has been successfully grafted onto the aromatic polyamide RO membrane surface, and the degree of grafting is more significant with increasing grafting concentration (Yang et al., 2020). The peaks at 2897 cm^{-1}, 2913 cm^{-1} are like the $C-O$ (amide I) stretching, the hydrogen-bonded $C-O$ (amide I) stretching, and $N-H$ (amide II) in-plane bending, respectively. Those stretchings are characteristics of polyamide in the barrier layer. The intense stretching at 3163 cm^{-1} is a $Ar-O-Ar$ stretching; to Ar is used to denote an aromatic ring, which is also characteristic of the membrane support layer (Liu et al., 2020). These findings are consistent with the findings reported by Wei et al., (2010) and, therefore, confirm the successful graft of ADMH on the membrane surface (Yang et al., 2020).

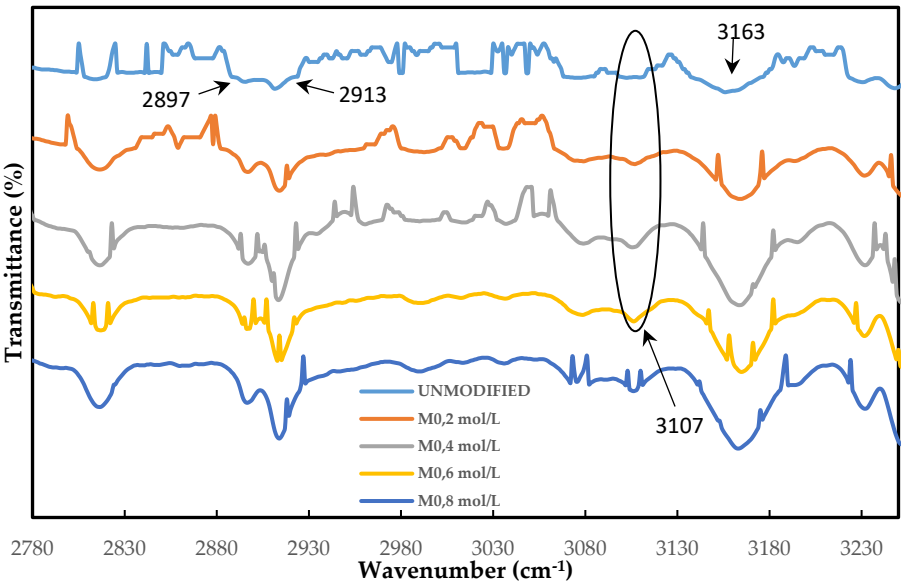


Figure 21: FTIR graphs for the Unmodified, M_0, $M_{0.2mol/L}$, $M_{0.4mol/L}$, $M_{0.6mol/L}$ and $M_{0.8mol/L}$ (modified membranes with 0.2 mol. L^{-1}, 0.4 mol. L^{-1}, 0.6 mol. L^{-1} and 0.8 mol. L^{-1} respectively) in the wavenumber range of 2780-3230 cm^{-1}.

SEM analysis was done to assess the membrane morphology before and after modification. Figure 22 shows the top-view SEM images of the RO membrane surface at 1 µm magnification and the cross-sectional images of the membranes on the left and the right, respectively. A typical multi-layered ridge-and-valley structure was observed in the unmodified membranes, as shown in Figure 23 (a1). Indeed, the top-view SEM images of the modified membranes show partial or complete filling of the XLE-4040 membrane pores by grafting chains. For the modified membranes, a less uniform appearance is observed, with irregularities in the form of matter. This observation is evident for the 0.6 mol/L grafted membrane shown in Figure 22 (d1). The irregularities observed on the membrane surface confirm the ADMH's adhesion, as suggested by Vatanpour & Zoqi, (2017).

Additionally, the irregularities become more pronounced with increasing concentration. The membrane surface modification caused the valleys of the commercial membranes to be filled with the grafting polymer ADMH.

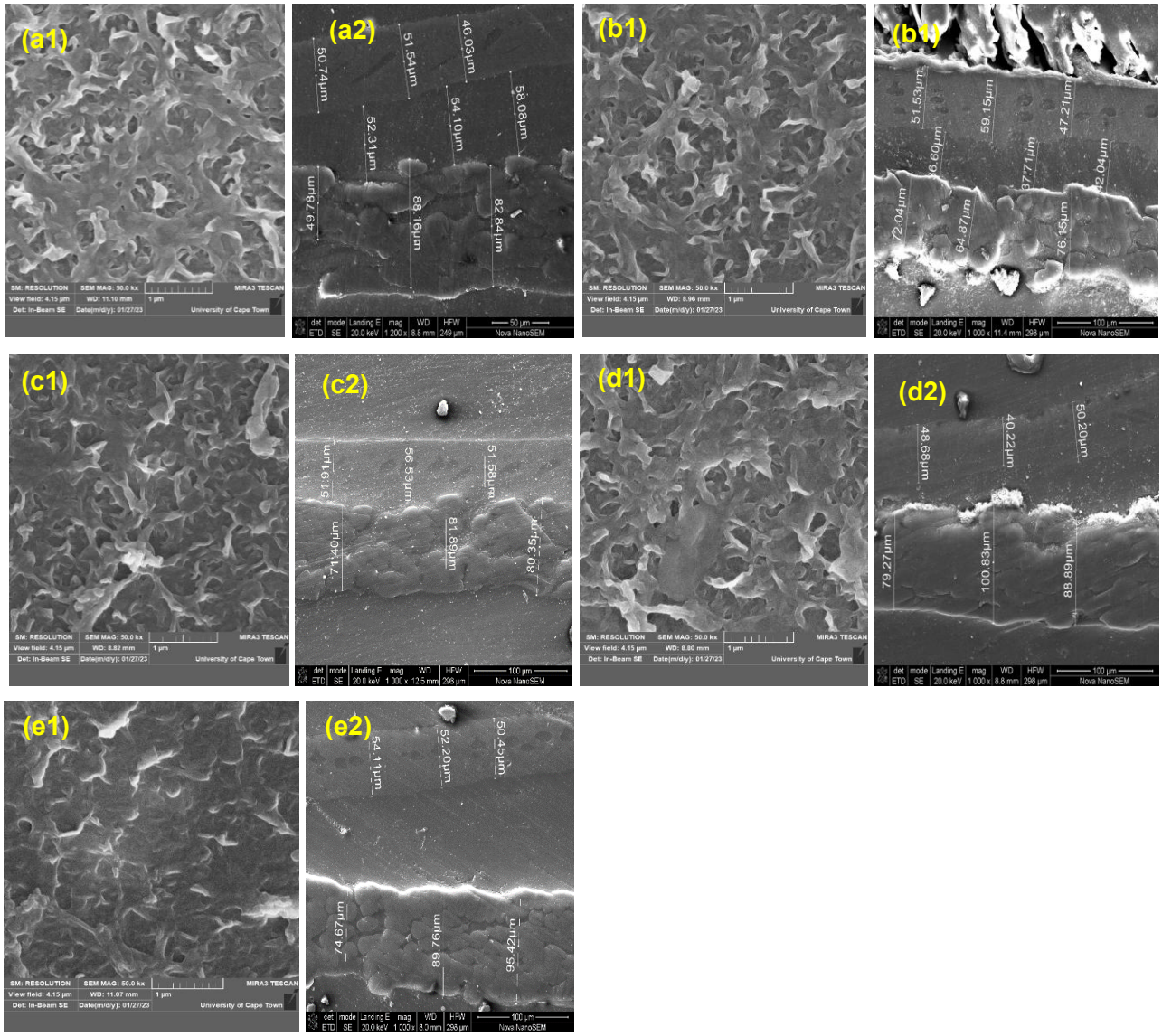


Figure 22: SEM images of the unmodified and ADMH grafted membranes (top-view & cross-section): (a) unmodified membrane, (b) 0.2 mol. L^{-1} ADMH, (c) 0.4 mol. L^{-1} ADMH, (d) 0.6 mol. L^{-1} ADMH, (e) 0.8 mol. L^{-1} ADMH.

Figure 22 also presents a cross-sectional view of the unmodified and grafted membrane samples. The cross-sectional thickness of the unmodified membrane is 88.16 µm, which differs from that of the modified membranes. The ADMH grafted membranes exhibit new characteristics in the top layer due to the addition of a thin layer. It confirms a successful modification of the membranes by ADMH grafting. Nuclear magnetic resonance spectroscopy was also used to analyse the structural alterations in the virgin reverse osmosis membrane and the modified membranes, as shown in Figure 23.

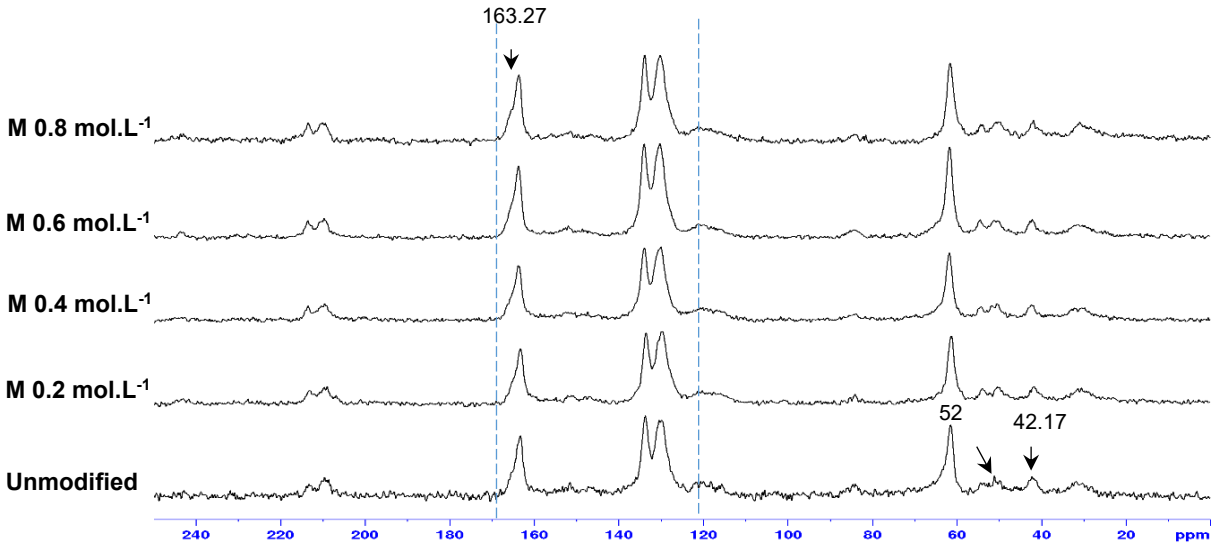


Figure 23: Solid C^{13} CPMAS NMR results for unmodified and all ADMH-modified membranes.

The carbonyl peak at 165 ppm belongs to the reverse osmosis membrane. Moreover, the chemical shift at 5.6–5.8 ppm was due to the methine proton in the pendant allyl groups. The spectrum of the neat bulk membrane displays resonances at (110 to 165) ppm, which belong to the reverse osmosis membrane. Liu et al., (2020) presented a nuclear magnetic resonance of ADMH and identified the elemental bonds of the agent. The pick-in at 52 ppm represents the (C $(CH_3)_2$) of the ADMH. The peak at 42.17 ppm corresponds to the (=$CHCH_2$) bond in ADMH, which increases with increasing concentration. The pick at 130.4 ppm is (=$CHCH_2$), while the pick at 163.27 ppm is the (C=O) bond in the ADMH structure. The variations observed from the membrane sample pick confirm the successful graft polymerisation (Liu et al., 2020).

The membrane surfaces were characterised using advancing contact angle measurements to assess hydrophilicity. As shown in Figure 24, the contact angle decreased progressively with increasing ADMH concentration: from 53.17° ± 1.73° for the unmodified membrane to 47.72° ± 2.29° for the 0.8 mol/L-modified membrane, with intermediate values of 52.80° ± 1.48°, 50.74° ± 1.75°, and 49.61° ± 1.65° for 0.2, 0.4, and 0.6 mol. L^{-1} modifications, respectively. This trend indicates that ADMH grafting effectively enhanced surface hydrophilicity. The introduction of hydrophilic amine and hydroxyl groups increases surface polarity, promoting water affinity and thereby lowering the contact angle (Wang et al., 2024). These findings align with previous reports indicating that the introduction of hydrophilic materials to the membrane surface reduces contact angles, thus improving membrane wettability (Wei et al., 2010).

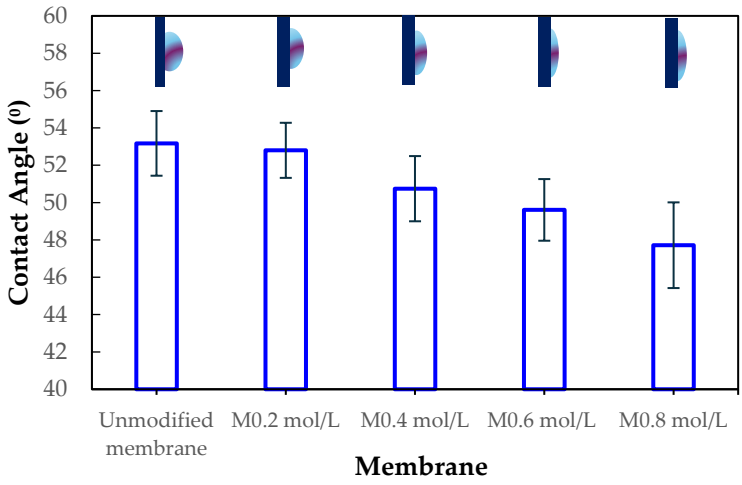


Figure 24: Contact angle measurements of unmodified and ADMH-modified RO membranes at different grafting concentrations (0.2 - 0.8 mol L^{-1}).

5.2.3 Biofouling Resistance

Figure 25 presents the mortality ratio of modified membranes compared to pristine membranes, tested with an *E. coli* solution. The membranes M0.2 mol. L^{-1} and M0.4 mol. L^{-1} (modified with 0.2 mol. L^{-1} and 0.4 mol. L^{-1} concentrations of ADMH, respectively) exhibits improved mortality rates of 45.23% and 58.93%, respectively. The membranes M 0.6 mol. L^{-1} and M 0.8 mol. L^{-1} (modified with 0.6 mol. L^{-1} and 0.8 mol. L^{-1} concentrations of ADMH, respectively) exhibit mortality ratios of 48.48% and 33.76%, respectively. One-way ANOVA showed a significant difference between unmodified and modified membranes when considering all mortality ratios ($p = 0.0253$). The grafting of ADMH onto the membrane introduces membrane functional groups that enable interfacial contact-killing, thereby reducing biofouling. Bromberg et al., (2024) demonstrated that N-halamine/hydantoin coatings provide durable contact-killing. Xiao et al., (2024) showed that grafting molecules, such as 2-aminoethanethiol, tunes interactions with foulants while maintaining permeance. This aligns with the present findings, where moderate ADMH concentrations enhanced hydrophilicity and foulant repellence without significantly compromising the membrane permeability.

It is observed that the membrane M0.4 mol. L^{-1} had the greatest improvement of 58.93% and appeared to be the optimal modified membrane against *E. coli*.

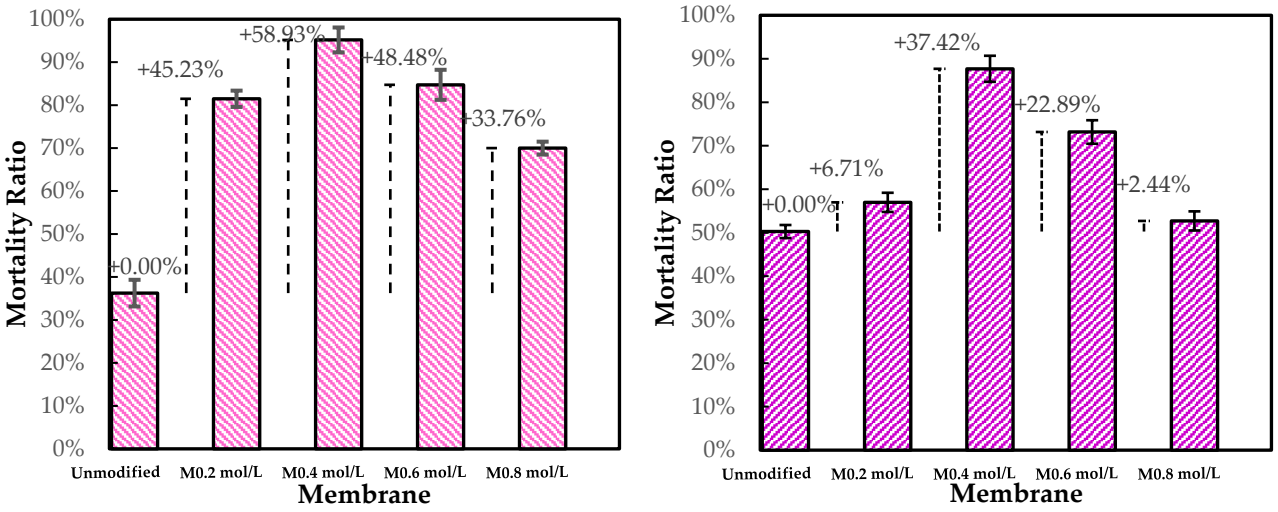


Figure 25: Static adhesion test results for unmodified and modified membranes against *E. Coli* (left) and *S. Aureus* (right).

Compared to *E. coli*, the mortality rate of the modified membranes is lower against *S. aureus*. Due to electrostatic interactions, gram-negative bacteria such as *E. coli* are repelled by the negatively charged surface of modified membranes, contrary to *S. aureus*, which has a positively charged outer surface (Ngo et al., 2017). This may also be explained by the fact that gram-positive bacteria can form more robust biofilms, which might offer better protection against the modified membrane surfaces and hence decrease mortality.

Moreover, the membrane M0.4 mol. L^{-1} shows the greatest improvement of 37.42% and appears to be the optimal modified membrane against *E. coli*. The success of the graft polymerisation of ADMH is observed by the behaviour of the 0.4 mol/L membranes. However, the membrane sample at 0.8 mol L^{-1} exhibited the lowest improvement, which could be due to the alteration of the membrane resulting in a reduction of electrostatic interactions necessary for an effective biofouling-resistant surface (Yang et al., 2020). The improved biofouling resistance activity observed at moderate ADMH concentrations (0.2–0.4 mol L^{-1}) can be attributed to adequate surface coverage that maintains accessibility of active groups while preserving permeability and electrostatic repulsion. At higher concentrations (>0.6 mol L^{-1}), however, excessive polymer deposition may cover functional groups, increase hydrogen bonding interactions, and hinder water transport (Suresh et al., 2021). Furthermore, it is observed that although surface hydrophilicity increases with ADMH concentration, antibiofouling performance peaks at 0.4 mol·L^{-1} and declines at 0.8 mol·L^{-1}. This suggests that enhanced hydrophilicity alone is not decisive; at moderate concentration, the denser hydrophilic groups promote a stable hydration layer that resists adhesion, whereas excessive concentrations cause surface heterogeneity, amplifying hydrophilicity but creating sites that facilitate microbial attachment and stronger foulant interactions (AlQasas & Johnson, 2024). The flux trend decreases over time, as shown in Figure 26, confirming the presence of microbial fouling, which is responsible

for the decline in flux. Modified membranes exhibited higher fluxes than unmodified ones, likely due to improvements in surface properties resulting from ADMH grafting. The anti-biofouling properties of ADMH are attributed to the strong bond formed on the membrane surface, which affects the flux of the membranes (Wei et al., 2010).

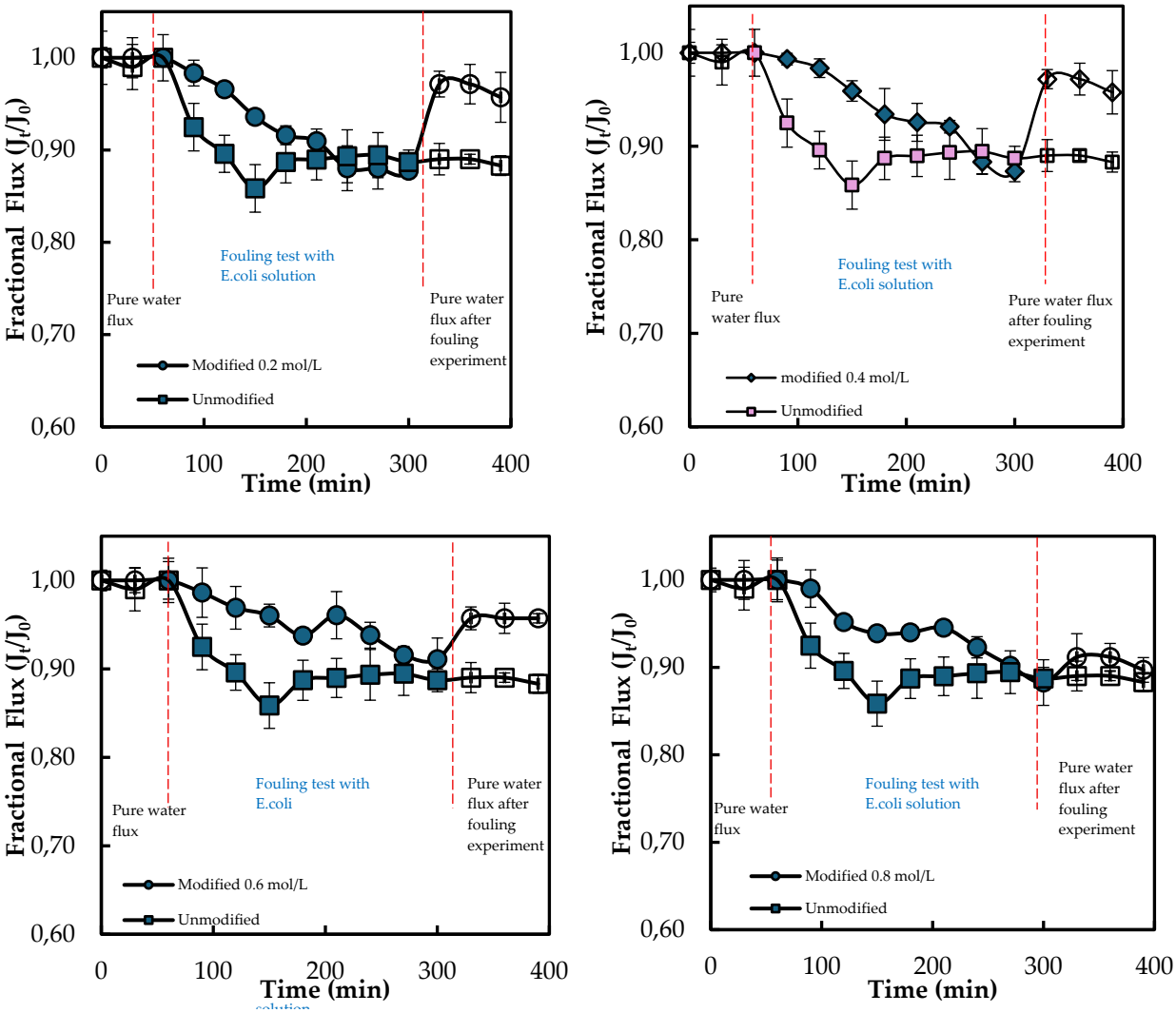


Figure 26: Flux of ADMH grafted membranes compared to the unmodified membrane during dynamic fouling tests with *E. coli* solution using an RO system.

Figure 27 shows that the flux decreases over time, confirming the presence of microbial fouling by *S. aureus*. The overall flux trend of the modified membranes is similar to that of the unmodified membrane. However, the fluxes of the modified membranes are slightly lower than those of the unmodified membrane, with a value of 33.58%, while the highest flux is 54.47% for the unmodified membrane. This observation could be due to the polymerisation of the aromatic layer of the grafted

membrane getting more compact due to heat treatment, which is responsible for increased water resistance (Zhang et al., 2013).

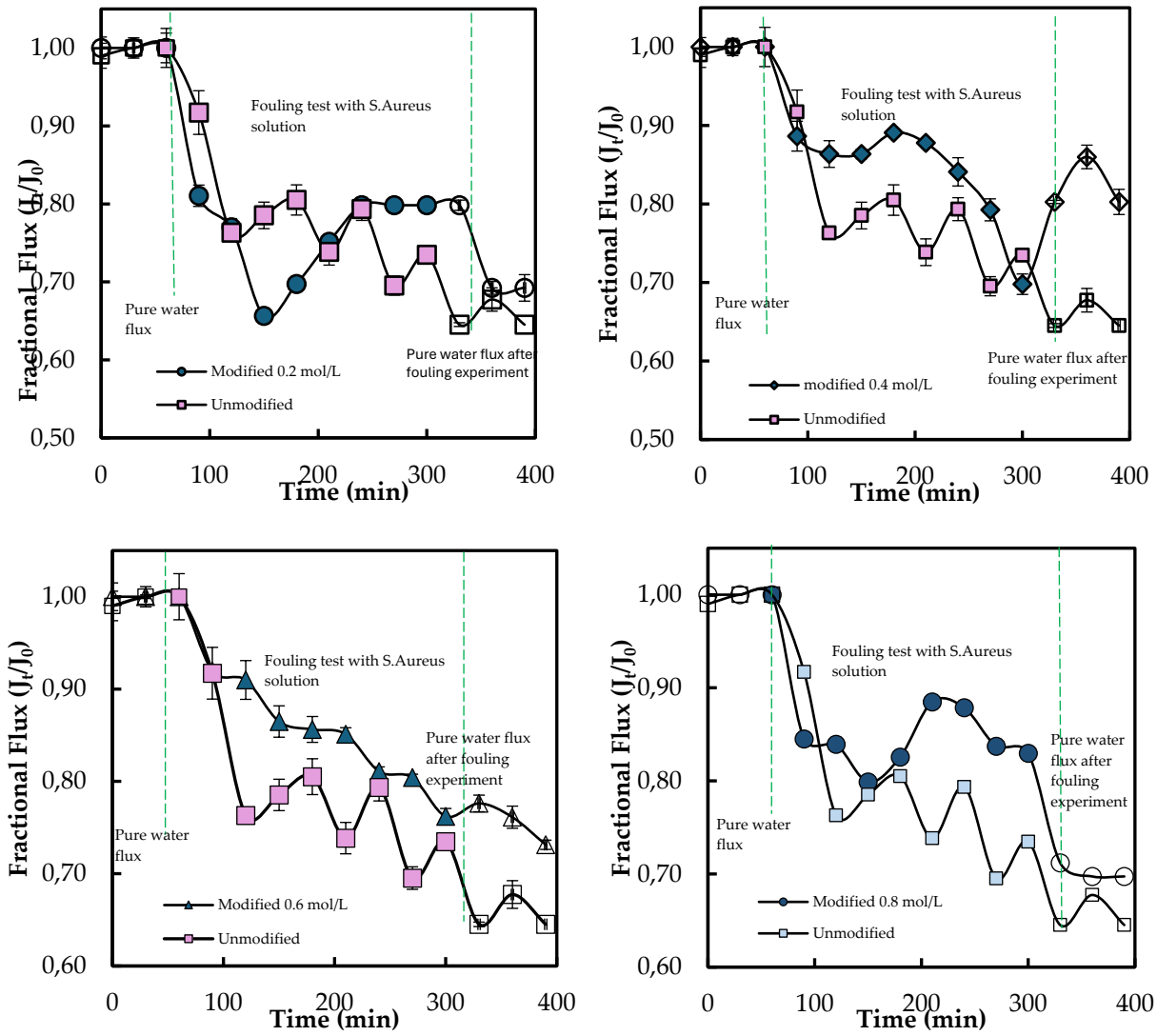


Figure 27: Flux of ADMH grafted membranes compared to the unmodified membrane during dynamic fouling tests with *S. Aureus* solution using a RO system.

The performance results of the modified and unmodified membranes are presented in Table 8. The salt rejection for the modified membranes was 80.99%, 81.62%, 80.81%, and 80.33% for the $M_{0.2mol/L}$, $M_{0.4mol/L}$, $M_{0.6mol/L}$, and $M_{0.8mol/L}$ membranes, respectively. It was observed that the salt rejection increased after surface modification.

Moreover, the membrane permeability of the modified membranes with ADMH concentrations of 0.2 $mol.L^{-1}$, 0.4 $mol.L^{-1}$, 0.6 $mol.L^{-1}$, and 0.8 $mol.L^{-1}$ was 9.52 $L.m^2\ h^{-1}\ bar^{-1}$, 9.51 $L.m^2\ h^{-1}\ bar^{-1}$, 9.18 $L.m^{-2}\ h^{-1}\ bar^{-1}$ and 9.02 $L.m^{-2}.h^{-1}\ bar^{-1}$. A decrease in permeability was observed with increased ADMH concentration, attributed to the addition of a layer on the membrane surface after modification. Wei et al., (2010) reported that grafting time affects permeability by altering the membrane's

hydrophilicity. Moreover, according to Wang et al., (2015), modifying the agent molecules at the membrane surface decreases hydrogen bonding between the carboxylic and amine groups of the polyamide layer, resulting in higher flux for the modified membrane.

Table 8: Mortality Ratio, FDR, and FRR values of ADMH grafted membranes.

	Salt Rejection (%)	Permeability (L/m².h.bar)	FDR (%)		FRR (%)	
			E. coli	S. aureus	E. coli	S. aureus
M_0	76 ± 1.27%	7.26 ± 0.15	11.29 ± 0.72%	26.53 ± 1.12%	82.26 ± 0.89	48.39 ± 1.41%
$M_{0,2mol/L}$	81 ± 0.58%	9.52 ± 0.98	12.24 ± 0.53%	3.72 ± 2.03%	96.88 ± 1.38	69.23 ± 1.66%
$M_{0,4mol/L}$	82 ± 1.01%	9.51 ± 0.56	12.68 ± 0.81%	30.21 ± 0.93%	94.27 ± 1.77	59.70 ± 1.99%
$M_{0,6mol/L}$	81 ± 0.91%	9.18 ± 0.44	8.91 ± 0.89%	23.79 ± 1.51%	96.88 ± 1.26	70.15 ± 1.82%
$M_{0,8mol/L}$	80% ± 0.43	9.51 ± 0.67	11.74 ± 0.13%	17.03 ± 1.69%	88.40 ± 2.46	65.67+1.91%

After 240 minutes of fouling, the lowest FDR value of 8.91% with *E. coli* was observed for $M_{0.6mo/L}$, and the highest FRR value of 96.88% was observed for $M_{0.2mo/l}$. Furthermore, the $M_{0.2mo/L}$ membrane had the lowest FDR value of 3.72%, while the $M_{0.6mol/L}$ membrane had the highest FRR value of 70.15% when tested with *S. aureus*. The decline in fluxes of ADMH grafted membranes may have been caused by the recovery of the inter-chain hydrogen (Zhang et al., 2013).

5.2.4 Organic Fouling Resistance

Figure 28 below presents the flux behaviour of the ADMH-grafted membranes during the organic fouling test using humic acid solution.

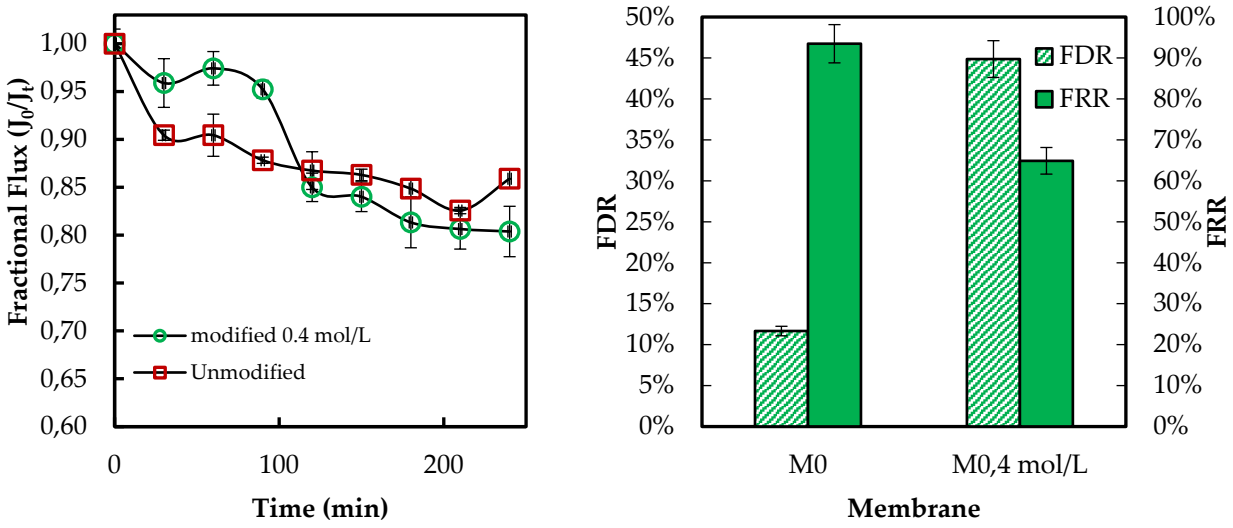


Figure 28: Membranes' antifouling properties during fouling tests with organic foulant solutions.

The overall fluxes through the modified membrane follow a similar pattern to those through the unmodified membrane. The FDR values are 11.66% and 44.87% for the unmodified and modified membranes. The FRR values are 93.47% and 64.89% for the unmodified and modified membranes, respectively. The modified membrane exhibited a lower flux than the unmodified membrane. This may be explained by the fact that ADMH's functional groups can form hydrogen bonds with the organic foulant, thereby increasing their adhesion to the membrane surface. In contrast to the adhesion of microorganisms, the grafting of ADMH may have provided more sites for organic molecules to adhere to, thereby promoting fouling. Similar trade-offs have been reported, where improvements in one property may compromise others (Suresh et al., 2021). Da'na et al., (2025) further confirmed that the polarity and type of surface functional groups are key factors governing fouling interactions.

5.2.5 Inorganic Fouling Resistance

Figure 29 below presents the flux behaviour of the ADMH-grafted membranes during the inorganic fouling test using sodium bicarbonate ($NaHCO_3$).

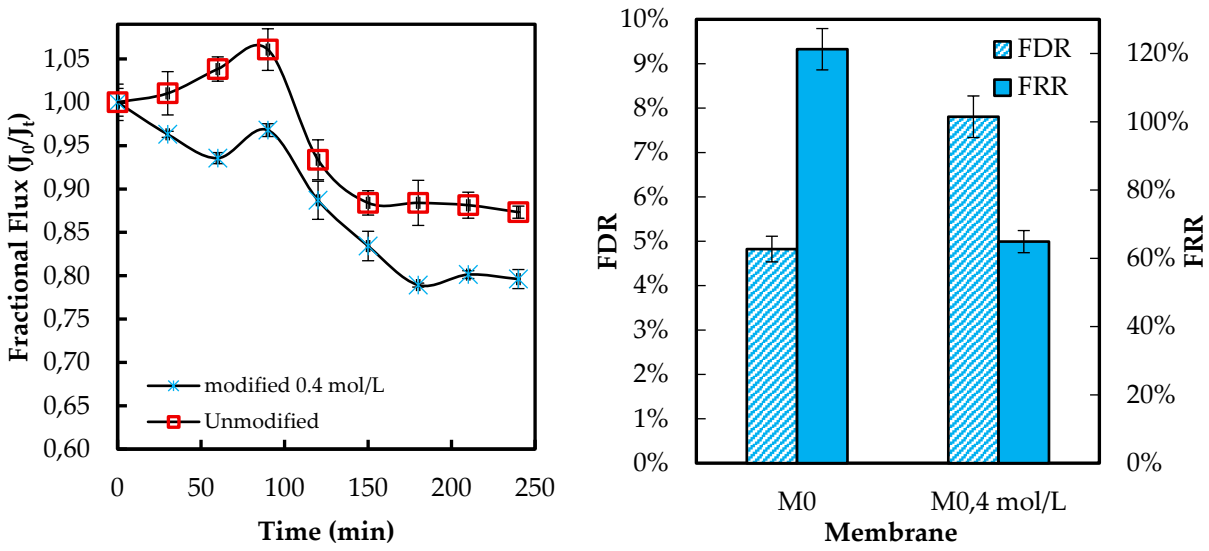


Figure 29: Membranes' antifouling properties during fouling tests with inorganic foulant solutions.

The FDR values are 4.82% and 11.34%.87% for the unmodified and modified membranes, respectively. Similarly, the unmodified membrane had a higher FRR than the modified membrane. The slight decline in resistance to both organic and inorganic fouling indicates that improved hydrophilicity was insufficient to prevent fouling, with foulant surface affinity exerting a more significant influence on the fouling mechanism. The decline in resistance to organic and inorganic fouling can be attributed to increased surface polarity from amide and hydantoin groups, which facilitate hydrogen bonding and dipole interactions with organic molecules and bicarbonate species.

Hence, functional groups and inorganic ions can jointly influence organic and inorganic fouling mechanisms (Xiao et al., 2024), while the same reactive surface enhances the contact-killing of microorganisms.

Mallah et al., (2025) reported that introducing hydrophilic nanocomposites enhanced permeability and reduced microbial attachment but slightly increased organic adsorption due to new polar interaction sites. Similarly, Bromberg et al. (2024) found that non-leaching N-halamine coatings maintained vigorous antibacterial activity yet exhibited moderate protein adsorption, while Xiao et al. (2024), demonstrated that grafted functional groups can alter foulant interaction energies, thereby influencing adsorption dynamics on RO membranes.

Despite a slight change in FDR, particularly with the modified membranes, the F-test ($p = 0.27$) indicates that this change is not statistically significant.

5.3 Summary

The study assessed the fouling resistance of reverse osmosis membranes after graft polymerisation of ADMH. The ADMH was used at varying concentrations to enhance the membrane surface's antibiofouling properties and was further tested for its resistance to both organic and inorganic fouling. Biofouling tests showed improved mortality ratios against both *E. coli* (45.23%, 33.76%, 48.48% and 58.93% for $M_{0.2\ mol/L}$ - $M_{0.8\ mol/L}$) and *S. aureus* (6.71%, 37.42%, 22.89% and 2.44% for $M_{0.2\ mol/L}$ - $M_{0.8\ mol/L}$). The biofouling resistance test demonstrated the improved biofouling resistance properties after the grafting of ADMH on the membrane surface. The $M_{0.2mol/L}$ and $M_{0.6mol/L}$ membranes exhibited the lowest FDR values of 3.72% against *S. aureus* and 8.91% against *E. coli*, respectively, with FRR values of 69.23% and 96.88%. The $M_{0.4mol/L}$ showed an FRR value of 94.27% against *E. coli* bacteria and 59.70% against S aureus.

The study reveals the impact of ADMH on improving membranes' biofouling resistance properties. However, after ADMH grafting, the membrane showed a slight decrease in resistance to both organic and inorganic fouling. Despite increasing hydrophilicity with ADMH concentration, fouling resistance peaked at 0.4 mol. L^{-1} and slightly declined at 0.8 mol. L^{-1}, indicating that surface heterogeneity can override hydrophilicity in governing foulants' adhesion.

5.4 References

AlQasas, N. & Johnson, D. 2024. Combined Effects of Surface Roughness, Solubility Parameters, and Hydrophilicity on Biofouling of Reverse Osmosis Membranes. *Membranes*, 14(11).

Ansari, A., Peña-Bahamonde, J., Wang, M., Shaffer, D.L., Hu, Y. & Rodrigues, D.F. 2021. Polyacrylic acid-brushes tethered to graphene oxide membrane coating for scaling and biofouling mitigation on reverse osmosis membranes. *Journal of Membrane Science*, 630(December 2020).

Bromberg, L., Magariños, B., Concheiro, A., Hatton, T.A. & Alvarez-Lorenzo, C. 2024. Nonleaching Biocidal N-Halamine-Functionalized Polyamine-, Guanidine-, and Hydantoin-Based Coatings. *Industrial and Engineering Chemistry Research*, 63(14): 6268–6278.

Da'na, D.A., Nawi, N.S.M., Sangor, F.I., Ashfaq, M.Y., Lau, W.J. & Al-Ghouti, M.A. 2025. Strategies for the use and interpretation of functionalized reverse osmosis membranes with improved antifouling and anti-scaling properties for the desalination process. *Desalination*, 600.

Hong Anh Ngo, T., Tran, D.T. & Hung Dinh, C. 2017. Surface photochemical graft polymerization of acrylic acid onto polyamide thin film composite membranes. *Journal of Applied Polymer Science*, 134(5).

Kasongo, G., Steenberg, C., Morris, B., Kapenda, G., Jacobs, N. & Aziz, M. 2019. Surface grafting of polyvinyl alcohol (PVA) cross-linked with glutaraldehyde (GA) to improve resistance to fouling of aromatic polyamide thin film composite reverse osmosis membranes using municipal membrane bioreactor effluent. *Water Practice and Technology*, 14(3): 614–624.

Liu, X., Li, L., Chen, Z., Duan, X., Yu, Y. & Sun, L. 2020. Curing behavior, thermal, and mechanical properties of N,N′-(4,4′-diphenylmethane)bismaleimide/2,2′-diallylbisphenol A/3-allyl-5,5-dimethylhydantoin resin system. *High Performance Polymers*, 32(6): 631–644.

Mallah, N.B., Shah, A.A., Pirzada, A.M., Ali, I., Ullman, J.L., Mahar, R.B. & Khan, M.I. 2025. Development of Antifouling Polyvinylidene Fluoride and Cellulose Acetate Nanocomposite Membranes for Wastewater Treatment Using a Membrane Bioreactor. *Water (Switzerland)*, 17(12).

Sisay, E.J., Al-Tayawi, A.N., László, Z. & Kertész, S. 2023. Recent Advances in Organic Fouling Control and Mitigation Strategies in Membrane Separation Processes: A Review. *Sustainability (Switzerland)*, 15(18).

Suresh, D., Goh, P.S., Ismail, A.F. & Hilal, N. 2021. Surface design of liquid separation membrane through graft polymerization: A state of the art review. *Membranes*, 11(11).

Wang, J., Hao, S., Qi, P., Wang, W. & Hu, Y. 2024. Superior chlorine-resistance of hyperbranched polyglycerol (hPG) grafted polyamide reverse osmosis membrane and its chlorine-resistant mechanism. *Journal of Membrane Science*, 709.

Wang, Jing, Wang, Z., Wang, Jixiao & Wang, S. 2015. Improving the water flux and bio-fouling resistance of reverse osmosis (RO) membrane through surface modification by zwitterionic polymer. *Journal of Membrane Science*, 493: 188–199.

Wang, T., Hou, Z., Yang, H. & Hu, J. 2024. A PEGylated PVDF Antifouling Membrane Prepared by Grafting of Methoxypolyethylene Glycol Acrylate in Gama-Irradiated Homogeneous Solution. *Materials*, 17(4).

Wei, X., Wang, Z., Zhang, Z., Wang, J. & Wang, S. 2010. Surface modification of commercial aromatic polyamide reverse osmosis membranes by graft polymerization of 3-allyl-5 , 5-dimethylhydantoin. *Journal of Membrane Science*, 351(1–2): 222–233. http://dx.doi.org/10.1016/j.memsci.2010.01.054.

Xiao, J., Hao, S., Qin, Y., Qi, P., Zhang, Z. & Hu, Y. 2024. Fouling-resistant reverse osmosis membranes grafted with 2-aminoethanethiol having a low interaction energy with charged foulants. *npj Clean Water*, 7(1).

Xing, M., Zhang, H., Li, Z., Zhang, L. & Qian, W. 2024. Long-lasting renewable antibacterial N-halamine coating enables dental unit waterlines to prevent and control of contamination of dental treatment water. *Frontiers in Materials*, 11.

Yang, Z., Saeki, D., Takagi, R. & Matsuyama, H. 2020. Improved anti-biofouling performance of polyamide reverse osmosis membranes modified with a polyampholyte with effective carboxyl anion and quaternary ammonium cation ratio. *Journal of Membrane Science*, 595(May 2019): 117529. https://doi.org/10.1016/j.memsci.2019.117529.

Zhang, Z., Wang, Z., Wang, J. & Wang, S. 2013. Enhancing chlorine resistances and anti-biofouling properties of commercial aromatic polyamide reverse osmosis membranes by grafting 3-allyl-5, 5-dimethylhydantoin and N, N ′ -Methylenebis (acrylamide). *DES*, 309: 187–196. http://dx.doi.org/10.1016/j.desal.2012.10.019.

Zheng, P., Yuan, S., Shen, Y., Wang, D., Liu, X. & Wang, Z. 2025. Superwetting-assisted preparation of high-density ultra-short zwitterion grafted membranes with outstanding antifouling performance. *Water Research*, 287.

Chapter 6

HYBRID MEMBRANE SURFACE MODIFICATION OF PA RO MEMBRANE TO ADDRESS BIOFOULING IN THE TREATMENT OF MUNICIPAL SECONDARY EFFLUENT

This chapter has been submitted as:

Kasongo, G., & Aziz, M. 2025. *Synergistic Antimicrobial Nanocomposite-Hydrophilic Monomer Surface Functionalization for Enhanced Biofouling Resistance in PA RO Membranes. Separation & Purification Technology.* Submitted (ID: SEPPUR-D-25-16866).

.

6.1 Introduction

The RO membrane, which has been used since the 1960s for desalination and wastewater treatment, faces significant challenges due to membrane fouling over long-term operation, the excessive use of chemical disinfectants to alleviate fouling, might damage the membrane and raise operating costs (Bromberg et al., 2024; Kasongo et al., 2025). Operating at moderate flux can delay fouling; however, preventing initial microbial attachment remains challenging due to the self-replicating nature of microorganisms (Habib et al., 2020; Kasongo et al., 2019).

Current research focuses on nano-structuring thin-film composite (TFC) reverse osmosis membranes to enhance performance and fouling resistance, while maintaining the essential trade-off in membrane design: achieving improved antifouling behaviour without compromising permeability or salt rejection. However, nanoparticle aggregation and weak compatibility between fillers and polymer matrices remain challenges in membrane nano-structuring. Researchers have explored various approaches to address particle aggregation and weak compatibility. One common approach is to pre-functionalize nanoparticles with a polymer before they enter the membrane matrix. The pre-functionalised nanoparticles improve bonding and stability. There is growing interest in the combined effects of polymers and nanoparticles. The hybrid modification that mixes polymers and nanoparticles strengthens antifouling behaviour and boosts the separation performance solution (Ahmad et al., 2022). Bagheripour et al., (2018) incorporated activated carbon nanoparticles into a Polyethersulfone (PES) casting solution mixed with chitosan. The chitosan coating improved the compatibility of the activated carbon nanoparticles with the PES casting solution. On the other hand, Suresh et al., (2025) reported a surface modification of polyamide thin-film composite reverse osmosis membranes using co-grafted copper and L-glutamine to exploit their complementary functions. Copper imparted antimicrobial activity, while L-glutamine adjusted the surface chemistry, resulting in reduced biofilm formation and improved resistance to biofouling without a significant penalty in desalination performance. The study showed that this synergistic co-grafting approach enhanced membrane operational stability while maintaining favourable water permeability and salt rejection compared with the unmodified membrane.

This section of the research project combines the hydrophilic monomer ADMH with a TiO_2-Ag nanocomposite to produce a hybrid surface layer that resists all common fouling modes while preserving salt rejection and improving permeability. ADMH forms a hydration-rich interface that minimises biological adhesion. The TiO_2-Ag phase causes antimicrobial action and addresses organic fouling. Together, these components act in concert: ADMH maintains a dense, selective PA skin that sustains high salt rejection, while the TiO_2-Ag network promotes water transport through favourable surface energetics and prevents biofilm establishment.

6.1 Membrane surface modification using ADMH\ TiO_2-Ag

6.1.1 ADMH and TiO_2-Ag characterisation: PSD

The particle size distribution of the nanoparticles was characterised in terms of percentile diameters D(10), D(50), and D(90), indicating the particle diameter below which 10%, 50%, and 90% of the distribution lie, respectively. Table 9 summarises the particle size distribution of the nanoparticles in terms of percentile values while Figure 30 shows the particle size distribution curves used to evaluate nanoparticle size and dispersion.

The particle size distributions measured for the TiO_2, Ag, and TiO_2-Ag suspensions provided insight into the stability and dispersion behaviour of the nanoparticles. The relatively narrow distribution observed for the TiO_2 particles (DX(50): 4.89 µm) and the limited extension toward larger particle sizes suggest a moderate level of agglomeration of TiO_2. On the other hand, the broader distribution of the Ag particles, characterised by a significant spread between D(10) and D(90) shows a tendency toward agglomeration (Fazekas et al., 2024). The TiO_2-Ag nanocomposite exhibited a narrower distribution, with reduced D(10) and D(90) relative to the Ag suspension and a median particle size approaching that of TiO_2. This suggests that the incorporation of Ag into TiO_2 effectively mitigates the formation of large Ag aggregates, resulting in a more uniform particle size distribution. Such improved dispersion may be advantageous for membrane modification as it promotes the formation of a more homogeneous surface and reduces the likelihood of pore blockage. Enhanced dispersion of Ag on TiO_2 not only stabilises the composite suspension but also increases the available surface area for interactions with foulants and microorganisms, which may be beneficial for membrane performance (Dou et al., 2025).

Table 9: Particles size distribution of nanoparticles presented in percentile

Particles size distribution	D[10] (µm)	D[50] (µm)	D[90] (µm)
TiO_2	2.69 ± 0.41	4.89 ± 0.89	8.28 ± 0.12
Ag	7.29 ± 1.25	37.29 ± 102	382.89 ± 2.6
TiO_2-Ag	0.66 ± 0.02	4.040 ± 0.76	7.48 ± 098

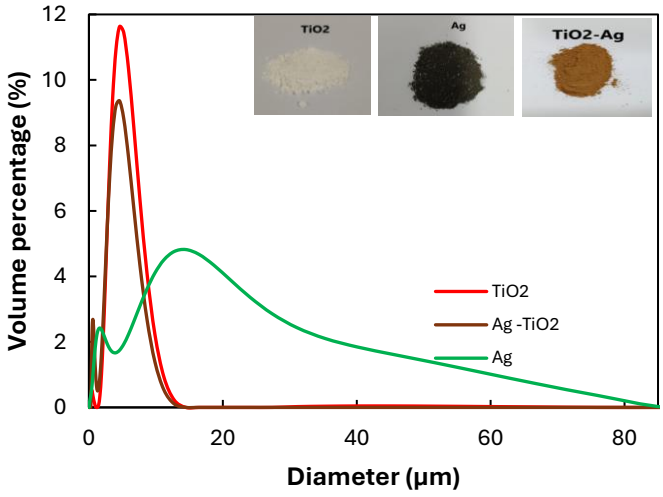


Figure 30: Zetasizer-derived particle size distribution of the nanoparticles

6.1.2 ADMH and TiO_2-Ag characterisation: FTIR and XRD

Figure 31 shows the characteristics spectra of ADMH, TiO_2, Ag and TiO_2-Ag nanoparticles using FTIR and XRD analyses. The XRD patterns of the TiO_2 and TiO_2 - Ag samples confirmed the presence of the anatase TiO_2 crystalline phase, with diffraction peaks at about 25.8° for the (101) plane, at about 38.0° for (004), and at about 48.19° for (200). In the Ag-TiO_2 composite, additional diffraction features attributable to metallic silver, such as reflections near 38.8° (Ag (111)), 44.2° (Ag (200)) and higher order planes, are shown. The retention of the anatase TiO_2 peaks in the composite suggests that the TiO_2 remains intact upon Ag integration, while the appearance or enhancement of Ag-related peaks supports the coexistence of both phases (Hong et al., 2020; Cao et al., 2017).

The FTIR spectra further showed the characteristics of the ADMH, nanoparticles, and nanocomposite structure. For the ADMH spectra, the peak at 3090 cm^{-1} shows the strong stretching vibration of $= CH$ bond with a weak stretching vibration peak of $C = C$ bond at 1642 cm^{-1}. Also, the peak in 1772 cm^{-1} is due to stretching vibrations of the $C = O$ bond peak H. Moreover, the peak at 1335 cm^{-1} is due to the in-plane bending vibration of the $= CH$ bond, while the absorption peaks at 942 cm^{-1} and 990 cm^{-1} are present because of the out-of-plane bending of the $= CH_2$ bond (Wei et al., 2010). The TiO_2 sample typically exhibits strong Ti-O-Ti stretching vibrations below 800 cm^{-1}, particularly in the 500-700 cm^{-1} region, which reflects the TiO_2 oxide as reported by several researchers (Al Mayyahi, 2018; Gayed et al., 2019). The surface-adsorbed hydroxyl groups is seen by broad bands around 3200-3700 cm^{-1} and bending vibrations near 1600-1640 cm^{-1}, reflecting -OH and H-O-H, often observed in both pure TiO_2 and Ag-TiO_2 materials due to surface hydration and Ag-TiO_2 composite, similar Ti-O-Ti bands are retained, with potential shifts or band broadening which suggest the interactions between the Ag phase and the TiO_2 surface (Fazekas et al., 2024).
Considering both analyses, the XRD and FTIR indicate that the Ag-TiO_2 sample consists of a crystalline anatase TiO_2 matrix with well-dispersed Ag nanoparticles, which aligns with other studies reporting that the nanocomposites preserve the oxide structure while integrating metallic phases, which is favourable for functional applications such as membrane surface modification. without compromising the fundamental TiO_2 (Dou et al., 2025; Habib et al., 2020; Gogoi et al., 2020).

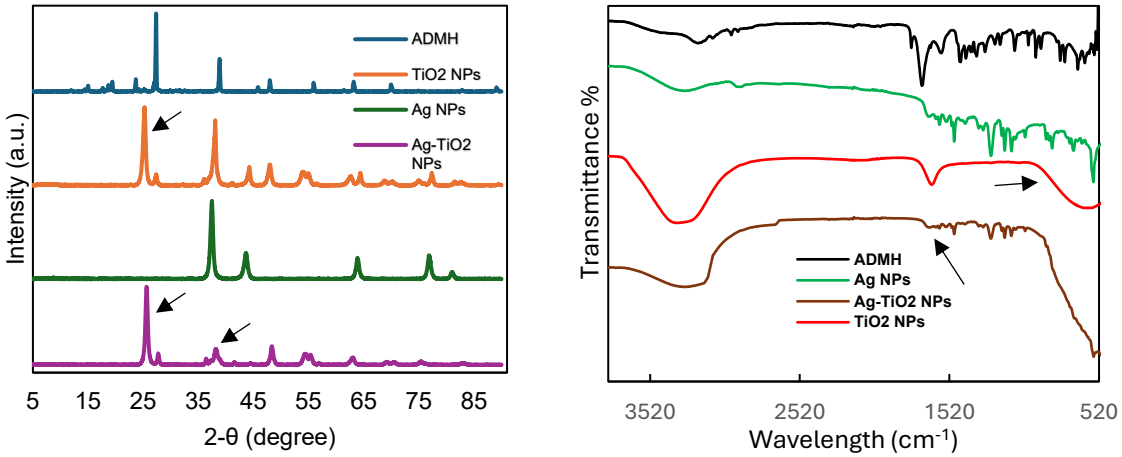


Figure 31: XRD (left) and FTIR (right) spectra of ADMH, the nanoparticles and nanocomposites used for the modification of the PA RO membrane in this work

6.1.3 Membrane surface characterisation: FTIR analysis

The unmodified and modified membranes were characterised by FTIR with a scan range of 400-3500 cm^{-1}. The FTIR spectra of the unmodified and modified membranes in Figure 32 show changes in both band intensity and spectral characteristics after surface modifications. The M-U membrane displays a broad absorption band around 3300 and 4000 cm^{-1}, which is characteristic of O-H and N-H stretching vibrations associated with adsorbed water and amide groups in the polyamide active layer (Yutao Hu et al., 2016; Liu et al., 2015). This band is also present in the spectra of the modified membranes but becomes broader and more intense for M-H and M-HTA, indicating an increase in surface polar functionalities and hydrogen-bonding capability after surface modification (Wei et al., 2010; Zhang et al., 2013). At the wavelength range 1500-1700 cm^{-1}, noticeable changes in peak intensity and shape are observed for the modified membranes compared with M-U. These bands are commonly associated with amide I and amide II vibrations of the polyamide layer. The attenuation of these peaks, particularly for M-TA and M-HTA, suggests surface interactions and partial coverage of the polyamide by the grafted layer and nanoparticle coatings (Dou et al., 2025; Fazekas et al., 2024). The unmodified and modified membranes were characterised by FTIR with a scan range of 400-3500 cm^{-1}. Figure 4 shows the FTIR graphs for the unmodified and modified membranes, as well as the results for ADMH after synthesis. The FTIR spectra show diagnostic bands that confirm the presence of the ADMH, the TiO_2 oxide and the presence of Ag on the membrane. The ADMH (hydantoin) is marked by carbonyl stretching bands (C=O stretches are common for hydantoin rings), which appear as the distinctive high-frequency carbonyl absorptions reported for hydantoin derivatives (Wei et al., 2010). Titanium dioxide modified membrane displays the expected metal-oxygen vibrations. The Ti-O-Ti\Ti-O stretching occurs in 400-800 cm^{-1} spectra (Al Mayyahi, 2018). The broad bands around 3200 and 3400 cm^{-1} indicate surface-

adsorbed hydroxyl groups and water on the oxide surface features, as reported for TiO_2 nanomaterials (Gayed et al., 2019b). The slight changes, i.e. slight shifts or decreased intensity of Ti-O-Ti bands, are consistent with structural interactions caused by the Ag-TiO_2 interface and have been observed in studies of Ag-decorated titania, where Ag stabilisation suppresses large agglomerates without destroying the oxide lattice (Dou et al., 2025; Fazekas et al., 2024). Overall, the FTIR spectra confirm the surface modification through increased surface polarity and the introduction of inorganic-related vibrational features, while preserving the chemical structure of the base membrane.

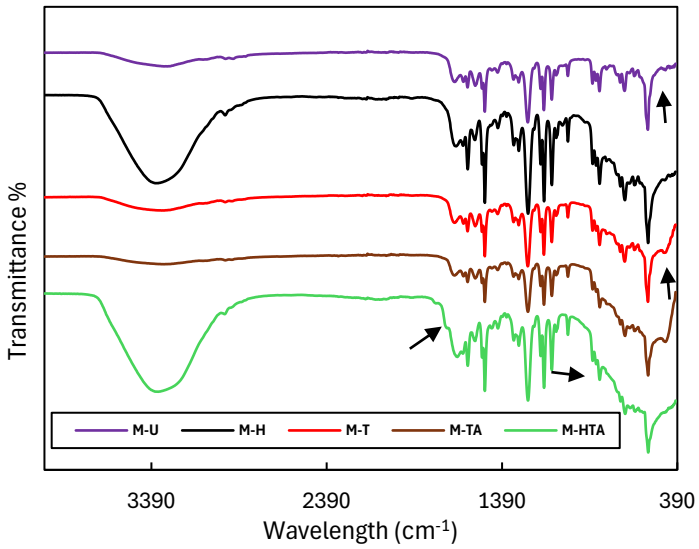


Figure 32: FTIR spectra of unmodified (M-U) and surface-modified membranes (M-H, M-TA, M-HTA), showing changes in functional groups after grafting

6.1.4 Membrane surface characterisation: Thermal stability TGA

Thermogravimetric Analysis (TGA) was conducted to assess the thermal stability of the membranes and confirm the attachment of the membrane-modifying agents by evaluating residual mass losses. The modified membranes caused a slight change in the membrane decomposition behaviour, as shown by the increase in inorganic residue. That is consistent with the other reported works that used nanoparticles as modifying agents. Armendáriz-Ontiveros et al., (2020) used chitosan and silver particles and reported that silver coatings increased residual mass but did not significantly raise the membrane decomposition temperature unless coupled with an inorganic reinforcing phase. From the TGA curves (zoomed) shown in Figure 33, the onset temperature of major degradation (Tonset) shifts slightly toward higher temperature for the modified membranes, particularly for the TiO_2-modified (M-T) and ADMH-modified (M-H) samples, compared with M-U. This indicates an improvement in initial thermal stability. The enhanced Tonset enhancement may be attributed to the heat-shielding effect imparted by inorganic materials (Batool et al., 2021). The hybrid membranes containing both inorganic and organic modifiers (HTA) showed intermediate Tonset behaviour. This suggests that the combined modification affects the degradation pathway; however, it does not imply a change in the PA backbone chemistry. The DTG curves further clarify the degradation kinetics. All membranes displayed a pronounced negative peak between approximately 430 and 460 °C, corresponding to Tmax, the temperature at which the maximum mass loss rate occurs. The similarity in Tmax across all samples confirms that the dominant degradation mechanism remains governed by the aromatic PA matrix. However, the modified membranes showed a slight shift in Tmax and changes in peak intensity. M-T and M-H exhibited slightly higher Tmax as compared to the M-U. These features suggest the presence of different degradation processes associated with modifier and polymer interactions or the improved thermal stability imparted by the presence of the inorganic nanoparticles (Maqsood et al., 2023; Batool et al., 2021).

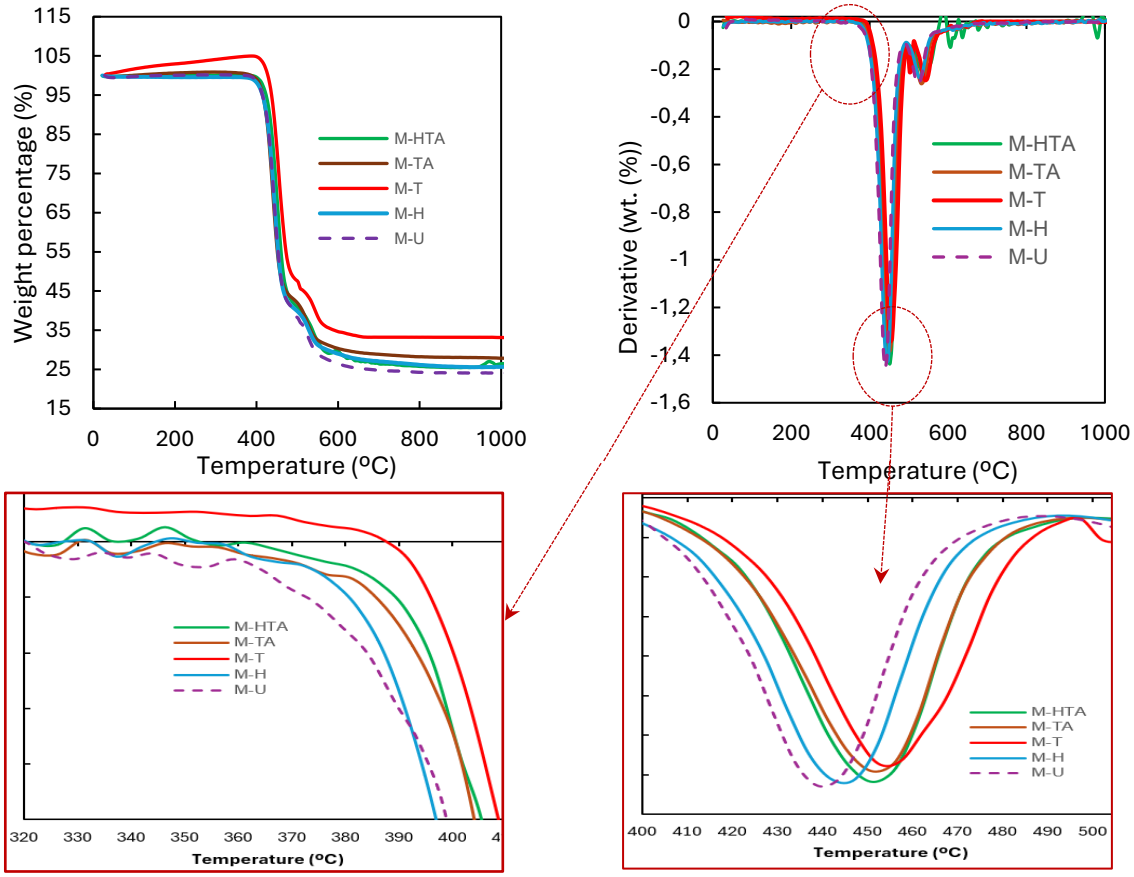


Figure 33: TGA (top left) and DTG (top right) curves of unmodified and surface-modified membranes, showing thermal degradation behaviour. Insets provide zoomed views (DTG curves) of key decomposition regions for detailed comparison.

6.1.5 Membrane surface characterisation: SEM-EDX and analysis

SEM analysis was done to assess the membrane morphology before and after modification. Figure 34 shows the top-view SEM images of the RO membrane surface. The ridge-and-valley structure was observed in the unmodified membranes, indicating the characteristic of the polyamide surface. After surface modification with ADMH, the M-H membrane displays partial filling of the PA membrane by grafting chains (Kasongo et al., 2025). The top-view SEM images of the modified membranes with nanoparticles indicate partial filling of the membrane pores by nanoparticles. The modified membranes have a less uniform appearance, with the presence of matter in the form of irregularities, suggesting the attachment of the modifiers used Kasongo et al., (2019). For the M-HTA, the membrane surfaces appear more uniform, suggesting improved nanoparticle distribution.

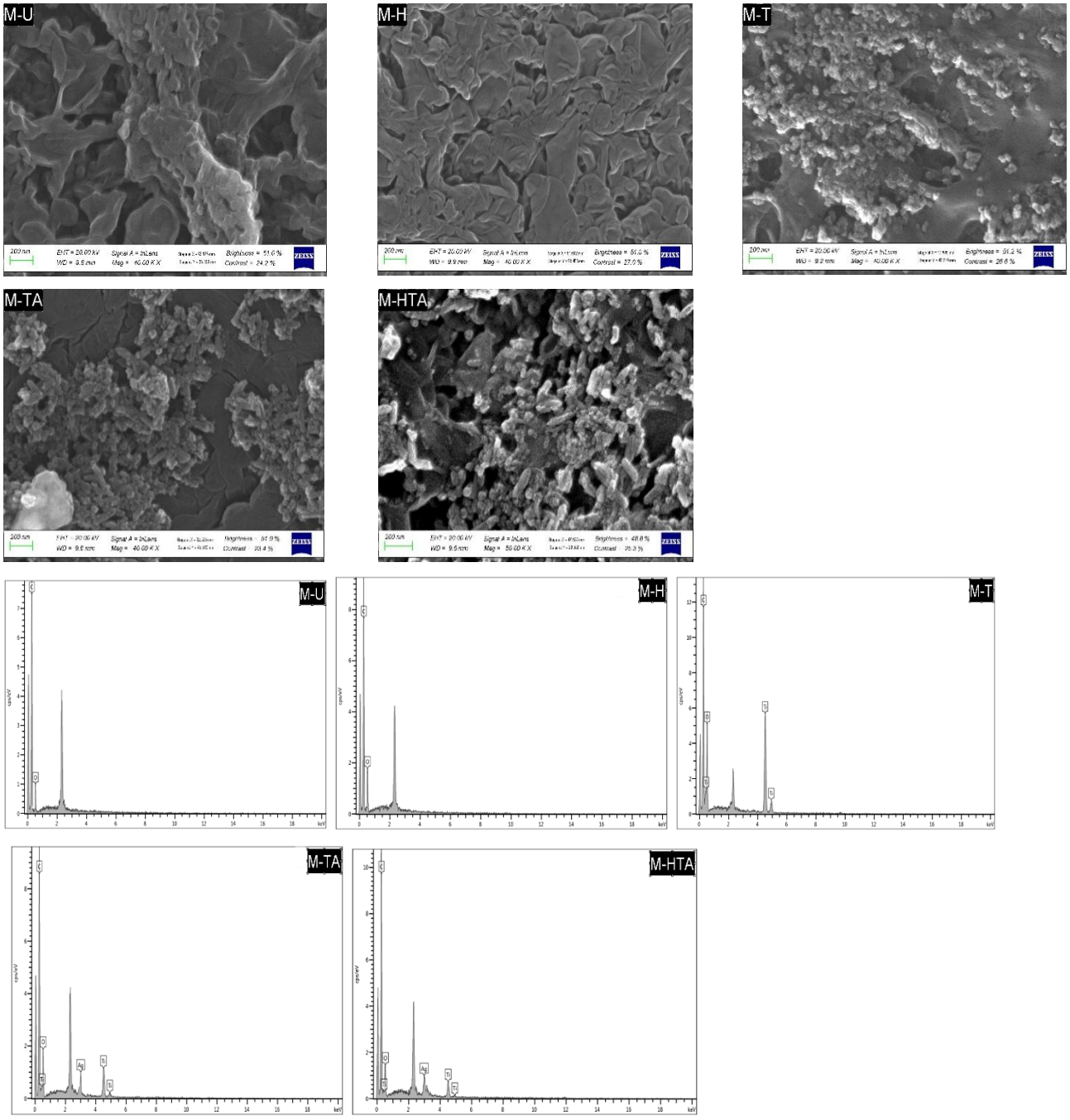


Figure 34: SEM images and corresponding EDX spectra of unmodified and surface-modified membranes, showing changes in surface morphology and elemental composition after grafting.

The EDX analysis confirms the presence of inorganic elements (Ti, Ag) on the membrane surface, noting that the reported values represent apparent surface concentrations. The unmodified membrane (M-U) shows the presence of carbon and oxygen, consistent with a polyamide layer (Wei et al., 2010). The appearance of titanium in M-T, M-TA and M-HTA membranes confirms the successful TiO_2 deposition, while the presence of both Ti and Ag in M-TA confirms the formation of TiO_2-Ag.

Table 10: Apparent concentration of elements on membranes obtained from EDX analysis

Membrane	C	O	Ti	Ag
M-U	74.00 ± 1.56	26.00 ± 1.56	-	-
M-H	67.37 ± 7.09	32.63 ± 7.09	-	-
M-T	67.94 ± 7.51	27.84 ± 4.94	14.22 ± 2.99	-
M-TA	66.62 ± 6.26	20.97 ± 4.03	6.90 ± 1.89	5.51 ± 1.51
M-HTA	69.54 ± 10.12	23.80 ± 7.66	4.07 ± 3.58	2.59 ± 3.79

6.1.6 TEM analysis

The membrane cross-section views were evaluated using TEM analysis. The cross-sectional images of the PA layer across membranes illustrate the structural changes observed in the modified membranes due to surface modification, as presented in Figure 35. The unmodified membrane displays a continuous layer, consistent with a typical thin-film composite RO membrane. The layer appears uniform across the imaged region, indicating that it is the membrane-selective layer before surface modification. The modified membranes exhibit new characteristics in the top layer, which are attributed to the presence of nanoparticles. In membranes containing nanoparticles, contrast regions are observed near the PA layer. According to Ngo et al., (2017), the appearance of a layer on the top of the membrane may explain the attachment of the modifying agents to the surface of the membrane, which in this case confirms the modification of the membranes by ADMH\TiO_2-Ag grafting. The TEM images also show that the modification predominantly occurs at or near the membrane surface, resulting in the formation of an additional layer on the existing PA structure rather than penetrating into the support layer. Despite the introduction of these particles, the overall PA thickness remains within the range of the unmodified membrane, indicating that nanoparticle attachment does not significantly disrupt the selective layer structure. The TEM images hence confirm that the applied modification strategies change the near-surface structure while preserving the PA layer structure.

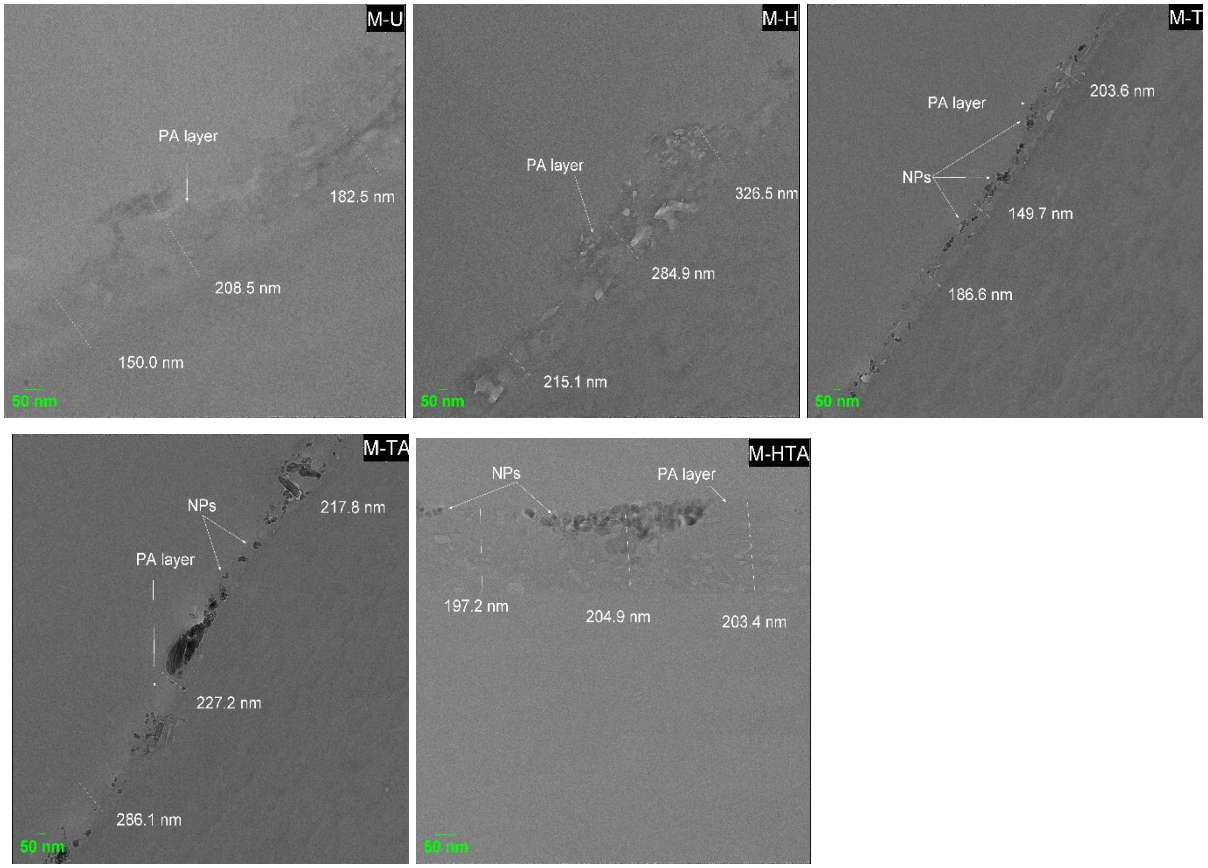


Figure 35: TEM cross-sectional images of unmodified and grafted membranes (cross-section), showing the membrane morphology and the distribution of nanoparticles within the active layer of the membranes

6.1.7 Membrane surface characterisation: Contact angle and charge measurements

The hydrophilicity of the membranes was evaluated with contact angle measurements. The contact angle measurements in Figure 36 show a clear trend towards enhanced surface hydrophilicity after membrane modification, with the unmodified membrane (M-U) exhibiting the highest contact angle and progressively lower values for M-H, M-T, M-TA and M-HTA. This reduction in contact angle is generally associated with increased surface wettability, which promotes water affinity and may be correlated with reduced fouling propensity of the membrane. Nanoparticles such as TiO_2 and Ag are fundamentally hydrophilic and may increase the surface energy of the membrane by introducing hydroxyl groups that attract water molecules, thereby lowering the contact angle (Xue et al., 2018). It has been reported that hydrophilic surfaces tend to form an adsorbed water layer that acts as a physical barrier against foulant adhesion (Baniamerian et al., 2024). This supports the trends in fouling and flux recovery observed in this study. The lowest contact angle for M-HTA suggests that the combined modification strategy most effectively enhanced membrane hydrophilicity, which aligns with reported studies indicating that hybrid modification of the surface can improve synergistically hydrophilicity and antifouling performance compared with single-component modifications.

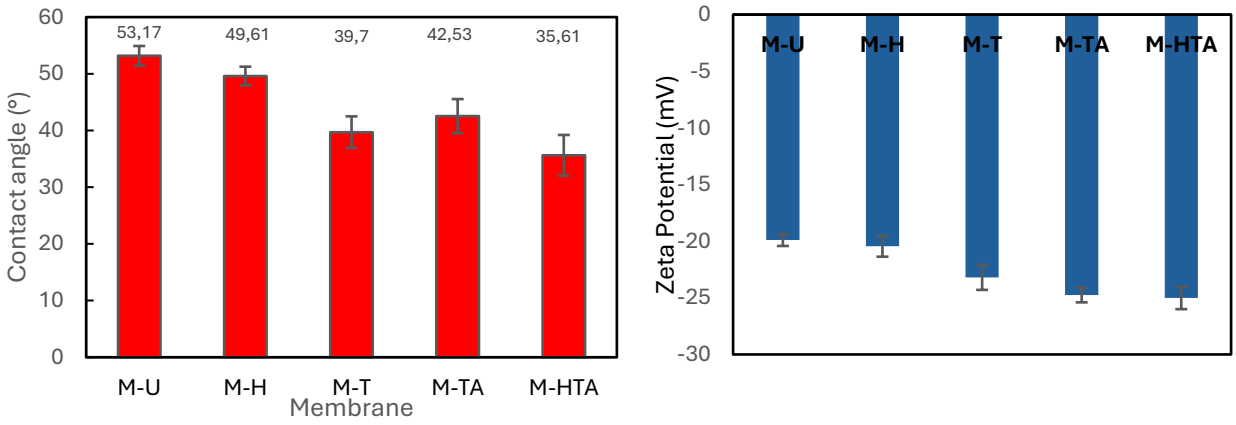


Figure 36: Contact angle (left) and zeta potential (right) of unmodified and surface-modified membranes, showing changes in surface hydrophilicity and surface charge after grafting and nanoparticle incorporation.

The zeta potential measurements indicate that all membranes are negatively charged at neutral pH, which is consistent with the behaviour of polyamide thin-film composite membranes (Mohammed et al., 2023). The M-H show only a slight increase in negative charge, which could be explained by the fact that the modification caused minor surface structure changes. The addition of TiO_2 and the TiO_2-Ag nanocomposite further increases the negative zeta potential. This trend indicates that the presence of nanoparticles increases surface charge, likely due to the negative surface groups on TiO_2 and Ag nanoparticles. M-HTA membrane exhibits the highest negative charge, showing the synergistic effect of hydrophilic treatment and nanocomposite immobilisation, which can improve antifouling properties by enhancing electrostatic repulsion of negatively charged foulants (Rajendran et al., 2025; Xiao et al., 2024).

6.2 Membranes biofouling resistance and performance tests

6.2.1 Static adhesion tests

Figure 37 presents the mortality ratios and membrane anti-fouling efficiencies of modified membranes compared to the pristine membrane. The modified membranes exhibited improved mortality ratios against both bacteria (*E. coli* and *S. Aureus*). The unmodified membrane (45 %) exhibits moderate antimicrobial. The addition of nanoparticles clearly enhanced bacterial mortality, indicating that both increased surface hydrophilicity and the presence of nanoparticles contribute to antimicrobial effects (Kasongo et al., 2025). The TiO_2-Ag nanocomposite further increases mortality, reflecting the strong biocidal activity of silver in combination with TiO_2. (Dou et al., 2025; Habib et al., 2020). The hybrid modified membrane (M-HTA, 94.64 %) achieves the highest mortality, suggesting a synergistic effect of hydrophilic monomer and inorganic nanoparticles.

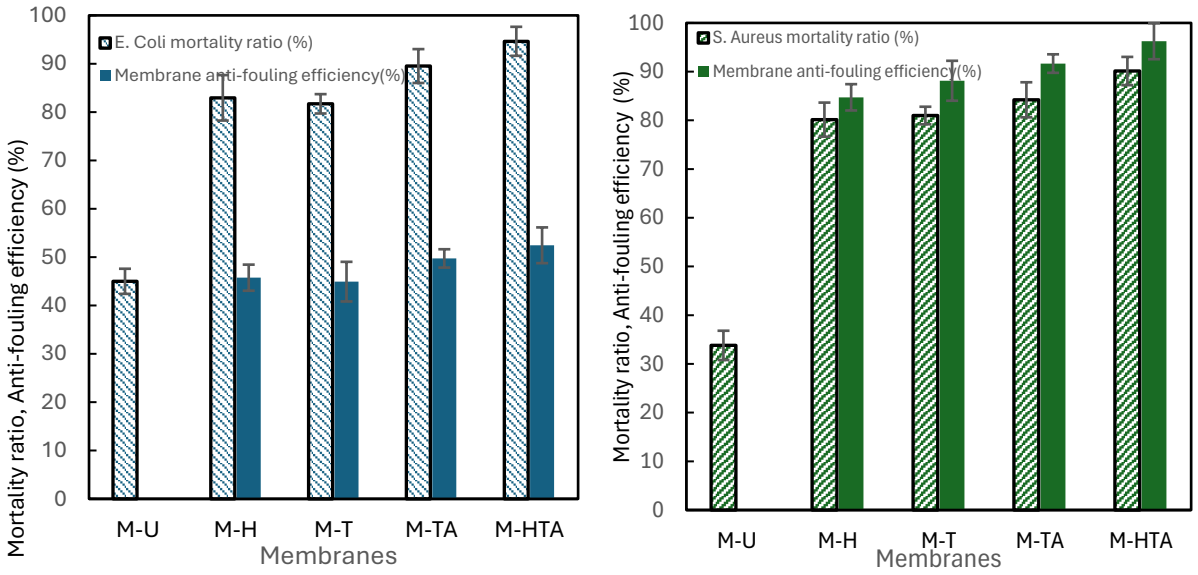


Figure 37: Mortality ratio and membrane antifouling efficiency obtained during the static adhesion test with *E. Coli* (left) and *S. Aureus* (right).

Compared to *E. coli*, the mortality ratio of the modified membranes is lower against S. aureus bacteria. Due to electrostatic interactions, gram-negative bacteria such as *E. coli* are repelled by the negatively charged surface of modified membranes, contrary to *S. aureus*, which has a positively charged outer surface (Ngo et al., 2017). This may also be explained by the fact that gram-positive bacteria can form more robust biofilms, which may offer better protection against the modified membrane surfaces and, therefore, decrease mortality.

6.2.2 Microbial dynamic adhesion and membrane performance tests

The membranes were further tested in a lab-scale crossflow filtration membrane operating at 10 bar and a velocity of 19 cm s^{-1} for a duration of 8 hours. The results in Table 11 show that all modified membranes maintained high salt rejection, indicating that the applied surface modifications did not compromise the structure of the polyamide selective layer. This is consistent with surface modification methods, where functional layers are formed primarily at the membrane solution (Zhao et al., 2017), and this suggests that the performance may be dominated by surface effects rather than the bulk structure of the membrane. However, clear trends were observed in permeability and fouling behaviour. The improved permeability of the modified membranes as compared to the unmodified membrane (M-U) can be attributed to enhanced surface hydrophilicity (AlQasas & Johnson, 2024) and altered interfacial interactions, which could have reduced the modified membranes' resistance to water transport. Similar permeability enhancements following the nanoparticle incorporation and surface functionalisation have been reported by several researchers (Hong et al., 2020; Boffa et al., 2016; Zhang et al., 2017).

TiO_2 and Ag-based modified polyamide membranes increased the membrane surface wettability, as also shown by the contact angle analysis. Biofouling resistance improved significantly after membrane surface modification, as reflected by lower FDR and higher FRR values for both *E. coli* and *S. aureus*. The reduced flux decline is attributed to decreased bacterial adhesion arising from increased surface hydrophilicity (Al-Juboori & Yusaf, 2012; Song et al., 2020; Wang et al., 2018) and the presence of antimicrobial components (Ghosh et al., 2025; Bashir et al., 2025), while the higher FRR values indicate that fouling was predominantly reversible(Xiao et al., 2024; Rajendran et al., 2025). The higher performance of M-TA membrane and particularly the M-HTA may suggest a synergistic effect between surface functionalisation and Ag-TiO_2 incorporation, where TiO_2 enhances dispersion and hydrophilicity, and Ag contributes antibacterial activity, which acts as a resistance to biofilm formation and microorganisms' attachment strength (Suresh et al., 2025). The consistently lower FRR observed for *S. aureus* compared with *E. coli* aligns with literature reports linking stronger adhesion of Gram-positive bacteria to their thicker cell walls (Schmitt & Flemming, 1998).
Overall, the results demonstrate that the combined modification strategy improves permeability and biofouling resistance without compromising salt rejection, confirming that controlled surface engineering is an effective approach for enhancing RO membrane operational performance.

Table 11: Mortality Ratio, FDR, and FRR values of ADMH grafted membranes.

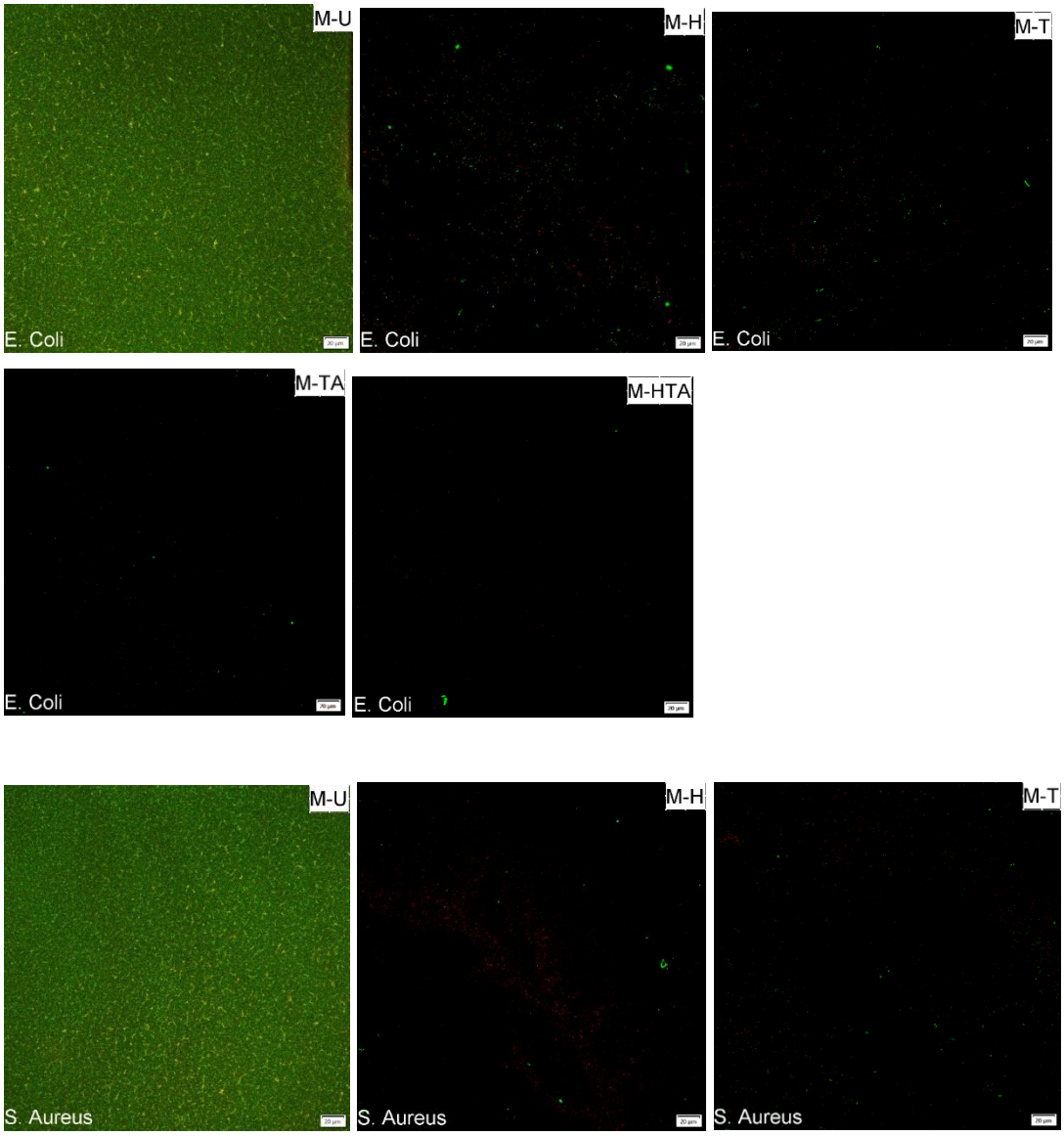
	Salt Rejection (%)	Permeability (L/m^2.h. Bar)	FDR (%)		FRR (%)	
			E. coli	S. aureus	E. coli	S. aureus
M-U	91 ± 2.27%	5.76 ± 1.81	20.29 ± 0.66%	25.15 ± 0.24%	80.66 ± 1.98	69.03 ± 0.32%
M-H	91 ± 0.49%	6.62 ± 1.79	13.45 ±1.29%	15.72 ± 0.25%	94.88 ± 2.67	89.02 ± 2.76%
M-T	91 ± 2.13%	6.79 ± 0.98	13.72 ± 1.14%	14.25 ± 2.13%	94.10 ± 0.83	88.55 ± 1.07%
M-TA	90 ± 1.75%	6.12 ± 0.79	10.08 ± 0.53%	13.14 ± 1.51%	95.01 ± 1.26	90.51 ± 1.71%
M-HTA	91% ± 0.5%	7.02 ± 2.30	7.04 ± 1.17%	11.03 ± 0.96%	97.01 ± 2.46	92.11+1.91%

6.2.3 Confocal Laser Scanning Microscopy (CLSM)

CLSM analysis was used to acquire direct visual and quantitative evidence of the antibiofouling behaviour of the modified membranes. Figure 38 shows CLSM results used to assess membrane biofouling behaviour under dynamic cross-filtration conditions. As summarised in Table 12, the unmodified membrane (M-U) displayed significant bacterial coverage for both *S. aureus* and *E. coli*, indicating strong cell adhesion and biofilm formation on the native polyamide surface. In contrast, all modified membranes showed a significant reduction in surface-attached cells, confirming that surface modification effectively alleviates bacterial attachment to the membrane surface (Kucera, 2019; Choi et al., 2020).

Among the modified membranes, a clear performance was observed with the M-HTA, showing the lowest cell counts and the highest antibiofouling efficiencies (94.60% for *S. aureus* and 97.36% for *E. coli*). This improved performance can be attributed to the combined effects of surface functionalization and TiO_2-Ag attachment onto the membrane surface, which enhances surface hydrophilicity and introduces antimicrobial functionality. TiO_2 contributes to reduced initial adhesion through increased wettability (Shao et al., 2017; Asadollahi et al., 2020), whereas Ag provides the membrane with anti-bacterial capability that inhibits bacterial survival and biofilm development (Jeon et al., 2021; Ghosh et al., 2025).

The consistently lower cell counts observed for *E. coli* compared with *S. aureus* across all membranes are consistent with literature reports that Gram-negative bacteria are generally more susceptible to antimicrobial surfaces, while Gram-positive bacteria exhibit stronger adhesion due to their thicker layers (Schmitt & Flemming, 1998; Maddah & Chogle, 2017).



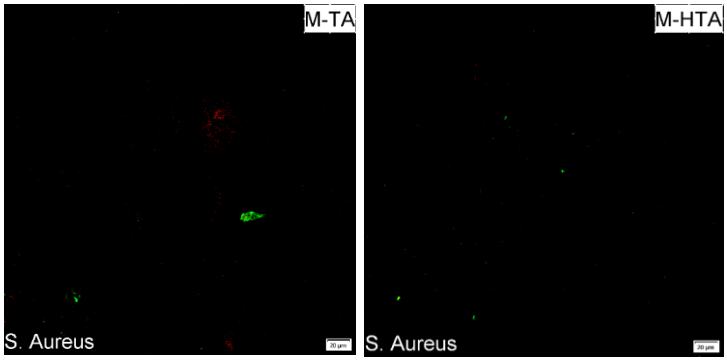


Figure 38: CLSM results of membranes after 8 hours of dynamic biofouling tests using Flux of modified membranes compared to the unmodified membrane during dynamic fouling tests with *E. Coli* and *S. Aureus* solution in the cross-filtration lab-scale RO system.

Table 12: Microorganisms cell count obtained using ImageJ software

Membrane	Cells count (CFU/20 μm^2)			
	S. Aureus	E. Coli	Membrane anti-biofouling efficiency (S. Aureus) (%)	Membrane anti-biofouling efficiency (E. Coli) (%)
M-U	23424	23290	-	-
M-H	11795	11020	49.64	52.68
M-T	4878	2749	79.17	88.19
M-TA	1974	1875	91.57	91.94
M-HTA	1263	614	94.60	97.36

6.2.4 Organic and inorganic fouling tests

The organic and inorganic fouling tests were conducted on a lab-scale RO cross-filtration system, with the initial flux of 32 L m^{-2} h^{-1} and the feed pressure maintained at 10 bar. Figure 39 compares the flux decline behaviour of the membranes during fouling with organic and inorganic model foulants.

During organic fouling with humic acid (150 mg/L), the unmodified membrane (M-U) showed a progressive flux decline, with the fractional flux decreasing to 0.65 (20.7 L m^{-2} h^{-1}) after 8 h, which indicates fouling on the membrane surface. On the other hand, the hybrid modified membrane (M-HTA) exhibited a slower flux decline and maintained a higher fractional flux of 0.80 (25.65 L m^{-2} h^{-1}) after 8 hours of filtration. The improved Flux decline of M-HTA demonstrates improved antifouling behaviour, attributed to increased surface hydrophilicity and stronger electrostatic repulsion, which reduces humic acid adsorption(Lee et al., 2006; Shafi et al., 2017). Overall, the results confirm that surface modification significantly mitigates organic fouling compared to the unmodified membrane.

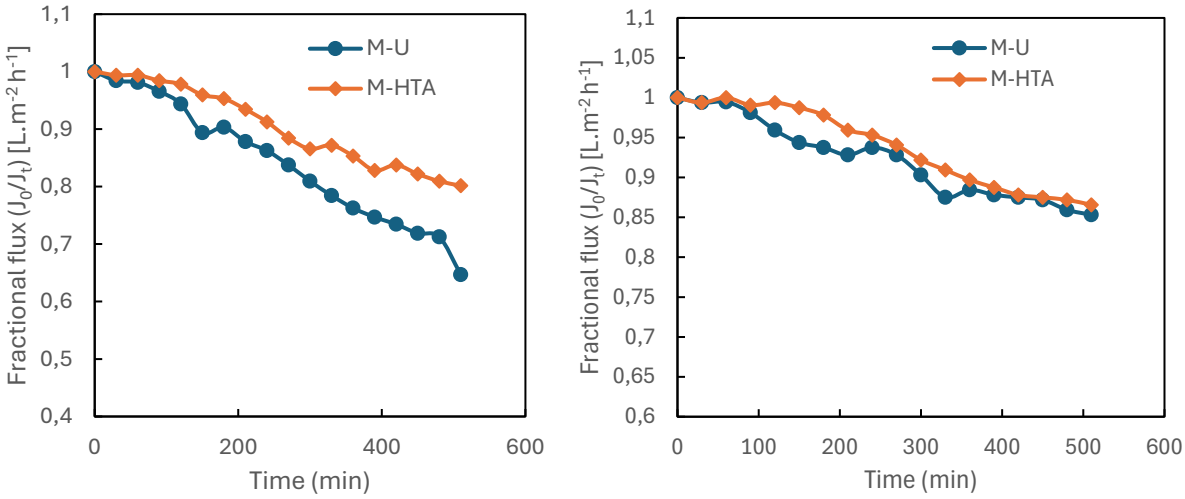


Figure 39: Membrane flux decline during fouling tests with the organic foulant humic acid (left) and inorganic foulant sodium bicarbonate (right) solutions.

During the inorganic fouling test using sodium bicarbonate (150 mg L^{-1}) over 8 h, both membranes exhibited a more gradual flux decline. The unmodified membrane (M-U) showed a decrease in fractional flux to approximately 0.85, corresponding to a flux decline from 32 L m^{-2} h^{-1} to 27.3 L m^{-2} h^{-1}. In contrast, the M-HTA membrane demonstrated improved resistance to fouling, maintaining a slightly higher fractional flux of 0.87 at the end of the fouling test, corresponding to 27.7 L m^{-2} h^{-1}. Although M-HTA consistently outperformed M-U, the difference between the two membranes was relatively small, indicating that inorganic fouling was less severe. The flux difference between M-U and M-HTA was more pronounced during organic fouling than inorganic fouling.

6.2.5 Membrane test using real secondary effluent

The M-U and M-HTA membranes were further tested using secondary effluent from a municipal wastewater treatment plant. During fouling tests, both membranes were operated under identical conditions (initial flux of 32 L m^{-2} h^{-1} and a constant feed pressure of 10 bar). Figure 40 presents the long-term flux behaviour and corresponding CLSM images of the membranes during filtration of real secondary effluent. Over the test duration, the unmodified membrane (M-U) showed a gradual but continuous flux decline, decreasing to 27.7 L m^{-2} h^{-1} after 72 hours of experimental test. The M-HTA maintained a higher and more stable flux, remaining at 30.1 L m^{-2} h^{-1}. This demonstrates a higher resistance to fouling under realistic wastewater conditions. The CLSM analysis aligned with the fouling test findings, as the results revealed significant biofouling on M-U, characterised by a predominantly green, fluorescent signal covering most of the membrane surface, which indicates viable microbial attachment. In comparison, the modified membrane showed very limited green fluorescence, confirming reduced bacterial adhesion. The hydraulic performance test and CLSM observations indicate that the surface modification effectively mitigates biofouling, likely through

enhanced surface hydrophilicity, increased negative surface charge, and the antimicrobial action of the incorporated (Jeon et al., 2021; Yang et al., 2021; Habib et al., 2020).

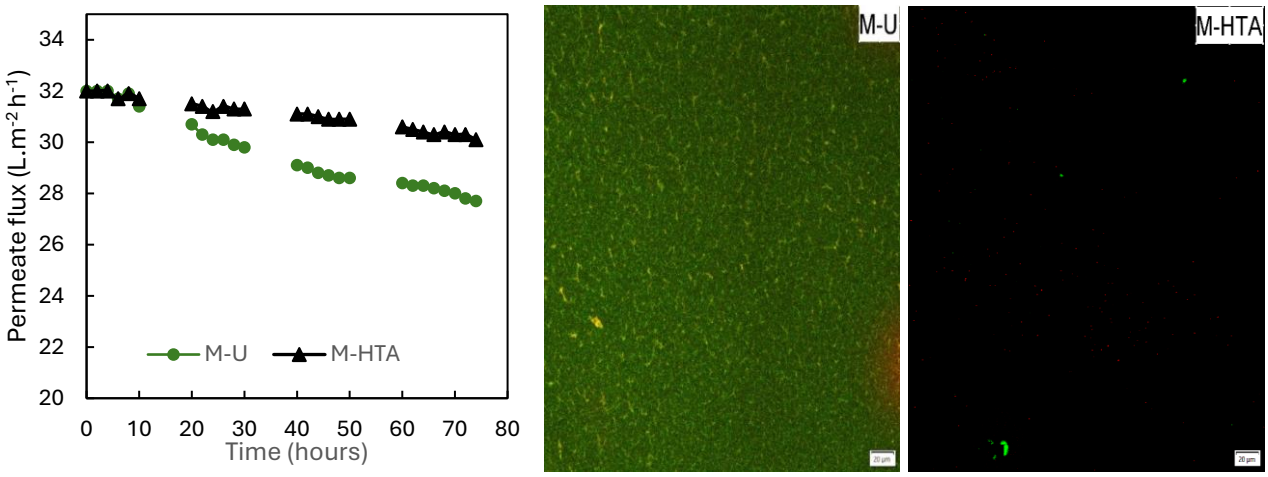


Figure 40: Membranes flux profile of the M-U membrane and M-HTA membrane during RO filtration with secondary effluent from municipal wastewater treatment plant (left) & CLSM images (right) of the membranes obtained after the experimental tests with the secondary effluent. The flux was recorded over 72 hours (3 days) with interval periods of 2 hours during the day, and 10 hours at night

6.3 Summary

This study investigated the modification of a polyamide RO membrane using a hybrid composition of ADMH and TiO_2-Ag. Membrane characterisation confirmed that the TiO_2-Ag nanocomposite exhibited improved thermal stability of the membrane, while FTIR, SEM–EDX, and TEM analyses confirmed the effectiveness of the modification method. The contact angle and zeta potential indicated that the modified membranes exhibited enhanced hydrophilicity and increasingly negative surface charges, with the hybrid membrane (M-HTA) displaying the lowest contact angle and the highest negative zeta potential. These changes had effects on fouling reduction and bacterial adhesion. Antibacterial tests and CLSM observations confirmed a significant reduction in the attachment and viability of both *E. coli* and *S. aureus* on modified membranes, with the highest antibiofouling performance achieved by M-HTA, highlighting the synergistic effect of hydrophilic modification.

Fouling experiments with organic (humic acid, 150 mg L^{-1}) and inorganic (sodium bicarbonate, 150 mg L^{-1}) foulants further confirmed the benefits of surface modification. M-HTA exhibited a slower flux decline during organic fouling (fractional flux 0.80 vs 0.65 for M-U) and moderate improvement against inorganic fouling (fractional flux 0.87 vs 0.85 for M-U), indicating that the hybrid modification approach is most effective against biofouling and organic fouling while slightly improving resistance to inorganic fouling.

6.4 References

Ahmad, N.N.R., Mohammad, A.W., Mahmoudi, E., Ang, W.L., Leo, C.P. & Teow, Y.H. 2022. An Overview of the Modification Strategies in Developing Antifouling Nanofiltration Membranes. *Membranes*, 12(12).

Al-Juboori, R.A. & Yusaf, T. 2012. Biofouling in RO system: Mechanisms, monitoring and controlling. *Desalination*, 302: 1–23. http://dx.doi.org/10.1016/j.desal.2012.06.016.

AlQasas, N. & Johnson, D. 2024. Combined Effects of Surface Roughness, Solubility Parameters, and Hydrophilicity on Biofouling of Reverse Osmosis Membranes. *Membranes*, 14(11).

Armendáriz-Ontiveros, M.M., Álvarez-Sánchez, J., Dévora-Isiordia, G.E., García, A. & Fimbres Weihs, G.A. 2020. Effect of seawater variability on endemic bacterial biofouling of a reverse osmosis membrane coated with iron nanoparticles (FeNPs). *Chemical Engineering Science*, 223: 1–10.

Asadollahi, M., Bastani, D., Mousavi, S.A., Heydari, H. & Mousavi, D.V. 2020. Improvement of performance and fouling resistance of polyamide reverse osmosis membranes using acrylamide and TiO2 nanoparticles under UV irradiation for water desalination. *Journal of Applied Polymer Science*, 137(11).

Bagheripour, E., Moghadassi, A.R., Hosseini, S.M., Ray, M.B., Parvizian, F. & Van der Bruggen, B. 2018. Highly hydrophilic and antifouling nanofiltration membrane incorporated with water-dispersible composite activated carbon/chitosan nanoparticles. *Chemical Engineering Research and Design*, 132: 812–821.

Baniamerian, H., Shokrollahzadeh, S., Safavi, M., Ashori, A. & Angelidaki, I. 2024. Visible-light-activated Fe_2O_3–TiO_2 nanoparticles enhance biofouling resistance of polyethersulfone ultrafiltration membranes against marine algae Chlorella vulgaris. *Scientific Reports*, 14(1).

Bashir, N., Afzaal, M., Khan, A.L., Nawaz, R., Irfan, A., Almaary, K.S., Dabiellil, F., Bourhia, M. & Ahmed, Z. 2025. Green-synthesized silver nanoparticle-enhanced nanofiltration mixed matrix membranes for high-performance water purification. *Scientific Reports*, 15(1).

Batool, M., Shafeeq, A., Haider, B. & Ahmad, N.M. 2021. Tio_2 nanoparticle filler-based mixed-matrix pes/ca nanofiltration membranes for enhanced desalination. *Membranes*, 11(6).

Bian, S., Wang, Y., Xiao, F., Tong, Y., Gao, C. & Zhu, G. 2022. Fabrication of polyamide thin-film nanocomposite reverse osmosis membrane with improved permeability and antibacterial performances using silver immobilized hollow polymer nanospheres. *Desalination*, 539: 115953. https://linkinghub.elsevier.com/retrieve/pii/S0011916422004088.

Boffa, V., Parmeggiani, L., Haaning, A. & Magnacca, G. 2016. Microporous and Mesoporous Materials Hydrophilicity and surface heterogeneity of TiO_2 -doped silica materials for membrane

applications. *Microporous and Mesoporous Materials*, 221: 81–90. http://dx.doi.org/10.1016/j.micromeso.2015.09.017.

Bromberg, L., Magariños, B., Concheiro, A., Hatton, T.A. & Alvarez-Lorenzo, C. 2024. Nonleaching Biocidal N-Halamine-Functionalized Polyamine-, Guanidine-, and Hydantoin-Based Coatings. *Industrial and Engineering Chemistry Research*, 63(14): 6268–6278.

Cao, C., Huang, J., Li, L., Zhao, C. & Yao, J. 2017. Highly dispersed Ag/TiO_2via adsorptive self-assembly for bactericidal application. *RSC Advances*, 7(22): 13347–13352.

Choi, W., Lee, C., Yoo, C.H., Shin, M.G., Lee, G.W., Kim, T.S., Jung, H.W., Lee, J.S. & Lee, J.H. 2020. Structural tailoring of sharkskin-mimetic patterned reverse osmosis membranes for optimizing biofouling resistance. *Journal of Membrane Science*, 595(August 2019): 117602. https://doi.org/10.1016/j.memsci.2019.117602.

Dou, H., Wang, J., Zhao, Y., Liu, J. & Li, Y. 2025. Preparation of Ag-Decorated TiO_2 Composite Materials and Study on Photocatalytic Performance. *Nanomaterials*, 15(18).

Fazekas, Á.F., Gyulavári, T., Ágoston, Á., Janovák, L., Kopniczky, J., László, Z. & Veréb, G. 2024. Enhanced Photocatalytic and Filtration Performance of TiO_2-Ag Composite-Coated Membrane Used for the Separation of Oil Emulsions. *Separations*, 11(4).

Gao, Q., Duan, L., Jia, Y., Zhang, H., Liu, J. & Yang, W. 2023. A Comprehensive Analysis of the Impact of Inorganic Matter on Membrane Organic Fouling: A Mini Review. *Membranes*, 13(10).

Gayed, H.M., El Fadl, F.I.A., Maziad, N.A., El-Aassar, A.H.M. & Abdel-Mottaleb, M.S.A. 2019. Surface modification of composite polyamide reverse osmosis membrane by irradiated chitosan and TiO_2 nanoparticles. *Desalination and Water Treatment*, 160: 32–40.

Ghosh, S., Imboon, T., Layek, R., Salunke, G., Parihar, V.S., Khumphon, J., Webster, T.J., Sutar, S., Kityakarn, S., Issro, C., Khamboonrueang, D. & Thongmee, S. 2025. Catechin-capped silver-doped titanium dioxide nanoparticle enhanced photocatalytic toxic dye degradation. *Frontiers in Chemistry*, 13.

Gogoi, D., Namdeo, A., Golder, A.K. & Peela, N.R. 2020. Ag-doped TiO_2 photocatalysts with effective charge transfer for highly efficient hydrogen production through water splitting. *International Journal of Hydrogen Energy*, 45(4): 2729–2744.

Habib, Z., Khan, S.J., Ahmad, N.M., Shahzad, H.M.A., Jamal, Y. & Hashmi, I. 2020. Antibacterial behaviour of surface modified composite polyamide nanofiltration (NF) membrane by immobilizing Ag-doped TiO_2 nanoparticles. *Environmental Technology (United Kingdom)*, 41(28): 3657–3669.

Hong Anh Ngo, T., Tran, D.T. & Hung Dinh, C. 2017. Surface photochemical graft polymerization of acrylic acid onto polyamide thin film composite membranes. *Journal of Applied Polymer Science*, 134(5).

Hong, T., Ngo, A., Thi, C., Nguyen, M., Do, K.D., Duong, Q.X., Tran, N.H., Vuong Nguyen, H.T. & Tran, D.T. 2020. *Improvement of Hydrophilicity for Polyamide Composite Membrane by Incorporation of Graphene Oxide-Titanium Dioxide Nanoparticles*.

Hu, Y., Lu, K., Yan, F., Shi, Y., Yu, P., Yu, S. & Li, S. 2016. Enhancing the performance of aromatic polyamide reverse osmosis membrane by surface modi fi cation via covalent attachment of polyvinyl alcohol (PVA). , 501: 209–219.

Jeon, S., Shin, S.S., Park, C.H. & Lee, J.H. 2021. Star polymer-mediated in-situ synthesis of silver-incorporated reverse osmosis membranes with excellent and durable biofouling resistance. *Journal of Membrane Science*, 639(August): 119778. https://doi.org/10.1016/j.memsci.2021.119778.

Kasongo, G., Nkombe, A.M. & Aziz, M. 2025. Biofouling Resistance Improvement in Membrane-Based Secondary Effluent Treatment: A Focus on Membrane Surface Modification by Graft Polymerization with 3-Allyl-5, 5-Dimethyl Hydantoin. *Membranes*, 15(10).

Kasongo, G., Steenberg, C., Morris, B., Kapenda, G., Jacobs, N. & Aziz, M. 2019. Surface grafting of polyvinyl alcohol (PVA) cross-linked with glutaraldehyde (GA) to improve resistance to fouling of aromatic polyamide thin film composite reverse osmosis membranes using municipal membrane bioreactor effluent. *Water Practice and Technology*, 14(3): 614–624.

Kucera, J. 2019. Biofouling of polyamide membranes: Fouling mechanisms, current mitigation and cleaning strategies, and prospects. *Membranes*, 9(9).

Lee, S., Ang, W.S. & Elimelech, M. 2006. Fouling of reverse osmosis membranes by hydrophilic organic matter : implications for water reuse. , 187(February 2005): 313–321.

Liu, M., Chen, Q., Wang, L., Yu, S. & Gao, C. 2015. Improving fouling resistance and chlorine stability of aromatic polyamide thin- fi lm composite RO membrane by surface grafting of polyvinyl alcohol (PVA). *DES*, 367: 11–20. http://dx.doi.org/10.1016/j.desal.2015.03.028.

Maddah, H. & Chogle, A. 2017. Biofouling in reverse osmosis: phenomena, monitoring, controlling and remediation. *Applied Water Science*, 7(6): 2637–2651.

Maqsood, K., Jamil, A., Ahmed, A., Sutisna, B., Nunes, S. & Ulbricht, M. 2023. Effect of TiO_2 on Thermal, Mechanical, and Gas Separation Performances of Polyetherimide–Polyvinyl Acetate Blend Membranes. *Membranes*, 13(8).

Al Mayyahi, A. 2018. TiO_2 polyamide thin film nanocomposite reverses osmosis membrane for water desalination. *Membranes*, 8(3).

Mohammed, S., Aburabie, J. & Hashaikeh, R. 2023. Facile morphological tuning of thin film composite membranes for enhanced desalination performance. *npj Clean Water*, 6(1).

Mujahid Aziz & Godwill Kasongo. 2021. Improving Resistance to Fouling of Aromatic Polyamide Thin-Film Composite Reverse Osmosis Membrane by Surface Grafting of N,N'-Dimethyl Aminoethyl Methacrylate (DMAEMA). *Journal of Water Chemistry and Technology*, 43(4): 312–320.

Nchoe, O.B., Matshetshe, K., As' Ballim, M., Tetyana, P., Sikhwivhilu, K. & Moloto, N. 2023. Fabrication of Ag2S-incorporated polyamide thin film nanocomposite reverse osmosis membranes with antifouling properties. *Journal of Applied Polymer Science*, 140(41).

Nguyen, M.N., Jue, M.L., Buchsbaum, S.F., Park, S.J., Vollnhals, F., Christiansen, S., Fornasiero, F. & Schäfer, A.I. 2024. Interplay of the forces governing steroid hormone micropollutant adsorption in vertically-aligned carbon nanotube membrane nanopores. *Nature Communications*, 15(1).

Rajendran, D.S., Devi, E.G., Subikshaa, V.S., Sethi, P., Patil, A., Chakraborty, A., Venkataraman, S. & Kumar, V.V. 2025. Recent advances in various cleaning strategies to control membrane fouling: a comprehensive review. *Clean Technologies and Environmental Policy*, 27(2): 649–664.

Schmitt, J. & Flemming, H. 1998. FTIR-spectroscopy in microbial and material analysis. *International Biodeterioration & Biodegradation*, *41*(1):1-11.

Shafi, H.Z., Matin, A., Akhtar, S., Gleason, K.K., Zubair, S.M. & Khan, Z. 2017. Organic fouling in surface modified reverse osmosis membranes: Filtration studies and subsequent morphological and compositional characterization. *Journal of Membrane Science*, 527(January): 152–163.

Shao, F., Xu, C., Jin, W., Dong, H., Sun, Q., Yu, L. & Dong, L. 2017. Layer-by-layer self-assembly TiO_2 and graphene oxide on polyamide reverse osmosis membranes with improved membrane durability. *Desalination*, 423: 21–29.

Song, M., Im, S.J., Jeong, D. & Jang, A. 2020. Reduction of biofouling potential in cartridge filter by using chlorine dioxide for enhancing anti-biofouling of seawater reverse osmosis membrane. *Environmental Research*, 180(October 2019): 108866. https://doi.org/10.1016/j.envres.2019.108866.

Suresh, D., Goh, P.S., Lau, W.J., Lim, J.W., Abdullah, M.S., Ng, B.C. & Ismail, A.F. 2025. The synergistic actions of copper/L-glutamine co-grafting in improving anti-biofouling and desalination performances of reverse osmosis thin film composite membrane. *Desalination*, 593.

Tuttle, A., Trahan, N. & Son, M. 2021. Growth and Maintenance of Escherichia coli Laboratory Strains. *Current Protocols*, 1.

Wang, Jing, Wang, Z., Wang, Jixiao & Wang, S. 2015. Improving the water fl ux and bio-fouling resistance of reverse osmosis (RO) membrane through surface modi fi cation by zwitterionic polymer. *Journal of Membrane Science*, 493: 188–199. http://dx.doi.org/10.1016/j.memsci.2015.06.036.

Wang, Y., Wang, Z., Wang, J. & Wang, S. 2018. Triple antifouling strategies for reverse osmosis membrane biofouling control. *Journal of Membrane Science*, 549(August 2017): 495–506. https://doi.org/10.1016/j.memsci.2017.12.047.

Wei, X., Wang, Z., Zhang, Z., Wang, J. & Wang, S. 2010. Surface modification of commercial aromatic polyamide reverse osmosis membranes by graft polymerization of 3-allyl-5, 5-

dimethylhydantoin. *Journal of Membrane Science*, 351(1–2): 222–233. http://dx.doi.org/10.1016/j.memsci.2010.01.054.

Xiao, J., Hao, S., Qin, Y., Qi, P., Zhang, Z. & Hu, Y. 2024. Fouling-resistant reverse osmosis membranes grafted with 2-aminoethanethiol having a low interaction energy with charged foulants. *npj Clean Water*, 7(1).

Xue, W., Sint, K.K.K., Ratanatamskul, C., Praserthdam, P. & Yamamoto, K. 2018. Binding TiO_2 nanoparticles to forward osmosis membranes: Via MEMO-PMMA-Br monomer chains for enhanced filtration and antifouling performance. *RSC Advances*, 8(34): 19024–19033.

Yang, Z., Takagi, R., Zhang, X., Yasui, T., Zhang, L. & Matsuyama, H. 2021. Engineering a dual-functional sulfonated polyelectrolyte-silver nanoparticle complex on a polyamide reverse osmosis membrane for robust biofouling mitigation. *Journal of Membrane Science*, 618(May 2020): 118757. https://doi.org/10.1016/j.memsci.2020.118757.

Zhang, T., Zhang, K., Li, J. & Yue, X. 2017. Simultaneously enhancing hydrophilicity, chlorine resistance and anti-biofouling of APA-TFC membrane surface by densely grafting quaternary ammonium cations and salicylaldimines. *Journal of Membrane Science*, 528(January): 296–302. http://dx.doi.org/10.1016/j.memsci.2017.01.013.

Zhang, Z., Wang, Z., Wang, J. & Wang, S. 2013. Enhancing chlorine resistances and anti-biofouling properties of commercial aromatic polyamide reverse osmosis membranes by grafting 3-allyl-5, 5-dimethylhydantoin and N, N ′ -Methylenebis (acrylamide). *DES*, 309: 187–196. http://dx.doi.org/10.1016/j.desal.2012.10.019.

Zhao, Y., Zhang, Z., Dai, L., Mao, H. & Zhang, S. 2017. Enhanced both water flux and salt rejection of reverse osmosis membrane through combining isophthaloyl dichloride with biphenyl tetraacyl chloride as organic phase monomer for seawater desalination. *Journal of Membrane Science*, 522: 175–182. http://dx.doi.org/10.1016/j.memsci.2016.09.022.

Chapter 7

CONCLUSION AND RECOMMENDATIONS

7.1 Conclusion

This research addressed the persistent challenge of fouling in polyamide reverse osmosis membranes used for treating municipal secondary effluent. The focus of the research was on biofouling. Improving resistance to biofouling through enhancements to membrane materials remains crucial, given the self-replicating nature of microorganisms and the membrane's vulnerability to various disinfectants over extended periods. This work demonstrated that membrane fouling behaviour is defined by coupled structure and performance relationships involving surface chemistry, hydrophilicity, surface charge, and antifouling functionality.

Initial surface modification using N,N′-dimethylaminoethyl methacrylate (DMAEMA) demonstrated that graft polymerisation can enhance biofouling resistance while largely preserving membrane permeability. The increased flux recovery and reduced flux decline confirmed the enhancement of membrane fouling resistance. The modification indicated that a higher concentration of the modifying agent (DMAEMA) adversely affects salt rejection.

Subsequent grafting with the hydrophilic monomer ADMH significantly improved membrane antibiofouling performance against both *E. coli* and *S. aureus*. The results showed that biofouling resistance depended on grafting concentration, with moderate ADMH levels (0.6 mol. L^{-1}) providing the most effective balance between hydrophilicity and fouling resistance. While ADMH grafting improved resistance to biofouling, its effect on organic and inorganic fouling remained comparable to that of the unmodified membrane, emphasising the complexity of fouling mechanisms in real wastewater systems.

The hybrid surface functionalization (ADMH with TiO_2-Ag nanocomposites) exhibited the highest permeability (7.02 L m^{-2} h^{-1} bar^{-1}), the lowest FDR values (7.04 % for *E. coli* and 11.03 % for *S. aureus*), and the highest flux recovery of 97.01 % and 92.11 %, for *E. coli* and *S. aureus,* respectively. The biofouling static adhesion tests further confirmed this synergistic effect, with bacterial mortality increasing from 45% for the unmodified membrane to 94.64% for the hybrid-modified membrane. The surface modification enhanced hydrophilicity, as shown by the contact angle analysis (53.17º and 35.61º for the unmodified and hybrid modified membranes, respectively).

During 72-hour filtration of municipal secondary effluent, the unmodified membrane experienced a continuous flux decline from 32 to 27.7 L m^{-2} h^{-1}, whereas the hybrid membrane had a significantly higher flux of 30.1 L m^{-2} h^{-1}. Furthermore, the CLSM analysis observations confirmed that the hybrid membrane exhibited higher resistance to microbial adhesion on its surface and reduced biofilm formation.

Overall, this study demonstrates that hybrid surface modification integrating a hydrophilic antimicrobial monomer with a biocidal nanocomposite provides an effective and scalable strategy for mitigating fouling, particularly biofouling, in PA RO membranes. These findings provide valuable insights into the relationships between membrane structure and performance that govern membrane fouling behaviour, offering a practical guide to developing more fouling-resistant RO membranes for wastewater reuse applications.

7.2 Recommendations

Based on the findings of this study, the following recommendations are proposed to further advance the development and practical application of fouling-resistant polyamide reverse osmosis membranes for wastewater reuse:

Future studies should investigate the long-term chemical stability of ADMH\TiO_2-Ag modified membranes under actual operating conditions. While this work demonstrated improved performance during extended lab-scale filtration tests, longer exposure to cleaning cycles, disinfectants, and variable feed water compositions would provide further insight into the durability of the modification method employed.

Optimisation of grafting concentrations of the modifying agents should be investigated to further improve membrane performance. The results clearly showed that moderate grafting concentrations provide higher antifouling capacity to the membrane, whereas excessive concentrations of the modifying agents affect the membrane's effectiveness and performance.

The interaction between surface-modified membranes and complex microbial communities warrants further study. This research primarily focused on model Gram-positive and Gram-negative bacteria; however, real wastewater contains a diverse array of microbial groups embedded in extracellular polymeric substances (EPS).

APPENDICES

APPENDIX A: sample calculations

Sample calculation of modifying solution (ADMH):

$Molecular\ weight = (12 \times 8) + (1 \times 12) + (14 \times 2) + (16 \times 2) = 168\ g/mol$

Calculations for 0.6 mol/L ADMH modified solution

Table 13: Table of concentration and mass labels

Concentrations	Required AMDH Mass
$C_1 = 0.2\ mol/L$	m_1
$C_2 = 0.4\ mol/L$	m_2
$C_3 = 0.6\ mol/L$	m_3
$C_4 = 0.8\ mo/L$	m_4

$$C_1 = \frac{n}{V}$$

$$n_1 = C_1 \times V$$

$$\frac{m_1}{M} = C_1 \times V$$

$$m_1 = C_1 \times V \times M$$

$$m_1 = 0.6\frac{mol}{L} \times 1L \times 168\frac{g}{mol}$$

$$m_1 = 100.8\ g$$

Sample calculation of RO performance indicators:

Flux

At time 30 min for 0.6 mol/L ADMH-grafted (organic foulant as feed solution);

$$J = \frac{V}{A \times \Delta t}$$

$$J = \frac{0.001792\ L}{0.013775 \times 0.004166667} = 31.22\ L/m^2.h$$

Salt Rejection

Salt rejection calculated using the electroconductivities of the feed and permeate.

ADMH grafted membrane:

$$R = \frac{C_f - C_P}{C_f} \times 100$$

$$R = \frac{1058 - 145.5}{1058} \times 100$$

$$R = 8625\%$$

Salt rejection is calculated using the total dissolved solids (TDS) of the feed and permeate.

ADMH\TiO_2-Ag grafted membrane:

$$R = \frac{C_f - C_P}{C_f} \times 100$$

$$R = \frac{2000\ mg.l^{-1} - 179\ mg.l^{-1}}{2000\ mg.l^{-1}} \times 100$$

$$R = 91.05\%$$

Flux Decline Ratio (FDR)

Sample calculations for 0.4 mol/L ADMH-grafted membrane against inorganic:

$$FDR = \left(\frac{Jw_i - J}{Jw_i}\right) \times 100$$

$$FDR = \left(\frac{32 - 30.01}{32}\right) \times 100$$

$$FDR = 6.22\ \%$$

Flux Recovery Ratio (FRR)

ADMH\ TiO_2-Ag grafted membrane (*S. Aureus*):

$$FRR = \left(\frac{J_{wf}}{J_{wi}}\right) \times 100$$

$$FRR = \left(\frac{28.84}{32}\right) \times 100 = 90.12\%$$

Mortality Ratio

Sample calculation for unmodified membrane antimicrobial abilities against *E. coli*:

$$R = \left(\frac{B - A}{B}\right) \times 100$$

$$R = \left(\frac{1.0 \times 10^8 - 9.19 \times 10^7}{1.0 \times 10^8}\right) \times 100 = 94.46\%$$

APPENDIX B: membrane surface modification data

Membrane surface modification using ADMH\TiO_2-Ag: Membrane characterization

Table 14: The mass of polyamide TFC RO membranes before and after grafting with ADMH, TiO_2, TiO_2-Ag and ADMH\TiO_2-Ag

Modification	Avg. Mass before (g)	Avg. Mass after (g)	Mass difference
M-H	5,38	6,09	0,71
M-T	4,21	5,37	1,16
M-TA	4,17	5,55	1,38
M-HTA	4,88	6,78	1,9

Table 15: membrane charge (Zeta Potential) tested at pH 7

	Zeta Potential (mV)				
Membrane	Run 1	Run 2	Run 3	Avg. ZP (mV)	Std. Dev
M-U	-19.3	-19.9	-20.5	-19.90	0.6
M-H	-19.5	-20.45	-21.4	-20.45	0.95
M-T	-22	-23.2	-24.4	-23.20	1.2
M-TA	-24.1	-24.75	-25.4	-24.75	0.65
M-HTA	-24	-25.01	-26	-25.00	1.00

Table 16: membrane contact angle measure with deionized water at ambient temperature

	Contact Angle (°)				
Membrane	Run 1	Run 2	Run 3	Contact Ang (°)	Std. Dev
M-U	54.8	53.2	51.5	53.17	1.65
M-H	47.9	51.3	49.6	49.60	1.70
M-T	42.5	36.9	39.7	39.70	2.80
M-TA	39.5	42.5	45.6	42.53	3.05
M-HTA	39.2	35.6	32.1	35.63	3.55

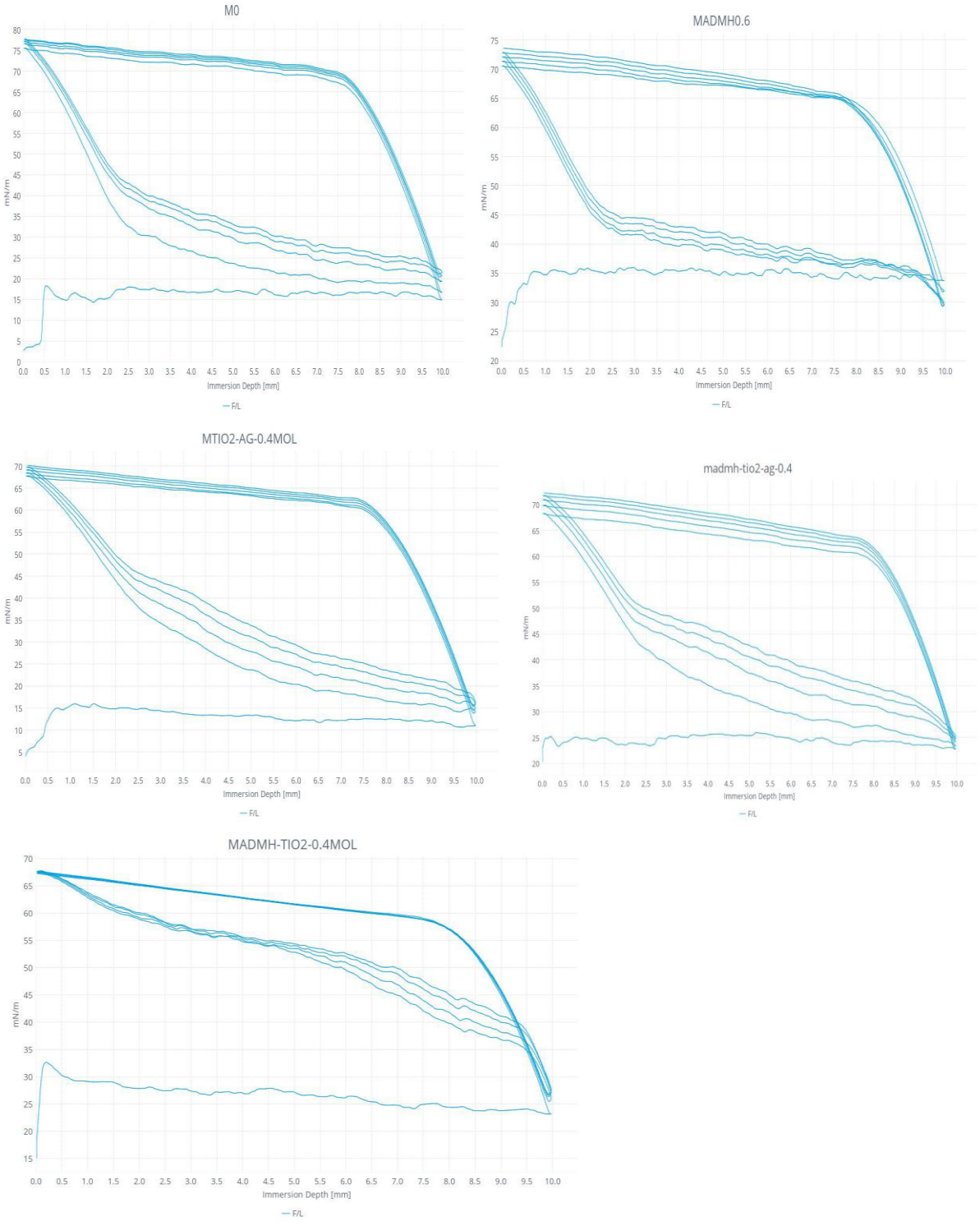


Figure 41: Contact angle cycles of membranes obtained in the analysis of membranes' hydrophilicity

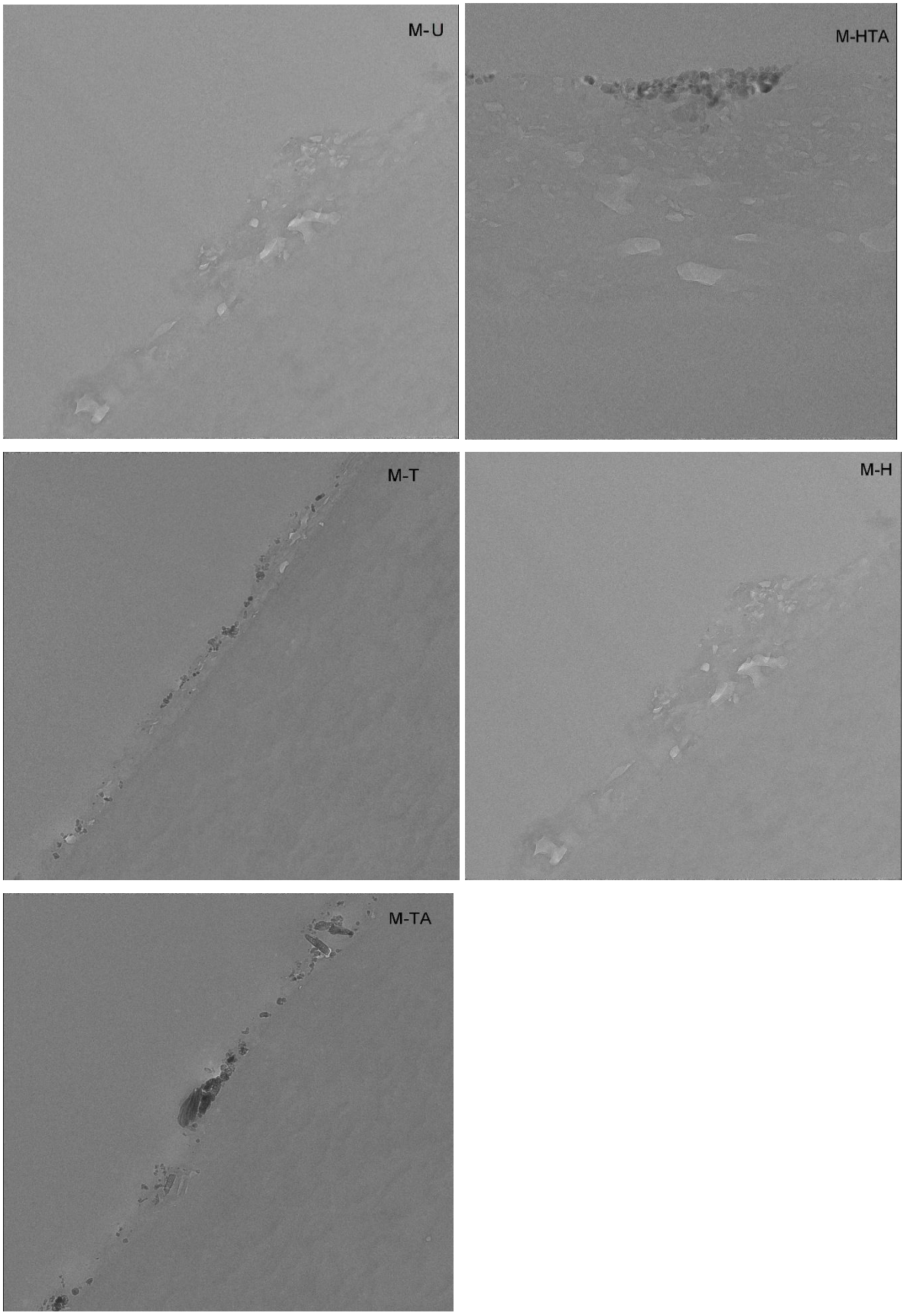


Figure 42: TEM images of membranes (Raw data)

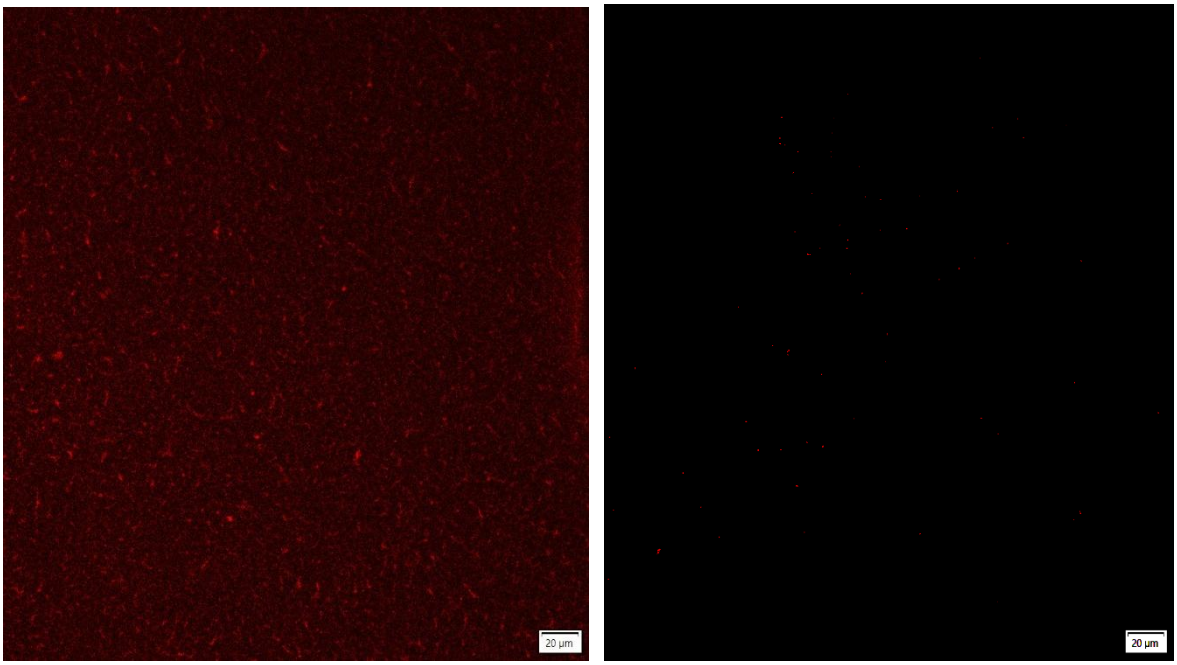


Figure 43: CLSM images of the M-U (left) and M-HTA (right) membranes after the long-term fouling test (dead bacteria)

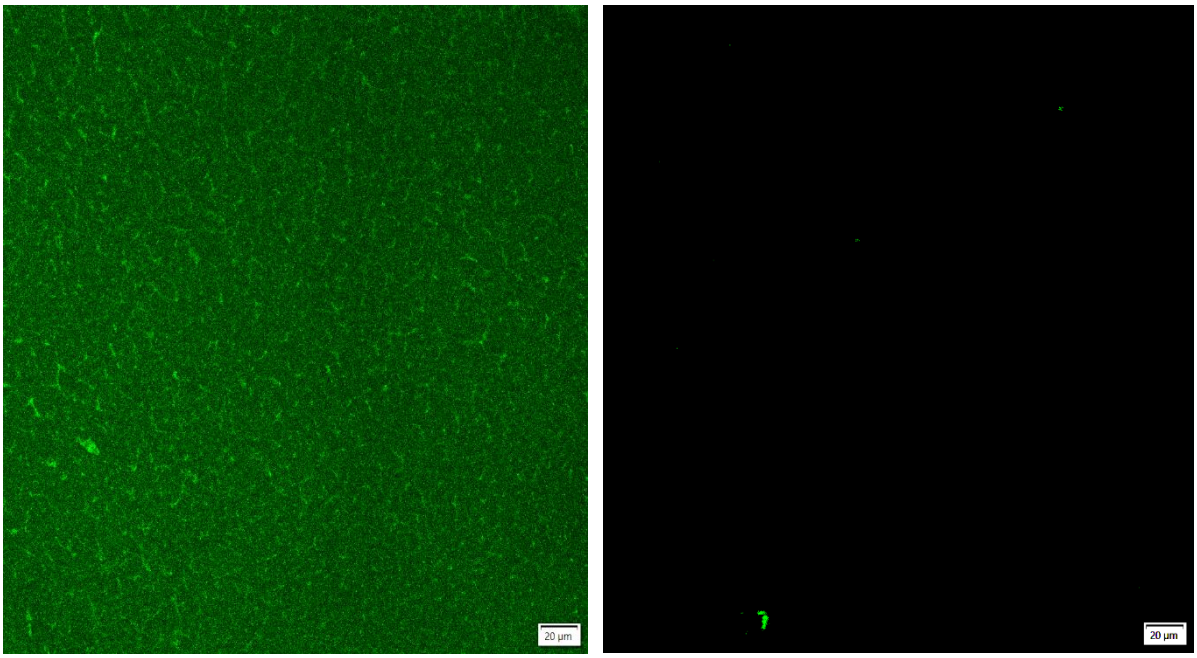


Figure 44: CLSM images of M-U (left) and M-HTA (right) membrane after the long-term fouling test (live bacteria)

APPENDIX C: Membrane performance assessment data

Membrane surface modification using ADMH\TiO$_2$-Ag: Batch Experimental Data of fouling tests

Table 17: *E. Coli* Mortality Ratio for tested membranes

Membrane	E. Coli Mortality Ratio				
	Run 1	Run 2	Run 3	Avg. MR (%)	Std. Dev
M-U	42.5	45	47.5	45.00	2.5
M-H	78.4	83	87.4	82.93	4.50037
M-T	79.7	81.7	83.7	81.70	2
M-TA	86	89.5	92.1	89.20	3.06105
M-HTA	91.6	94.6	97.7	94.63	3.05

Groups	*Count*	*Sum*	*Average*	*Variance*
M-U	3	138.42	46.14	0.09
M-H	3	141.87	47.29	0.16
M-T	3	134.25	44.75	0.49
M-TA	3	132.09	44.03	0.81
M-HTA	3	211.14	70.38	0.3481

ANOVA

Source of Variation	*SS*	*df*	*MS*	*F*	*P-value*	*F crit*
Between Groups	3102.96	6.00	517.16	1028.94	1.09E-17	2.85
Within Groups	7.04	14.00	0.50			
Total	3110.00	20.00				

Table 18: *S. Aureus* Mortality Ratio for tested membranes

Membrane	S. Aureus Mortality Ratio				
	Run 1	Run 2	Run 3	Avg. MR (%)	Std. Dev
M-U	31	33.8	36.6	33.80	2.80
M-H	76.8	80.2	83.5	80.17	3.35
M-T	79.2	81	82.8	81.00	1.80
M-TA	80.6	84.2	87.8	84.20	3.60
M-HTA	87.3	90.1	93	90.13	2.85

Groups	*Count*	*Sum*	*Average*	*Variance*
M-U	3	101.4	33.80	0.09
M-H	3	240.5	80.17	0.0225
M-T	3	243	81.00	0.1156
M-TA	3	252.6	84.20	0.0196
M-HTA	3	270.4	90.13	0.1225

ANOVA

Source of Variation	*SS*	*df*	*MS*	*F*	*P-value*	*F crit*
Between Groups	1965.323	6	327.5538	4297.532703	4.98E-22	2.847726
Within Groups	1.067067	14	0.076219			
Total	1966.39	20				

Table 19: FDR of membranes after 8 hours of filtration with *E. Coli*

Membrane	Bacteria	Run 1	Run 2	Run 3	Avg. FDR (%)
M-U	E. coli	19.6	20.4	20.9	20.30
	S. aureus	24.9	25.2	25.4	25.17
M-H	E. coli	12.2	13.6	14.6	13.47
	S. aureus	15.5	15.7	16	15.73
M-T	E. coli	12.6	3.81	14.8	10.40
	S. aureus	12.2	14.3	15.2	13.90
M-TA	E. coli	9.5	10.1	10.6	10.07
	S. aureus	11.8	13.2	14.4	13.13
M-HTA	E. coli	5.9	7.1	8.1	7.03
	S. aureus	10.1	11	12	11.03

Table 20: FRR of membranes after 8 hours of filtration with *E. Coli*

Membrane	Bacteria	Run 1	Run 2	Run 3	Avg. FRR (%)
M-U	E. coli	78.6	80.9	82.5	80.67
	S. aureus	68.7	69	69.4	69.03
M-H	E. coli	92.5	95.3	96.8	94.87
	S. aureus	86.2	89.4	91.5	89.03
M-T	E. coli	93.2	94.4	94.7	94.10
	S. aureus	87.7	88.6	89.4	88.57
M-TA	E. coli	93.9	95.1	96	95.00
	S. aureus	88.9	90.7	91.9	90.50
M-HTA	E. coli	94.5	97.2	99.4	97.03
	S. aureus	90.2	92.3	93.8	92.10

Table 21: Salt Rejection of tested membranes with 2000 mg. L^{-1} of NaCl solution Feed

Membrane	Permeate TDS (mg/L)			Avg. Salt Rejection (%)
	Run 1	Run 2	Run 3	
M-U	180	200	160	91.00
M-H	175	180	170	91.25
M-T	210	190	150	90.83
M-TA	180	200	210	90.17
M-HTA	177	182	187	90.90

Table 22: Permeability of tested membranes with DI water

Membrane	Permeate TDS (mg/L)			Permeability (L. m^{-2} h^{-1} bar^{-1})
	Run 1	Run 2	Run 3	
M-U	5.61	5.76	5.87	5.76
M-H	6.27	6.6	6.93	6.62
M-T	6.35	6.79	7.21	6.79
M-TA	5.88	6.14	6.42	6.12
M-HTA	6.4	7.02	7.6	7.04

Table 23: Fouling test using the organic foulant (150 mg. L^{-1} HA): Permeate Flux Decline

Min	M-U		M-HTA	
	Avg. Flux ($L.m^{-2}$ h^{-1})	Fractional flux (J_i/J_t)	Avg. Flux ($L.m^{-2}$ h^{-1})	Fractional flux (J_i/J_t)
0	32	1	32	1
30	31.5	0.98438	31.8	0.99375
60	31.4	0.98125	31.8	0.99375
90	30.9	0.96563	31.5	0.98438
120	30.2	0.94375	31.3	0.97813
150	28.6	0.89375	30.7	0.95938
180	28.9	0.90313	30.5	0.95313
210	28.1	0.87813	29.9	0.93438
240	27.6	0.8625	29.2	0.9125
270	26.8	0.8375	28.3	0.88438
300	25.9	0.80938	27.7	0.86563
330	25.1	0.78438	27.9	0.87188
360	24.4	0.7625	27.3	0.85313
390	23.9	0.74688	26.5	0.82813
420	23.5	0.73438	26.8	0.8375
450	23	0.71875	26.3	0.82188
480	22.8	0.7125	25.9	0.80938
510	20.7	0.64688	25.65	0.80156

Table 24: Fouling test using the inorganic foulant (150 mg. L^{-1} $NaHCO_3$): Permeate Flux Decline

Min	M-U		M-HTA	
	Avg. Flux ($L.m^{-2}$ h^{-1})	Fractional flux (J_i/J_t)	Avg. Flux ($L.m^{-2}$ h^{-1})	Fractional flux (J_i/J_t)
0	32	1	32	1
30	31.8	0.99375	31.8	0.99375
60	31.83	0.9946875	32	1
90	31.4	0.98125	31.7	0.990625
120	30.7	0.959375	31.8	0.99375
150	30.2	0.94375	31.6	0.9875
180	30	0.9375	31.3	0.978125
210	29.7	0.928125	30.7	0.959375
240	30	0.9375	30.5	0.953125
270	29.7	0.928125	30.1	0.940625
300	28.9	0.903125	29.5	0.921875
330	28	0.875	29.1	0.909375
360	28.3	0.884375	28.7	0.896875
390	28.1	0.878125	28.4	0.8875
420	28	0.875	28.1	0.878125
450	27.9	0.871875	28	0.875
480	27.5	0.859375	27.9	0.871875
510	27.3	0.853125	27.7	0.865625

APPENDIX D: Lab-scale long term experimental tests using secondary effluent

Table 25: Long-term fouling test using municipal secondary: Flux Decline

Hours	M-U	M-HTA
	Avg. Flux ($L.m^{-2}\ h^{-1}$)	Avg. Flux ($L.m^{-2}\ h^{-1}$)
0	32	32
2	32	32
4	32	32
6	31.7	31.7
8	31.9	31.9
10	31.4	31.7
12	Night gap	Night gap
14		
16		
18		
20	30.7	31.5
22	30.3	31.4
24	30.1	31.2
26	30.1	31.4
28	29.9	31.3
30	29.8	31.3
32	Night gap	Night gap
34		
36		
38		
40	29.1	31.1
42	29	31.1
44	28.8	31
46	28.7	30.9
48	28.6	30.9
50	28.6	30.9
52	Night gap	Night gap
54		
56		
58		
60	28.4	30.6
62	28.3	30.5
64	28.3	30.4
66	28.2	30.3
68	28.1	30.4
70	28	30.3
72	27.8	30.3
74	27.7	30.1

APPENDIX E: Data recording sample for the lab-scale RO filtration tests

DMAEMA modified membrane

Table 26: RO process operating conditions for membrane performance evaluation

Dimensions	14.5 cm x 9.5 cm
Active Area (m^2)	0.013775
Nomination	XLE-4040
Feed P_0 (bar):	5
Piston P (bar):	14
Feed velocity (Cm/s):	19
Brine p (Kpa):	100

Table 27: Process parameters recorded during the fouling test using the lab-scale RO membrane system

	Feed			Brine		Permeate						
Time (min)	EC µS)	TDS (mg/L)	Temp (°C)	EC (µS)	TDS (mg/L)	EC (µS)	TDS (mg/L)	Temp (°C)	Time (h)	Volume (L)	Flow R (L/h)	Flux (L/h^{-1} m^{-2})
0	336	183	22	336	183	226	125	25	0.004	0.0033	0.792	57.5
45	336	183	22.1	337	184	221	121	24	0.004	0.0032	0.768	55.8
90	338	185	22.2	339	185	213	117	23.8	0.004	0.0032	0.768	55.8
135	340	186	22.2	340	186	211	115	24	0.004	0.0030	0.720	52.3
180	340	186	22.2	341	186	228	127	24	0.004	0.0031	0.744	54.0
225	342	187	22.2	340	186	264	148	23.4	0.004	0.0030	0.720	52.3
270	342	187	22.2	343	187	239	136	23	0.004	0.0029	0.696	50.5
315	347	187	22.7	347	187	336	132	22.4	0.004	0.0029	0.696	50.5
360	349	187	22.8	349	187	249	139	22.6	0.004	0.0028	0.672	48.8
405	350	188	22.9	353	187	236	131	21.6	0.004	0.0028	0.672	48.8
450	352	190	22.8	352	190	198	110	22.5	0.004	0.0029	0.696	50.5
495	352	190	22.7	355	192	123	75	23	0.004	0.0029	0.696	50.5
540	354	192	22.7	356	193	74	41	22.8	0.004	0.0029	0.696	50.5
945	333	184	21.8	334	185	31	19	22.8	0.004	0.0029	0.696	50.5
990	336	185	21.9	335	186	28	17	23	0.004	0.0029	0.696	50.5
1035	336	186	21.8	339	187	38	22	23	0.004	0.0029	0.696	50.5
1080	340	187	21.9	340	188	34	20	22.7	0.004	0.0028	0.672	48.8
1125	341	189	21.8	343	190	39	24	22.8	0.004	0.0028	0.672	48.8
1170	342	190	21.9	343	190	44	26	23.1	0.004	0.0028	0.672	48.8

1215	345	191	21.9	345	191	52	28	23.3	0.004	0.0029	0.696	50.5
1260	345	191	22	346	191	64	36	23	0.004	0.0028	0.672	48.8
1305	347	191	22.1	348	192	70	39	22.7	0.004	0.0027	0.648	47.0
1350	348	192	22.2	349	193	61	35	21.9	0.004	0.0025	0.600	43.6
1395	349	192	22.2	350	193	56	32	21.7	0.004	0.0026	0.624	45.3
1440	350	193	22.2	351	194	57	32	21.9	0.004	0.0024	0.576	41.8
1485	351	194	22.3	354	195	60	34	21.8	0.004	0.0025	0.600	43.6
1530	353	194	22.4	354	195	55	31	22	0.004	0.0024	0.576	41.8
1575	356	195	22.4	357	195	56	31	21.9	0.004	0.0024	0.576	41.8
1620	357	196	22.4	359	197	55	30	22	0.004	0.0025	0.600	43.6
1665	358	196	22.4	360	197	57	32	22	0.004	0.0025	0.600	43.6
1710	359	197	22.5	360	198	54	30	22.1	0.004	0.0024	0.576	41.8
1755	358	196	22.4	359	197	54	30	22.1	0.004	0.0024	0.576	41.8
1800	360	197	22.4	360	198	55	31	22.1	0.004	0.0023	0.552	40.1
1845	361	197	22.3	363	199	56	32	22	0.004	0.0024	0.576	41.8
1890	362	198	22.3	363	199	55	31	21.8	0.004	0.0024	0.576	41.8
1935	365	199	22.2	366	199	57	32	21.8	0.004	0.0023	0.552	40.1
1980	366	199	22.2	368	201	59	33	21.9	0.004	0.0023	0.552	40.1
2475	355	195	21.9	358	197	50	28	21.9	0.004	0.0023	0.552	40.1
2520	357	196	21.8	360	198	49	27	21.7	0.004	0.0022	0.528	38.3
2565	359	198	21.8	361	199	49	27	21.6	0.004	0.0023	0.552	40.1

F-Test

	Normalized flux 2	*Normalized flux 1*
Mean	47.49753906	43.68835693
Variance	35.14705695	34.0913
Observations	38	40
df	37	39
F	1.030968516	
P(F<=f) one-tail	0.461671794	
F Critical one-tail	1.713211604	

t-Test: Two-Sample Assuming Equal Variances

	Normalized flux 1	*Normalized flux 2*
Mean	43.68835693	47.49753906
Variance	34.0913	35.14705695
Observations	40	38
Pooled Variance	34.60528694	
Hypothesized Mean Difference	0	
df	76	
t Stat	-2.858478985	
P(T<=t) one-tail	0.002745245	
t Critical one-tail	1.665151353	
P(T<=t) two-tail	0.005490489	
t Critical two-tail	1.99167261	